LA-UR- 94-1206

EXPERIMENTAL AND THEORETICAL INVESTIGATION OF OPERATIONAL AND SURVIVABILITY ISSUES IN THERMAL RADIATORS FOR THERMIONIC SPACE NUCLEAR POWER SYSTEMS

Final Report

Submitted to

Lt. Eric Critchley
Phillips Laboratory
Kirtland Air Force Base 87117-6008
Albuquerque, New Mexico

Prepared by

Michael D. Keddy
Los Alamos National Laboratory

15 March 1994

ABSTRACT

Heat pipes are a promising candidate for spacecraft radiators. They combine low weight with high thermal efficiency. Liquid metal heat pipes operated at power throughputs well below their design point for long durations may fail as a result of the working fluid migrating to a cold region within the pipe, freezing there, and not returning to the evaporator section. Eventually sufficient working fluid inventory may be lost to the cold region to cause a local dry-out condition in the evaporator, a condition which may lead to complete and permanent failure.

This report describes a program designed to investigate the mass migration phenomenon in heat pipes. The program involved experiments to observe and measure the mass migration rates in both high and low operating temperature heat pipes. The low-temperature experiments were intended to simulate the operation of high-temperature, liquid metal heat pipes. Octadecane was the selected low-temperature working fluid. It is a paraffin and exhibits some of the characteristics of liquid metal working fluids. Sodium was the working fluid used in the high temperature experiment. The various heat pipe experiments were successful, producing temperature profile, heat throughput and mass distribution data.

A one-dimensional compressible flow model was developed for describing the hydrodynamics of rarefied vapor flow in heat pipe condensers. This model was compared with experimental data for the low-temperature octadecane heat pipes and the high-temperature sodium heat pipe. The

model was found to satisfactorally predict the temperature profiles and location of freeze-fronts for the low-temperature heat pipes. Mass migration rate predictions using the model were satisfactory for the low-temperature heat pipes as well. However, the mass migration prediction for the high-temperature, sodium heat pipe was not in agreement with experimental data. An analytical model which accounts for property variations in the radial as well as longitudinal directions is recommended. A one-dimensional model was unsatisfactory for predicting mass migration rates in liquid metal heat pipes.

The experimental data provides a benchmark for estimating mass migration rates in liquid metal heat pipe radiators. This led to the development of design approaches which should mitigate the deletrious effects of the mass migration phenomenon on heat pipe radiators performance.

TABLE OF CONTENTS

TABLE OF CONTENTS (CONT.)

LIST OF FIGURES

LIST OF FIGURES (CONT.)

LIST OF FIGURES (CONT.)

LIST OF FIGURES (CONT.)

LIST OF FIGURES (CONT.)

LIST OF FIGURES (CONT.)

LIST OF TABLES

NOMENCLATURE

A	cross section area [m^2]
a	arbitrary constant
B	arbitrary constant
b	arbitrary constant
C.G.	center of gravity
D	diameter [m]
d1	distance from freeze front to location 1 [m]
d2	distance from freeze front to location 2 [m]
dA	differential cross section area [m^2]
dM	differential Mach number
dP	differential pressure [N/m^2]
dQ	differential heat transfer rate [W]
dV	differential vapor velocity [m/s]
dw	differential mass flowrate [kg/s]
dx	differential axial length [m]
E	arbitrary constant
F	arbitrary constant
f	friction factor
f'	constant in friction factor relation
f1, $f1_i$	first natural frequency [Hz]
f2, $f2_i$	second natural frequency [Hz]
G	arbitrary constant
g_c	gravitational constant
h_{fg}	latent heat of vaporization [J/kg]
$\bar{H}$	average hoat transfer coefficient [$W/m^2/K$]
J	moment of inertia
k	spring constant [
L	distance measured from center of gravity [m]
M	Mach number
m	mass [N/m]
P	pressure [N/m^2]
Q	heat transfer rate [W]
R	gas constant [$atm*cm^3$]
R	Reaction Force [N]

Re_D	Reynolds number
rat_i	ratio of first to second natural frequency
S1	restoring force at location 1 [N]
S2	restoring force at location 2 [N]
T	temperature [K]
t	time [s]
V	vapor velocity [m/s]
w	mass flowrate [kg/s]
W1(x)	distributed weight [N/m]
W2(x)	distributed weight [N/m]
x	axial length along the heat pipe condenser beginning at the evaporator exit [m]
y	ratio of axial component of velocity for condensing vapor to that for the main stream
y	vertical coordinate [m]
$\ddot{y}$	vertical acceleration [m/s^2]
γ	specific heat ratio
δQ	incremental heat transfer rate [W]
δw	incremental mass flowrate [kg/s]
δx	incremental length [m]
Θ	angular coordinate [rad]
$\ddot{\Theta}$	angular acceleration [rad/s^2]
μ	vapor viscosity [$N*s/m^2$]
ρ	vapor density [kg/m^3]
τ_w	wall shear stress [N/m^2]
$\dot{X}$	flow characterization parameter
Ψ	phase angle [rad]
ω	frequency of ocillations [rad/s]

<u>subscripts</u>

sink	environment (i.e., heat sink)
i	arbitrary
o	stagnation
1, 2	points 1 and 2

INTRODUCTION

Liquid metal heat pipes operated at power throughputs well below their design point for long durations may fail as a result of the working fluid migrating to a cold region within the pipe, freezing there, and not returning to the evaporator section. Eventually sufficient working fluid inventory may be lost to the cold region to cause a local dry-out condition in the evaporator.

In the interest of developing heat pipes not subject to failure by this mass migration phenomenon, a joint experimental and analytical effort between the Air Force Phillips Laboratory and Los Alamos National Laboratory was initiated. Experiments included both high temperature liquid metal and low temperature organic heat pipes. The objectives of this effort were to experimentally observe and measure the rate of mass migration into the frozen region within heat pipes and develop a combined analytical and empirical model capable of predicting those rates for liquid metal heat pipes operating well below their design points. The intent of the model is to be first-order and semi-analytical. It will include important parameters and will enable an evaluation of the sensitivity of modeled results to those parameters to be made. As a result, the operating parameters for heat pipes intended for this type of operation, such as is the case for some spacecraft radiators, will be defined. This will ultimately lead to the formulation of heat pipe designs not subject to failure as a result of internal migration of working fluid.

This introductory section will outline the problems associated with heat

rejection in space and the incentives for developing heat pipes for waste heat rejection from spacecraft. A brief discussion is included describing normal heat pipe operation and the problems associated with their long term operation at power levels substantially below their design points. This introductory section will conclude with a discussion of related work and the specific goals for this program.

1.1. Background: Heat Rejection in Space

The unique environment of space presents unusual heat rejection problems. Due to the absence of a convective medium, heat rejection in space is accomplished by either radiation or mass rejection. Mass rejection systems present the risk that they may interfere and possibly even permanently damage sensitive detectors, acquisition, and communications instruments or other sensitive instruments aboard the spacecraft. In addition, for spacecraft with high net heat loads over their design life, the mass for rejection systems exceeds that for passive radiator designs. For these reasons and because radiator systems have been successfully employed in the past, mass rejection systems are seldom considered. Most future spacecraft will probably employ waste heat radiators of some design.

Future spacecraft will require greater power sources to meet the needs of ever increasingly sophisticated instruments. As these craft travel greater distances, their power requirements for propulsion and communications will also increase. Consequently, the waste heat rejection and thermal control requirements will increase proportionately.

With all spacecraft, weight is a premium. Every system aboard is designed to achieve maximum performance and reliability while minimizing weight. This applies to the thermal control system or systems, and in particular to the waste heat radiators which often can be the largest single component in these systems.

Heat pipes are a promising candidate for spacecraft radiators. They combine low weight with high thermal efficiency. The heat pipe, whose operation is described in later paragraphs, is capable of low thermal resistances, many times lower than the best metals. Because of this, a heat pipe can transport heat over appreciable distances and then reject that heat to a sink under the most favorable conditions. In some cases, the temperature losses are so low that the heat rejection is accomplished at temperatures very near the source temperature, making the device extremely efficient.

The waste heat rejection temperatures for future spacecraft will be on the order of 700 to 1000 K. Alkali liquid metals are best suited as working fluids at these temperatures.

1.2. Backgrcund: An Overview of Heat Pipe Operation

Before discussing the problem of long term, low-power operation of a heat pipe, it is beneficial to first provide a brief history of the invention and describe the basic principles by which it operates.

Figure 1 illustrates schematically the principal components and operation of a heat pipe. A heat pipe is a sealed tube containing a working fluid existing under saturation conditions. That is, the working fluid is in

equilibrium between its phases. In normal operation, the fluid exists simultaneously as a liquid and a saturated vapor. When operating, heat is absorbed by the working fluid in a region called the evaporator, where the liquid is vaporized. The amount of thermal energy absorbed by the liquid in the evaporator is proportional to the fluid's latent heat of vaporization. Some representative heat pipe working fluids and their latent heats are listed in Table 1 below.

The vaporized working fluid flows from the evaporator to the cooled region, called the condenser, where the working fluid condenses giving up its latent heat of vaporization. The condensate is circulated back to the heated region where it again vaporizes. The two principal means by which liquid circulation is accomplished are by gravity or by capillary action. In space applications, where gravitational forces are negligible, capillary wick structures are used for liquid circulation. Wire mesh screens, foams, felts and sintered powders are some of the more common wick structure materials. Container materials are usually metals; however, ceramics, glasses and composites have also been used in specialized applications.

Heat pipes are being developed for a wide variety of heat transfer and temperature control applications, some of which include solar energy conversion, waste heat recovery, temperature control for irradiation experiments in nuclear reactors and temperature control of electronic and optical sensor equipment and also temperature control of spacecraft. In most applications, a properly designed heat pipe will transfer heat between two different reservoirs while operating at a nearly uniform

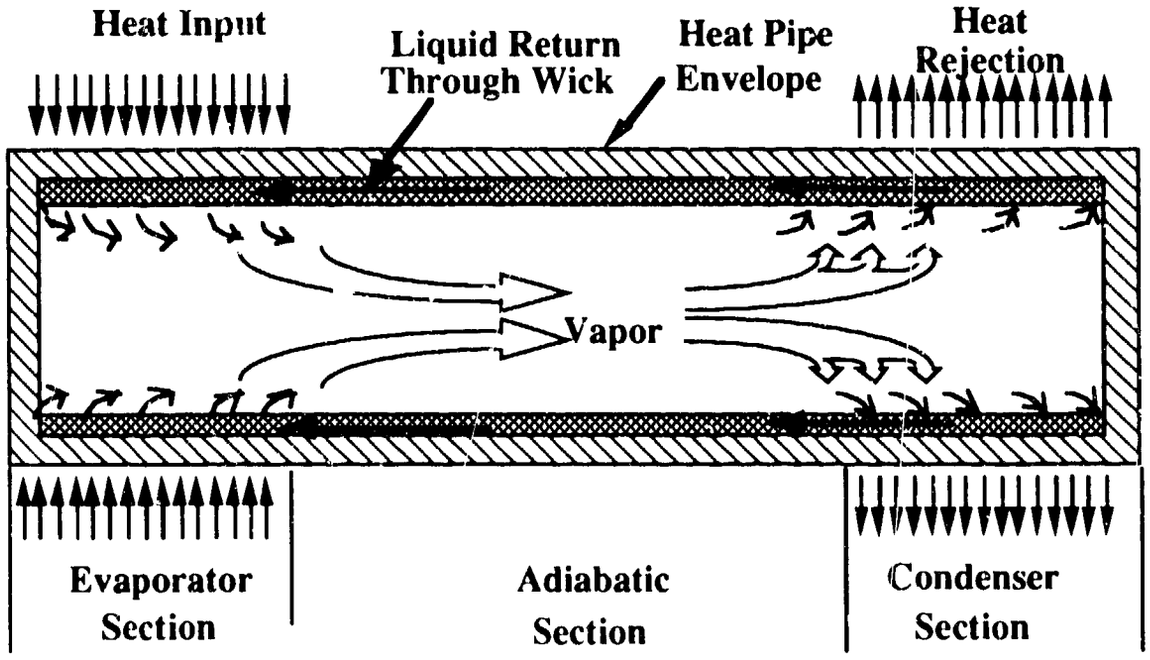

Figure 1. Schematic Representation of a Heat Pipe

Table 1. Latent Heats of Vaporization for Representative Heat Pipe Working Fluids

Fluid	Temperature (°C)	Latent Heat of Vaporization (J/gm)
Ammonia	0	1263
Freon 11	0	190
Acetone	0	564
Methanol	0	1178
Water	0	2492
Mercury	500	291
Cesium	500	512
Potassium	500	2040
Sodium	500	4370
Lithium	1000	20525

temperature. However, in some situations, a heat pipe may be required to operate with a non-uniform temperature profile.

1.3. Background: The Problem of Long Term, Low-Power Heat Pipe Operation

In most applications a heat pipe will be operated under a specific and well defined set of conditions. And, accordingly it will be designed to those conditions. When a heat pipe is operated at power levels substantially different than those it was designed for, it may fail to perform satisfactorily and may even fail altogether. One scenario of interest where these circumstances may arise is as follows: Consider a spacecraft traveling for a period of tens of months or years in a low-power mode as it makes its planned journey. Upon arrival at its intended destination, the spacecraft powers up and begins to gather and send data. The heat rejection system is required to operate in two distinctly different modes. The first is a long-term, low-power mode during the transit. The second is a high-power or full-power mode as the craft gathers, records and sends data back to the experimenters. The design constraints imposed by the high-power operating mode will, to a large extent, dictate the heat pipe design. Materials, geometries, relative sizes and wick structures are all influenced by the high-power operating requirements. The low-power mode, in general, imposes less severe constraints on the design; however, if the heat pipe is operated for extended periods at low power, it may fail as a result of migration of the working fluid. Working fluid can migrate to the cold region within the pipe, freeze there, and not return to the evaporator section. Eventually sufficient working fluid inventory may be lost to the cold region to cause

a local dry-out condition in the evaporator, a condition which may lead to complete and permanent failure.

Low-power, quasi-steady state heat pipe operation has been demonstrated in the Laboratory. Heat pipe tests have demonstrated that in operating radiative coupled heat pipes below their heat throughput design point, a part of the condenser will operate near the evaporator exit temperature, essentially isothermal. At the end of this region, the temperature falls sharply and can reach values below the fusion temperature for the working fluid. This temperature decline occurs over a length corresponding to a few heat pipe diameters.

To illustrate this, Figure 2 shows a temperature profile for a potassium heat pipe operated well below its design point. This heat pipe is constructed of niobium-1.0% zirconium; has an annular screen wick; is 1.52 centimeters in diameter; and is approximately 1.0 meter long. The heated length was 11 cm. Heat removal was by radiation over the entire length. The heat pipe was operated at steady state, with an approximate power throughput at the evaporator exit of 65 Watts. It was designed to transport 650 Watts at 800 K.[1]

A heat pipe operating well below its design point will slowly deplete its inventory of usable working fluid as a result of fluid freezing in the condenser and not being cycled back to the evaporator. For long-term, low-power operation of heat pipe radiator elements in space power systems, this mode of operation may lead to system failure.

In order to determine the rate at which the working fluid migrates from the molten region to the frozen region, it is necessary to establish the point where freezing begins. To do so by analytic means requires the use of a model for the flowing vapor in the condenser. The heat pipe wall temperature is strongly dependent upon the vapor stream temperature, and freezing will start to occur at the point along the wall where the temperature is equal to the working fluid fusion temperature. A useful model must account for the changing nature of the vapor as it travels down the condenser,

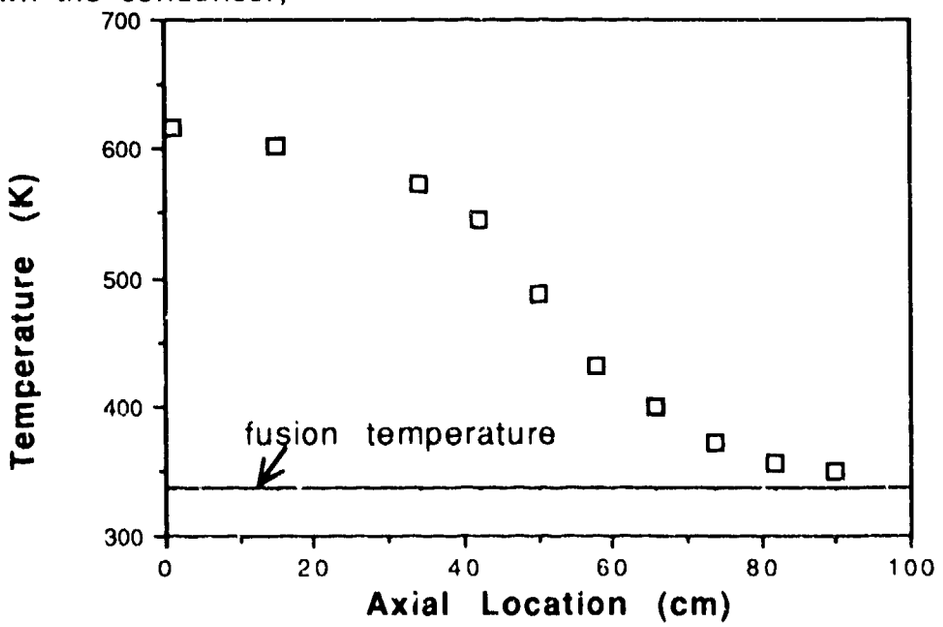

Figure 2. Temperature Profile Data for a Potassium-Niobium 1%Zirconium Heat Pipe Operated at Quasi Steady-State for a Power Substantially Below its Design Level

progressively becoming more rarefied. The vapor stream as it leaves the evaporator exit is in continuum flow. Eventually a sufficient amount of vapor condenses out of the stream so that the assumption of zero velocity for the vapor at the wall is no longer valid.[2] This type of flow is termed

slip flow, or transition flow. Eventually, the flowing vapor becomes so rarefied as to be in free molecular flow. Molecular flow occurs when the mean free path for the molecules is approximately equal to the characteristic dimension for the channel,[3] in this case the heat pipe inside diameter. It is in these regions of slip flow and free molecular flow that the sharp temperature decline along the outside heat pipe surface is observed.

1.4. Technical Approach : An Overview

The overall objectives for this program are to experimentally observe and measure the rate of mass migration into the frozen region within heat pipes and develop a combined analytical and empirical model capable of predicting those rates for heat pipes operating well below their design points.

The technical approach was as follows:

- Strategies for measuring mass distributions and the changes in mass distributions with operation of the heat pipe were formulated and evaluated. Strategies included both direct and indirect techniques and were both non destructive and destructive. Evaluations were based on accuracy, complexity, cost and repeatability.
- Candidate working fluids for use in the low-temperature heat pipe experiments were evaluated. The evaluation criteria included: operating temperature, rarefied flow behavior near the triple point, triple point

above the dew point, low saturation vapor pressure, materials compatibility, and low toxicity and hazard potential.

- Qualification experiments were designed and conducted to help assess the selected low-temperature heat pipe working fluid.
- A one dimensional analytical model was developed and programmed on a desk top computer. The computer model was designed to predict pressure and temperature profiles, freeze-front locations, and mass migration rates within operating heat pipes.
- Low-temperature experiments were designed with the objective of simulating the operation of high-temperature, liquid metal heat pipes operated at power levels substantially below their design points. The use of low temperature heat pipes simplifies the required experimental and fabrication techniques.
- Heat pipes for use in the low-temperature experiments were designed and fabricated.
- The low-temperature experiments were conducted and the test data reduced.
- The low-temperature heat pipe test data was compared with the computer model predictions and the results were reviewed.
- A high temperature experiment was designed employing a liquid metal heat pipe.
- A Heat pipe for use in the high-temperature experiments was designed and fabricated.
- The high temperature experiment was conducted and the test data reduced.
- The high-temperature heat pipe test data was compared with the computer model predictions and the results were reviewed.

1.5. Background: Related Work

Several studies have been conducted in the past on rarefied flows in heat pipes.[4][5][6] These studies focused on the start-up dynamics of heat pipes and not on long term, low power operation. However, parallels between the operating modes exist. During start-up of some heat pipes, regimes of free molecular flow, transition flow and continuum flow can exist. The flow can be compressible or incompressible. Vapor velocities can be sonic or even supersonic. A review of the dynamics of vapor flow in heat pipes during start-up and the methods by which these dynamics are studied is beneficial for the study of the mass migration phenomena in heat pipes operated for long durations at low power.

In a heat pipe, the vapor stream accelerates or decelerates as a result of the addition or removal of mass. Mass addition in a heat pipe evaporator and mass removal in a heat pipe condenser are analogous to the converging and diverging sections in a nozzle. The changes in velocity for a flow in a converging-diverging nozzle are the result of a constant mass flow through a variable cross-section area duct. In a heat pipe, the changes in velocity are caused by changes in the mass flow through a constant cross-section area. Figure 3 illustrates the pressure in a converging-diverging for various flows. As the vapor velocity increases, the pressure decreases in the converging section of the nozzle. In the diverging section, the velocity can increase further and become supersonic provided the outlet pressure is low enough, or the velocity can decrease with a corresponding recompression of the vapor. The amount of recompression depends on the magnitude of the outlet pressure, P_l. Supersonic flows

will occur for outlet pressures below P_{II}. As the outlet pressure is decreased from P_I to P_{II}, the flow in the converging section increases to a maximum, attaining sonic velocity at the throat. This is considered the choked condition as no further reductions in outlet pressure result in increased mass flow. As the outlet pressure is reduced below P_{II}, the flow in the diverging section becomes supersonic, and pressure recovery usually occurs in the form of a shock wave. There is one value of outlet pressure, P_{IV} for a given area ratio which results in a continuous acceleration of the vapor over the entire length of the duct. Further reductions in the outlet pressure have no effect upon the vapor flow in the nozzle section.

Vapor flow in a heat pipe is similar to that in a converging-diverging nozzle. Choked flow, high vapor velocities and pressure recovery in heat pipes have been demonstrated by experiment.[5][7] Results of experiments with a sodium heat pipe by Kemme are presented in Figure 4.[7] Shown is a plot of temperature versus axial location. Heat pipe wall temperatures were used because they can be more readily measured than pressures and, because the heat pipe is a two phase system, there is a direct relation between temperature and pressure. A constant, uniform heat input of 6400 W was supplied at the evaporator. Heat rejection was controlled using a gas-gap calorimeter. The mixture of argon and helium in the gas-gap calorimeter can be controlled to give a factor of four variation in the heat sink thermal resistance. Curve A exhibits a subsonic flow condition with some pressure recovery in the condenser. The vapor accelerated in the evaporator section as a result of mass addition due to evaporation.

The corresponding vapor stream pressure decreased as manifested by the declining temperature.

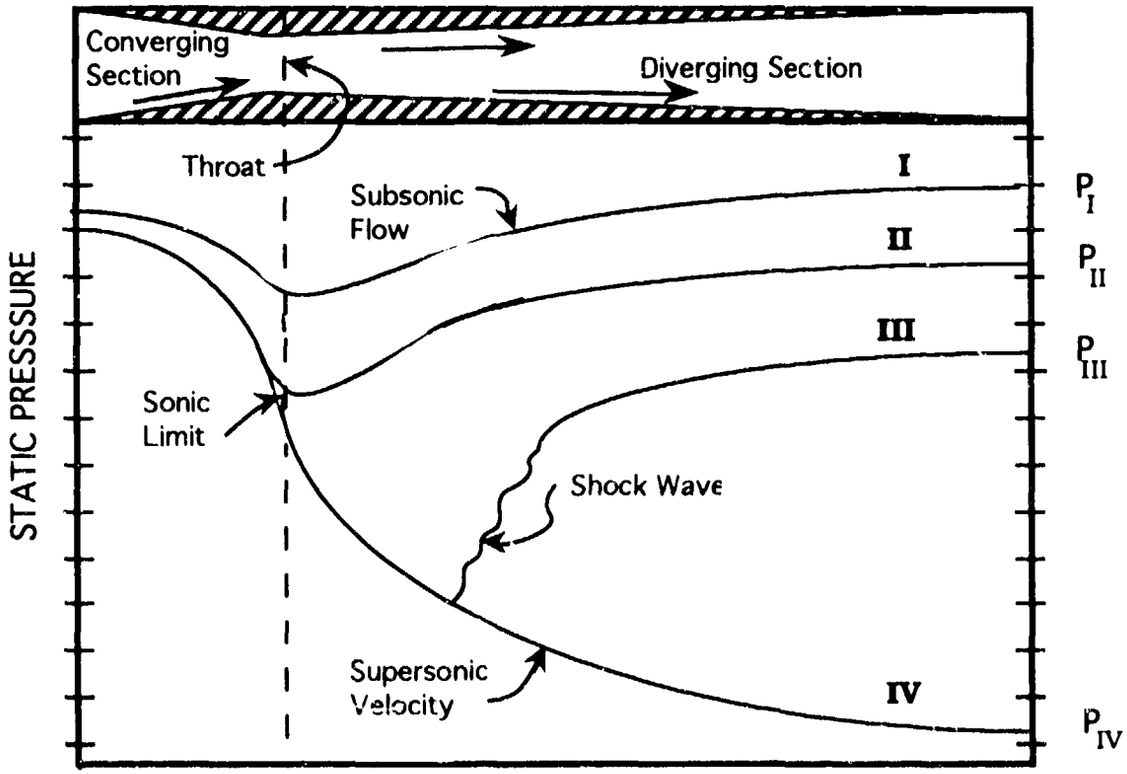

Figure 3. Pressure Profiles in a Converging-Diverging Nozzle

As the heat rejection rate was increased, thus lowering the condenser temperature and pressure, the evaporator temperature was also lowered until sonic velocity was achieved at the evaporator exit as shown in curve B. Increasing the heat rejection further only decreased the condenser temperature and had no effect on the evaporator as shown in curves C and D. Choked flow at the evaporator exit and the sonic limit of heat pipe operation was demonstrated.

The flow dynamics are similar for heat pipes and converging-diverging nozzles, but the expressions for predicting temperature, pressure and density changes in the vapor stream are necessarily different. The derivation of the expressions for heat pipes should be based on flow through a constant area duct with mass addition or removal. Appendix A outlines a one-dimensional compressible flow model for heat pipe evaporators as originally presented by Deverall et al [5]. This model forms the basis for the following discussion.

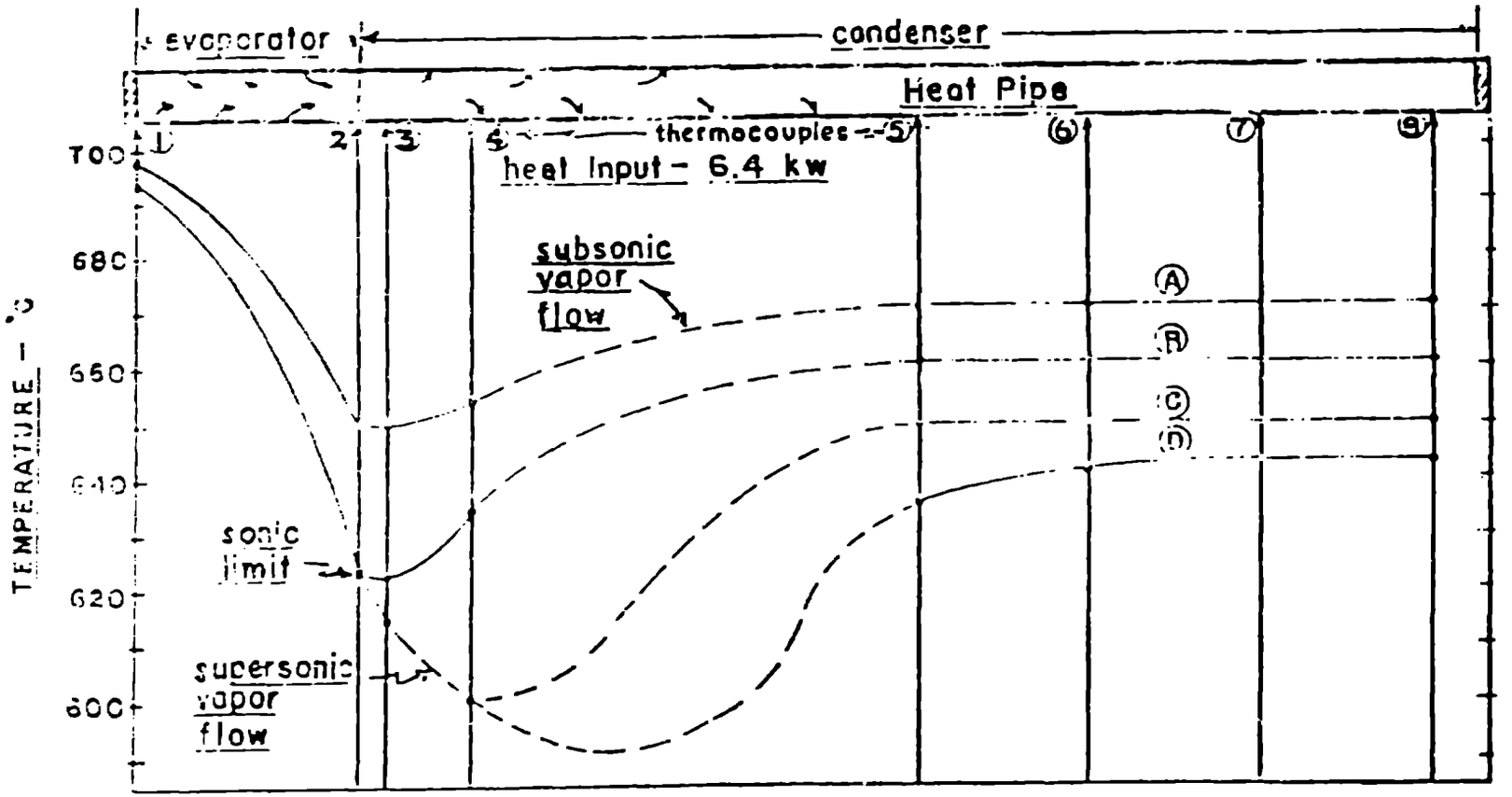

Figure 4. Temperature Profiles in a Sodium Heat Pipe

2. Theoretical and Experimental Methods

2.1 Modeling of the Mass Migration Phenomena in Heat Pipes

Consider the control surface of length dx shown in Figure 5. Mass flows into the surface at a rate w on the left side, and flows out at a rate w + dw on the right. Heat flows out of the volume at a rate dQ as a result of the condensation of vapor which occurs at a mass flow rate of dw.

The mass flowrate is directly related to the heat throughput. Assuming sensible heat is negligible compared to the latent heat of vaporization, then the mass throughput at any given location along the heat pipe condenser can be written as

$$w = \frac{Q}{h_{fg}} \tag{1}$$

The rate of change of mass throughput, or condensation rate is then defined by the relation

$$\delta w = \frac{\delta Q}{h_{fg}} \tag{2}$$

And the heat transfer rate is described by

$$\delta Q = H\left(\pi D \delta x\right)\left|T - T_{sink}\right| \tag{3}$$

For a discrete element of length δx, we designate the upstream location as point 1 and the downstream location as point 2. A one-dimensional compressible flow with constant specific heat and molecular weight is assumed. Further assume that the vapor is an ideal gas; that the stagnation temperature is constant; that the cross sectional area is constant; and that body forces, such as gravity and dynamic accelerations are negligable. Then, following the derivations of

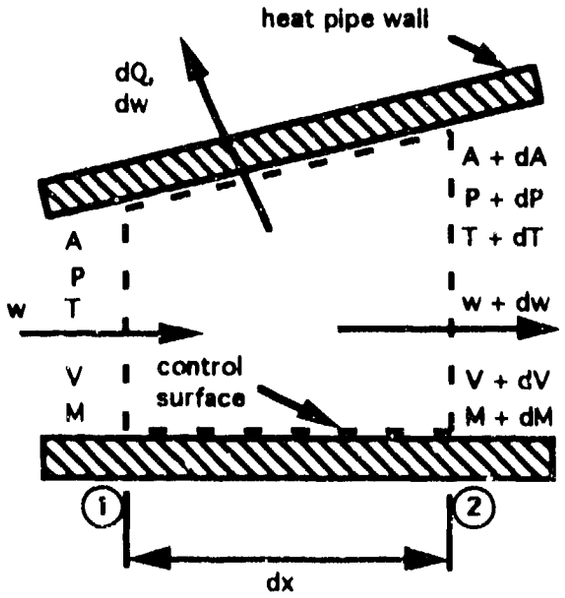

Figure 5. Control Surface for Vapor Flow in a Heat Pipe Condenser

Shapiro[8], the change in pressure across the control surface can be described by

$$\frac{P_2}{P_1} = \frac{w_2}{w_1}\frac{M_1}{M_2}\left[\frac{1 + \frac{\gamma - 1}{2}M_1^2}{1 + \frac{\gamma - 1}{2}M_2^2}\right]^{1/2} \qquad (4)$$

And an expression for the change in Mach number as a function of location along the condenser and mass removal rate can be written in differential form as

$$\frac{dM^2}{M^2} = \frac{\gamma M^2\left(1 + \frac{\gamma - 1}{2}M^2\right)}{1 - M^2}\left(4f\frac{dx}{D} - 2y\frac{dw}{w}\right) + \frac{2\left(1 + \gamma M^2\right)\left(1 + \frac{\gamma - 1}{2}M^2\right)}{1 - M^2}\frac{dw}{w} \qquad (5)$$

With the coefficient of friction defined in the following manner

$$\tau_w \equiv \frac{f\rho V^2}{2} \qquad (6)$$

Where τ_w is the wall shearing stress. The factor y is defined as the ratio of the component of velocity for the injected flow (i.e., condensation or evaporation) in the direction of the main flow to the velocity for the main flow.

Making certain assumptions about heat rejection and friction, it is possible to integrate equation (5) in closed form. Assume that for a sufficiently small interval, dx, between points 1 and 2, the heat rejection rate (i.e., mass removal rate) is constant. Thus, the mass throughput is a linear function of location, resulting in

$$w = w_1 - Bx \quad \text{and} \quad dw = -Bdx \tag{7}$$

Where the subscript 1 refers to the upstream location. Further assume that y=1. Substitution into equation (5) results in

$$\frac{dM^2}{M^2} = \left[\frac{1 + \frac{\gamma - 1}{2} M^2}{1 - M^2}\right]\left(\gamma M^2 * 4f\frac{dx}{D} - 2\frac{Bdx}{w_1 - Bx}\right) \tag{8}$$

Assuming the friction factor to be a linear function of Reynolds number

$$f = \frac{f'}{Re_D} = f'\frac{\mu\pi D}{4w} \tag{9}$$

yields the following differential equation

$$\frac{dM^2}{M^2} = \left[\frac{1 + \frac{\gamma - 1}{2} M^2}{1 - M^2}\right] * \left(\gamma M^2 * f'\frac{\mu\pi}{w} - 2\frac{B}{w_1 - Bx}\right)dx \tag{10}$$

Which may be rearranged as

$$\frac{dM^2}{M^2} = \left[\frac{1 + \frac{\gamma - 1}{2} M^2}{1 - M^2}\right] * \left(2 - \gamma M^2 * f'\frac{\mu\pi}{B}\right)\left(\frac{-Bdx}{w_1 - Bx}\right) \tag{11}$$

or

$$\frac{dM^2}{M^2} = \left[\frac{1 + aM^2}{1 - M^2}\right]\left(2 - bM^2\right)\frac{dw}{w}$$

where

$$a = \frac{\gamma - 1}{2} \quad \text{and} \quad b = \gamma^* f' \frac{\mu\pi}{B} \tag{12}$$

This expression can then be integrated by the technique of separation of variables. The result is

$$\frac{w_1}{w_2} = \frac{M_2}{M_1}\left(\frac{1 + aM_1^2}{1 + aM_2^2}\right)^{\frac{a+1}{2a+b}}\left(\frac{2 - bM_2^2}{2 - bM_1^2}\right)^{\frac{1-b}{2a+b}} \tag{13}$$

Equations (1) through (13) comprise the analytical model. Implementation of the model proceeds as follows. First the heat pipe condenser is divided into discrete sections, each of length δx. It is assumed that the distance δx is sufficiently small such that the properties for the entire section can be described by the upstream conditions. Solution of the various properties at each section then proceeds in a forward marching fashion. With knowledge of the upstream conditions at the first section, the properties at the section exit (i.e., inlet to the next section) are determined. The solution then proceeds for each subsequent section. First the heat sink is defined in terms of sink temperature and equivalent heat transfer coefficient (T_{sink} and H). The heat transfer coefficient may be a function of temperature as is the case for radiation, and to a lesser extent, convection; however, as with the other properties, it is considered constant over each discrete element. The stagnation temperature, sink temperature and heat transfer coefficient are treated as parameters in the model. Equation (3) is then solved for the incremental heat transfer

rate, δQ. Equation (2) is solved for the condensation rate, δw, and the downstream mass flowrate is thus determined. Equation (13) is used to determine the downstream Mach number, and then equation (4) is solved for the downstream pressure.

The working fluid in a heat pipe exists as a two-phase fluid, thus the vapor and liquid in the condenser region coexist under saturation conditions. This implies that the temperature and pressure are directly related (i.e., $T=T(P)$ only). With knowledge of an appropriate equation of state, the downstream temperature can be determined from the downstream pressure. This temperature then determines the heat rejection rate at the next downstream section, and the solution proceeds as before until the temperature reaches the fusion temperature for the working fluid. The physical location where this occurs is the freeze front for the working fluid. At this point the calculations are terminated. The mass throughput at this point is the predicted mass migration rate for the heat pipe design in question.

In order to start the model, it is necessary to characterize the flow conditions at the inlet to the condenser. The conditions that exist in throughout the heat pipe during start-up are analogous to those that exist in the condenser for a heat pipe being operated at power levels substantially below its design point. The flows are compressible and rarefied. At the evaporator exit, which is the condenser inlet in heat pipes without adiabatic sections, the vapor flow is said to be choked. That is, no additional mass can be added to the vapor stream without changing the operating constraints on the heat pipe (e.g., evaporator

temperature, heat sink temperature or respective heat transfer coefficients). Under these conditions (i.e., Mach number = 1), the heat pipe is said to be operating at its sonic limit. The heat transfer throughput at the evaporator exit is given by

$$Q_{sonic} = \frac{\rho_o A \sqrt{\gamma R T_o}}{\sqrt{2(\gamma + 1)}} h_{fg} \qquad (14)$$

And the temperature is

$$T_{sonic} = \frac{2}{\gamma + 1} T_o \qquad (15)$$

The saturation pressure can then be found from the saturation curve, so the evaporator exit conditions (i.e., condenser inlet conditions) are fully characterized. The information necessary to implement the mass migration model is thus complete.

This analytical model was coded in BASIC and programmed on a Macintosh SE/30. A listing of the code is included in Appendix B. Thermophysical properties are calculated by various separate subroutines. These are modular in nature, so the user need only substitute the appropriate routines for the desired working fluid. The user must then supply the appropriate physical dimensions, gas constant, specific heat ratio and molecular weight. These are hard wired in the code, but are still easily modified within the appropriate modules. To run the code, the user simply inputs the stagnation temperature at the prompt, and the code proceeds to

execute. The results for the Low and High Temperature Heat Pipe performance predictions are discussed in Section 3.

2.2 Experimental Methods

2.2.1 Alternative Mass Migration Measurement Techniques

Three techniques for measuring working fluid migration in heat pipes were formulated and evaluated. They were a direct balance technique; a vibration response technique; and a weighing of segments technique. The principles behind, procedures for implementation, and advantages and drawbacks of each technique are discussed separately below.

Some of the criteria used to evaluate the alternatives were:

- Technical feasibility, such as practicality of implementation and the likelihood for precise, accurate and repeatable data;

- Cost and ease of procedure;

- Versatility, that is, the adaptability of the technique to both the high and low temperature experiments.

Mass Balance (Sum of Moments) Technique

Figure 6 is a schematic diagram for a heat pipe shown supported on a fulcrum located at the interface between the frozen and operating regions

of the heat pipe. The reaction force at the fulcrum is denoted R. The forces which act to balance the heat pipe are designated S1 and S2 and their respective distances from the freeze front are designated d1 and d2. A hypothetical mass distribution for the working fluid along the longitudinal axis of the heat pipe is depicted graphically. The mass distribution in the frozen region is designated w1(x), and the mass distribution in the operating region is designated w2(x).

The balancing forces, S1 and S2, and their distances from the fulcrum can be measured. The reaction force at the fulcrum may be determined by a force balance, knowing the total weight for the heat pipe. The two remaining unknowns are the weight distributions, w1(x) and w2(x).

An iterative approximation for the mass distribution in the frozen region can be made by assuming the functional form for both distributions is linear, and further assuming the mass at the end of the frozen region furthest from the freeze front is zero.

The solution procedure is described below and makes use of the following free body diagrams. Free Body Diagram Figure 7(a) is for the entire heat pipe. Free Body Diagram Figure 7(b) is for the frozen region, and Free Body Diagram Figure 7(c) is for the operating region.

From the free body diagram for the entire heat pipe, Figure 7(a), a sum of forces in the y-direction yields:

$$\sum F_y = 0, \; S1 + R + S2 - \int_0^{d1} W1(x)dx - \int_{d2}^{0} W2(x)dx = 0 \qquad (16)$$

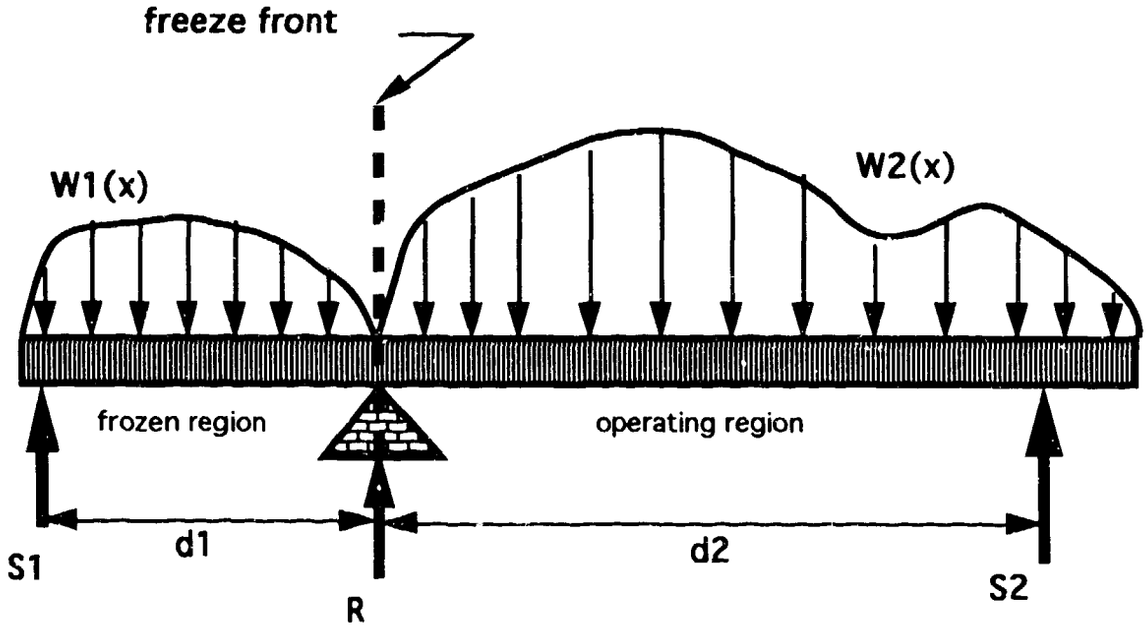

Figure 6 Schematic Representation of a Heat Pipe and its Supports as They Apply to the Mass Balance Technique.

The sum of the integrals for w1(x) and w2(x) is equal to the total weight for the heat pipe,

$$\int_0^{d1} W1(x)dx + \int_{d2}^{0} W2(x)dx = Wtot \qquad (17)$$

which is a measurable quantity, as are the quantities S1 and S2. The remaining supporting force, located at the fulcrum and denoted as R, is the only unknown in equation (1) and can be solved for directly. From the free body diagram for the frozen region, Figure 7(b), a sum of forces in the y-direction and a sum of the moments about the freeze-front yields:

$$\sum F_y = 0,\ S1 + R1 - \int_0^{d1} W1(x)dx = 0 \tag{18}$$

$$\sum M_{\text{freeze front}} = 0,\ \ S1*d1 - M - \int_0^{d1} x*W1(x)dx = 0 \tag{19}$$

Similarly, from the free body diagram for the operating region, Figure 7(c), a sum of forces in the y-direction and sum of moments about the freeze-front yields:

$$\sum F_y = 0,\ S2 + R2 - \int_{d2}^{0} W2(x)dx = 0 \tag{20}$$

$$\sum M_{\text{freeze front}} = 0,\ \ M - S2d2 + \int_{d2}^{0} x*W2(x)dx = 0 \tag{21}$$

Equations (19) and (21) can be combined to eliminate M. The resulting expression becomes,

$$S2d2 - S1d1 - \int_0^{d1} xW1(x)dx - \int_{d2}^{0} xW2(x)dx = 0 \tag{22}$$

The system of integral equations, equation (17) and equation (22), cannot be solved without first knowing the distribution functions, w1(x) and w2(x). However, as stated earlier, if w1(x) and w2(x) are both assumed linear and the mass at the end of the frozen region furthest from the freeze-front is assumed to be zero, then the linear distribution equations for w1(x) and w2(x) can be written as

$$W1(x) = E\left[1 - \frac{x}{d1}\right] \qquad (23)$$

and

$$W2(x) = Fx + G \qquad (24),$$

where E, F and G are constants and l is the length of the frozen region.

By the appropriate choice for one of the balancing forces, the other can be made zero (i.e., the problem as shown in Figure 7 is over constrained). Letting S2 be zero and substituting equations (23) and (24) into equations (17) and (22) results in

$$W = E\frac{d1}{2} - \left(\frac{F}{2}d2 + G\,d2\right) \qquad (25)$$

and

$$S1d1 = \frac{F}{3}d2^3 + \frac{G}{2}d2^2 - E\frac{d1^2}{6} \qquad (26),$$

which are two equations with three unknowns (i.e., the constants E, F and G). A solution for the constants in these equations can be determined by the iterative experimental approach explained below.

First a value for the constant E is assumed. Then the c rresponding values for F and G can be found from equations (25) and (26). Next, the point at which the balancing force is applied is moved to a new location, d1'. The force acting at this new location, S1', is measured. This measured value

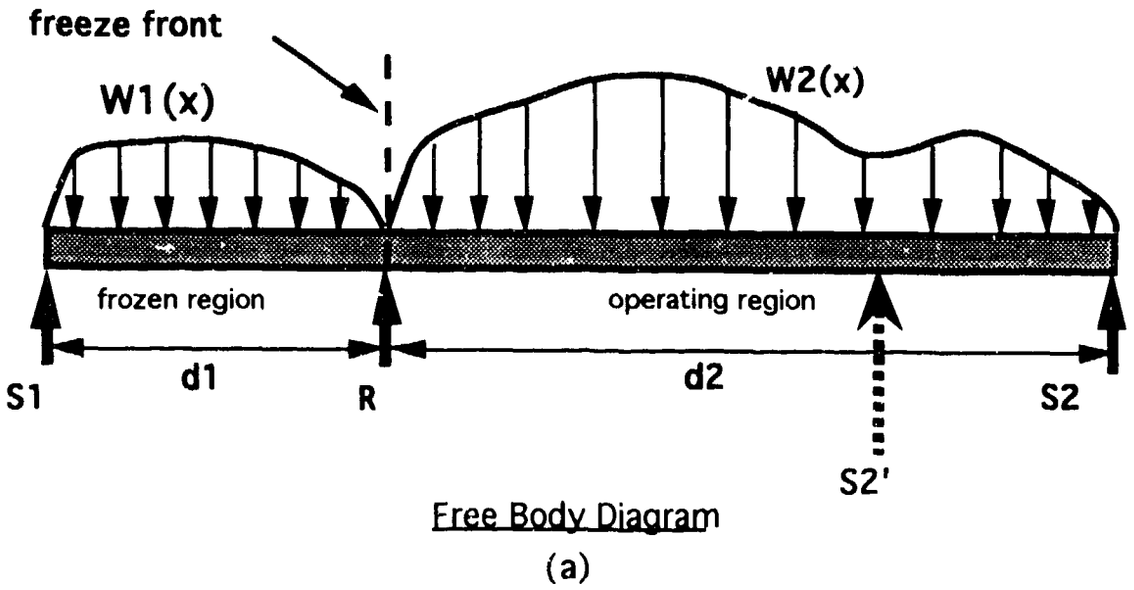

Free Body Diagram
(a)

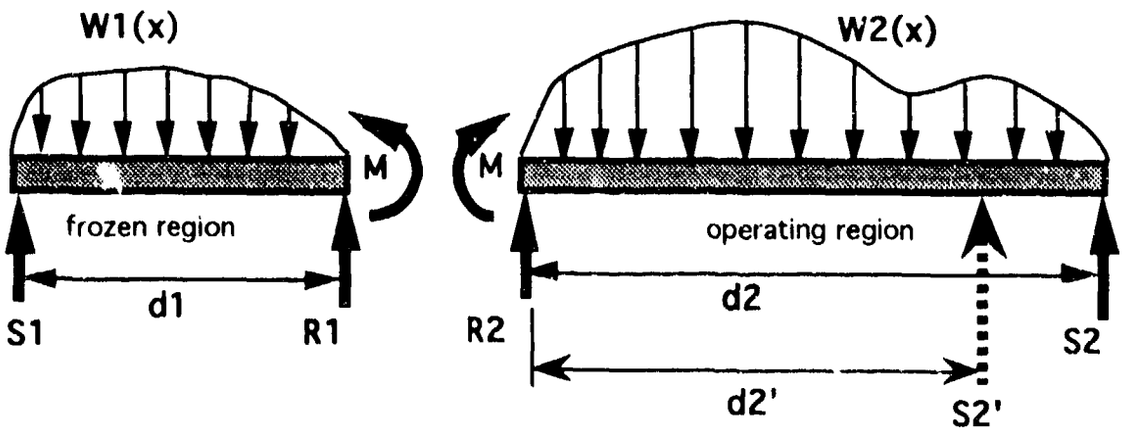

Free Body Diagram
(b)

Free Body Diagram
(c)

Figure 7 Free Body Diagrams for a Heat Pipe with a Non-Uniform Mass Distribution: (a) entire heat pipe length, (b) frozen region, and (c) operating region

is then compared with the value computed from equation (26). If the two values are not in agreement, a new value for the constant E is assumed, and the above process is repeated until agreement is achieved. Solutions for the mass distribution and net mass in the frozen region are thus determined.

This procedure could be repeated at successive time steps over the duration of an experiment.

This technique is relatively straightforward and requires no specialized equipment. However, its accuracy is limited to that for the mass distribution functions. It would be desirable to calibrate this approach against another, direct measurement approach. The sensitivity for the experiment depends on the particular size and weight of the heat pipe being tested. As an example, a heat pipe 1.0 meter long and 1.0 inch in diameter would have a total mass on the order of 0.5 kg. This is within the capacity of common triple beam balances or other common laboratory scales, which typically have accuracies on the order of ±0.001 gms. Now, were all the frozen material to deposit right at the freeze front (a worse case scenario), then the sensitivity for the experiment would be approximately twice the accuracy of the balance, or roughly 0.002 gms.

In order to utilize the mass balance technique, it is necessary to precisely locate the freeze front. One method of locating the freeze front is by visual observation using a transparent heat pipe. This would require the use of a working fluid which is compatible with the transparent material and whose liquid and solid phases are visually discernible. Figure 8 is an illustration of a possible experiment layout for a transparent heat pipe

which employs the Mass Balance technique. In this case the transparent heat pipe material is quartz. A camera may be used to record the freeze front location and the accumulation of frozen working fluid over the course of the experiment. Note that no wick structure is provided in the heat pipe region wherein the freeze front is located. This is not a design requirement for heat pipes using the mass balance technique, but it does make precise location of the freeze front easier and facilitates photography. No experiments using the Mass Balance technique were ever conducted. As such the experimental layout shown in Figure 8 was never used. However, the heat pipe design illustrated in this figure is approximately that used in the Low Temperature Heat Pipe working fluid validation experiments. Details of these experiments and the heat pipe design used therein are discussed in a later section.

Many organic and inorganic working fluids are compatible with transparent materials like glass and quartz, so fabrication of transparent heat pipes for the low temperature experiments is feasible. However, fabrication of a transparent liquid metal heat pipe is a difficult undertaking. Liquid metals tend to be strong oxidizers and operate at high temperatures. As such, they are incompatible with glasses and quartz. Use of the Mass Balance technique with liquid metal heat pipes requires that some method other than visual observation be developed for locating freeze fronts. One possible alternative is to locate freeze fronts, by means of precise temperature measurements along the length of the heat pipe's outer or inner surface. Before an approach like this could be used, experiments would need to be conducted to calibrate temperature measurements with freeze front locations. Unfortunately, experiments

utilizing liquid metals are inherently expensive. Much of the high costs are attributable to the handling and processing of the liquid metal and to the restrictions imposed on materials and test equipment due to high temperatures.

In summary, a shortcoming of the Mass Balance technique is that it may prove difficult and costly to apply to liquid metal heat pipes. Also, as stated previously, it would be desirable to compare this approach against a direct measurement approach in order to validate the leading assumptions used in the analytical development. This too would require additional experimentation, adding to the cost.

Vibration Response Technique

Consider the two degree of freedom system shown in Figure 9. This system represents a heat pipe supported by two springs which are free to move in the y-direction only. The spring constants, k1 and k2 are equal. The distances, L1 and L2, measured from the center of gravity to the springs may or may not be equal. The first two modes of vibration for this system are: the vertical motion of the center of gravity, measured by the y coordinate and the rotational motion about the center of gravity, measured by the Θ coordinate. Applying Newton's Second Law of Motion to the transverse and rotational directions yields the following coupled system of differential equations:

$$m\ddot{y} + k_1(y - L_1\Theta) + k_2(y + L_2\Theta) = 0$$

$$J\ddot{\Theta} + k_2(y + L_2\Theta)L_2 - k_1(y - L_1\Theta)L_1 = 0 \qquad (27)$$

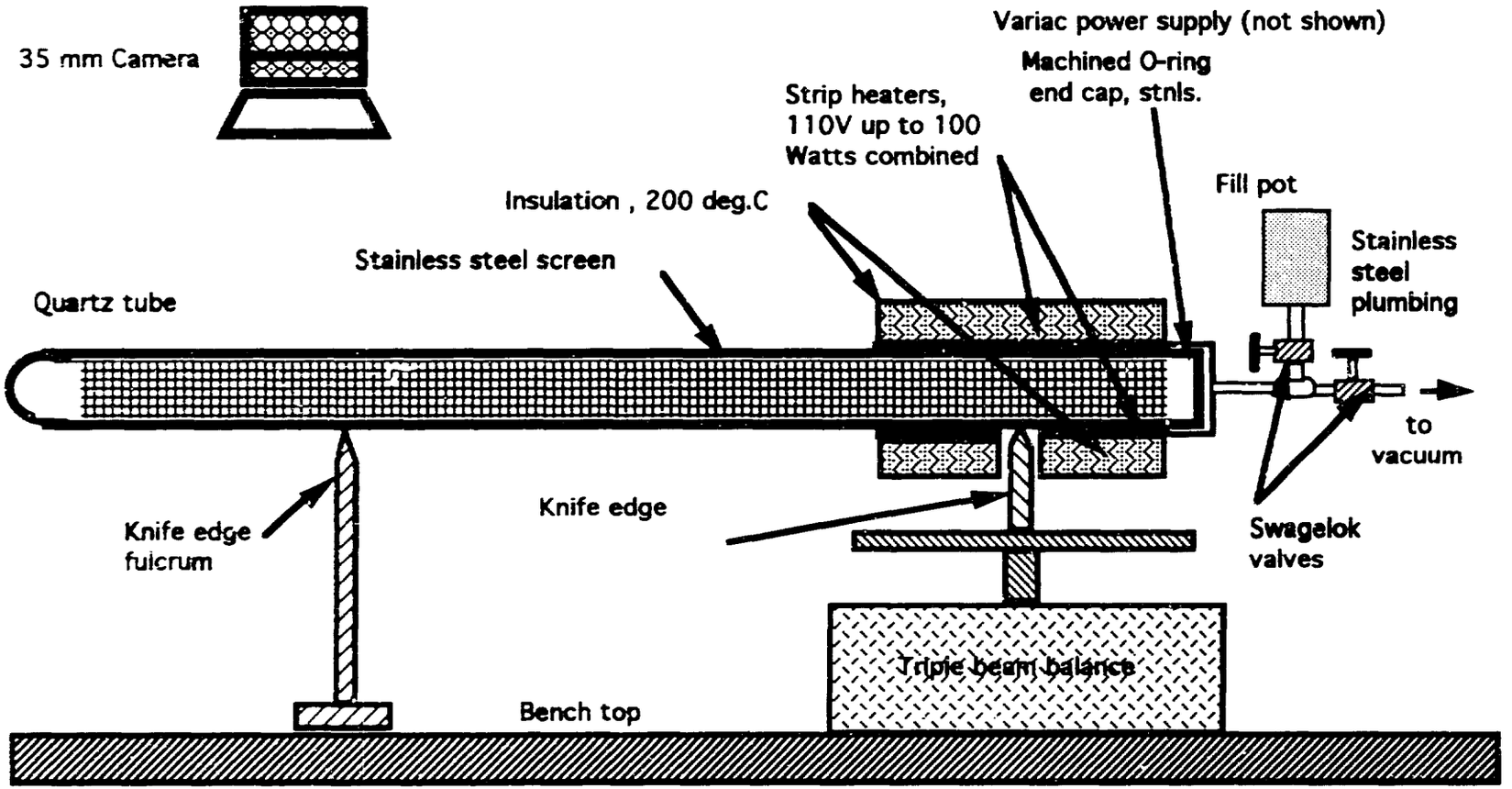

Figure 8. Conceptual Experiment Set-Up for a Heat Pipe Experiment Using the Mass Balance Technique.

Substituting

$$y = A\sin(\omega t + \psi) \text{ and } \Theta = B\sin(\omega t + \psi) \qquad (28)$$

into the above system results in the following:

$$(a - \omega^2)A + bB = 0$$
$$cA + (d - \omega^2)B = 0$$

where,

$$a = \frac{k_1 + k_2}{m} \qquad b = \frac{k_2L_2 - k_1L_1}{m}$$

$$c = \frac{k_2L_2 - k_1L_1}{J} \qquad d = \frac{k_1L_1^2 + k_2L_2^2}{J} \qquad (29)$$

Solutions for the first two natural frequencies, $\omega 1$ and $\omega 2$, can be found by setting the determinant of the coefficient matrix for the above system of equations equal to zero and solving the resulting polynomial.

For a balanced system, the coupling term (k_2L_2-k_1L_1) is zero. A force applied in the y-direction at the center of gravity will produce a translation in the y-direction only. As the center of gravity moves, the coupling term is no longer zero, and the system will have both a translational and rotational motion when a displacement or torque is applied. As the system becomes progressively more unbalanced, and

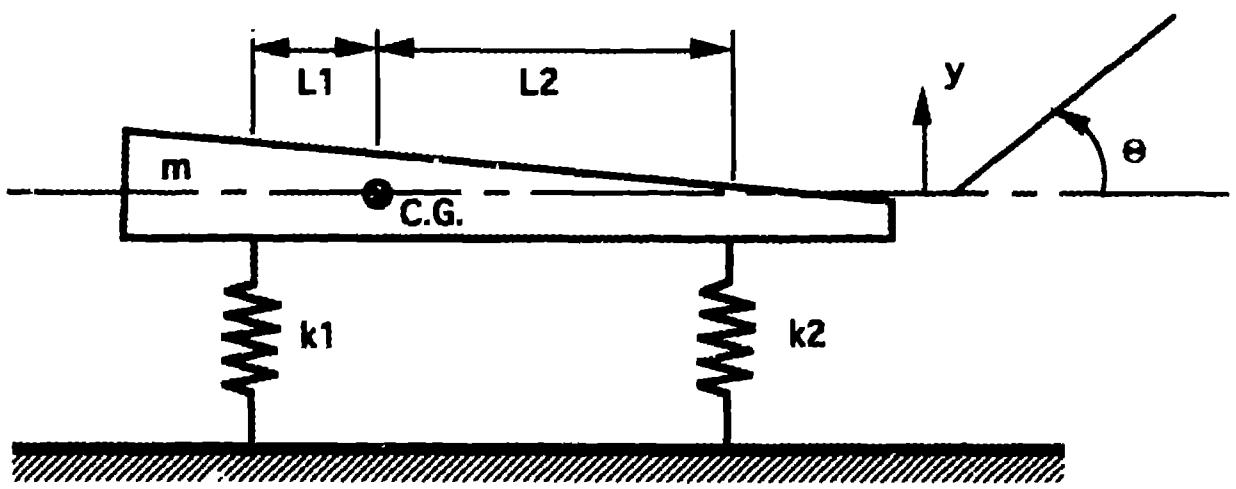

Figure 9. Two Degree of Freedom Mass-Spring System

thereby the coupling term increases, the ratio of frequencies for the two modes will change. Altering the mass distribution and thus shifting the center of gravity is one way of creating an imbalance in the system. Provided the translational and rotational frequencies are sufficiently spaced, such that their ratio is not nearly unity, it should be possible to measure changes in the frequency ratio due to shifts in the location of the center of gravity. It is conceivable that by measuring the frequency response of the system to some excitation and calibrating this to mass shifts within the system, a method for measuring mass migration in a heat pipe may be devised.

A series of parametric studies were conducted to determine whether this approach would be feasible for the size and shape of heat pipes planned for use in this program. It was assumed that the respective distances from the springs to the center of gravity in the baseline case were a

constant multiple (e.g., $L_2 = 1.001*L_1$). The total length was varied from 1 to 100 inches, and three tubular cross sections were used. The tubes were all stainless steel, one of 1.0 inch diameter by 0.035 inch wall, the next of 0.5 inch diameter by 0.035 wall and the last of 0.5 inch diameter by 0.010 inch wall. A set of sample calculations as used in this parametric study are included in Appendix C. The same calculation procedure was used for each of the three cross section geometries. The results of this parametric study are summarized in Figures 10 through 18. Figures 10 through 12 are for the 1.00 inch by 0.035 inch case. Figures 10 and 11 show the first two natural frequencies in terms of cycles per second (Hz) as a function of tube length in inches. Figure 12 shows the ratio of the two frequencies as a function of tube length. Figures 13 through 15 are analogous results for the 0.50 inch diameter by 0.035 inch wall case, and Figures 16 through 18 are analogous results for the 0.50 inch diameter by 0.010 inch wall case.

Of greatest interest are tube lengths in the range of 24 to 48 inches, lengths typical of what might be used on spacecraft. Comparing Figures 12, 15 and 18 at these lengths, it is apparent that the frequency ratio is much more affected by wall thickness than by tube diameter. It appears that a thin walled tube, on the order of 0.010 inch, would be best suited to this mass migration measurement technique.

A simple experiment was run to determine the viability of this technique as it applies to this program. Figure 19 illustrates the experiment layout. A stainless steel tube 23.6 inches long by 0.5 inch diameter by 0.010 inch wall thickness is fixed at either end to a mounting bracket by means of

leaf springs. This assembly is mounted to a shaker table. One accelerometer and an equivalent load to balance the system are mounted at opposite ends of the stainless steel tube. This accelerometer measures the response of the system to the dynamic load induced by the shaker table. An additional accelerometer (not shown) is attached to the shaker table to measure the driving frequency.

The planned experimental procedure was to excite the baseline system and identify its first two natural frequencies. This would then be repeated several times to verify the repeatability of the measurements. The system would then be balanced until only the first mode was present. The frequency response for the balanced system would form a baseline. Once the baseline has been achieved, a small known weight would be placed on the tube some prescribed distance from the center of gravity. For this, a rubber band or piece of tape might be used. The response of the system would again be measured. This process would be repeated for various other weights and weight locations. From the result of these measurements, an empirical relationship could be derived for relating mass shifts to frequency response.

Application of the Vibration Response technique to measurement of mass migration in a heat pipe is similar to the experimental procedure described above. Prior to subjecting the heat pipe to induced vibration loads, a dummy heat pipe, identical in all structural and physical properties is tested. Testing of the dummy heat pipe is exactly analogous to the procedure described above. That is, the dummy heat pipe is shaken for a series of varying weights and weight distributions. The results are then correlated into an empirical relationship for vibration response as a

function of mass distribution for that specific heat pipe. To determine the mass migration within the actual heat pipe, it is necessary to compare the vibration response signature for the actual heat pipe to that for the dummy heat pipe. The correlation between the two should be direct.

Using the experimental approach described earlier, the system illustrated in Figure 19 was tested. The system was twice subjected to an excitation, and its response measured. The results are compiled in Figures 20 through 23. These results represent averages taken over ten sweeps of readings.

The equipment used to record and compile the data as well as control the excitation frequency was a Hewlett Packard HP-3565S signal processing system and a Hewlett Packard HP-360 workstation using SMS Modal Analysis 3.0 software. The accelerometers were Endevco Isotron PE type with sensitivities of 509 mV/g. A random excitation over a span of 0-100 Hz was used to drive a 500 pound shaker to which the test assembly was mounted. The shaker was manufactured by Vibration Tester Systems.

Figures 20 and 21 are for the first run, and Figures 22 and 23 are for the second run. Figure 20 shows the frequency response in terms of output voltage over input voltage as a function of frequency. It is evident that at least one mode is present and has a frequency around 39 Hz. It also appears that a second mode may exist at a frequency near 52 Hz; although, it is not clearly discernible. Figure 21 shows phase versus frequency for the same run. This figure shows a phase shift approaching 180° at approximately 40 Hz, verifying this frequency as a natural frequency.

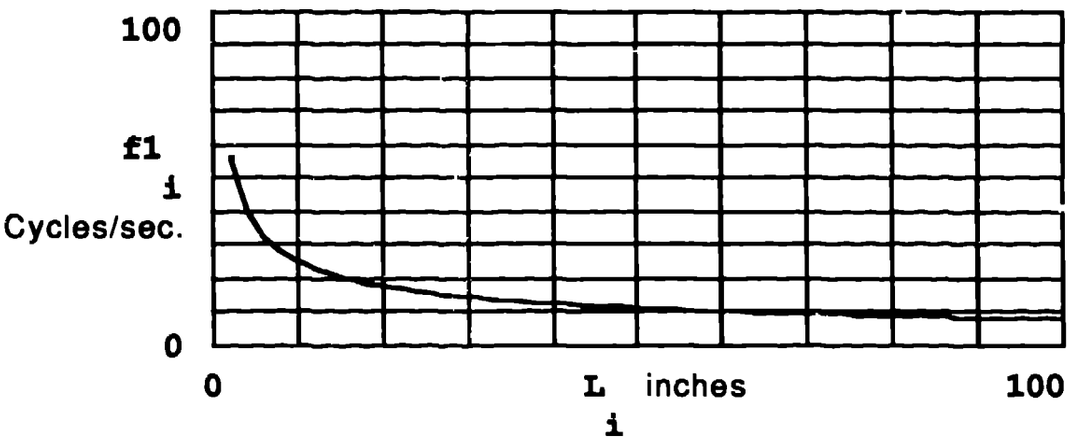

Figure 10. First Natural Frequency for 1.00" dia. X 0.035" wall Tube

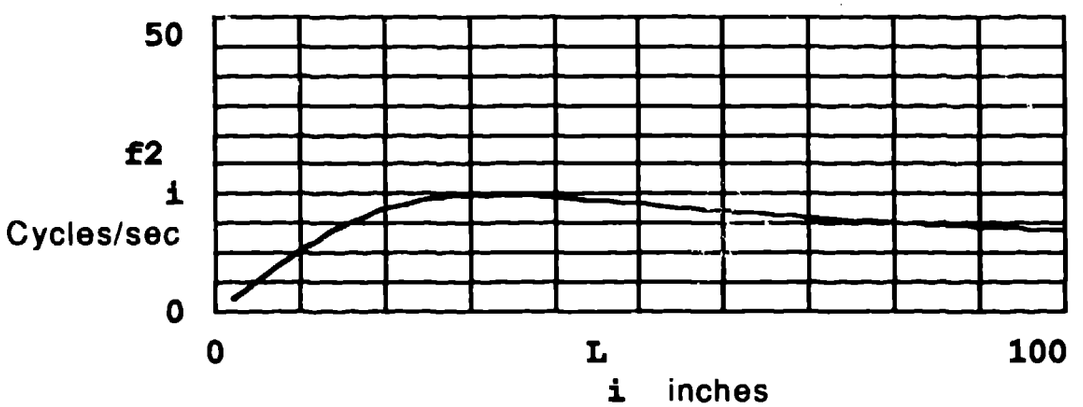

Figure 11. Second Natural Frequency for 1.00" dia. X 0.035" wall Tube

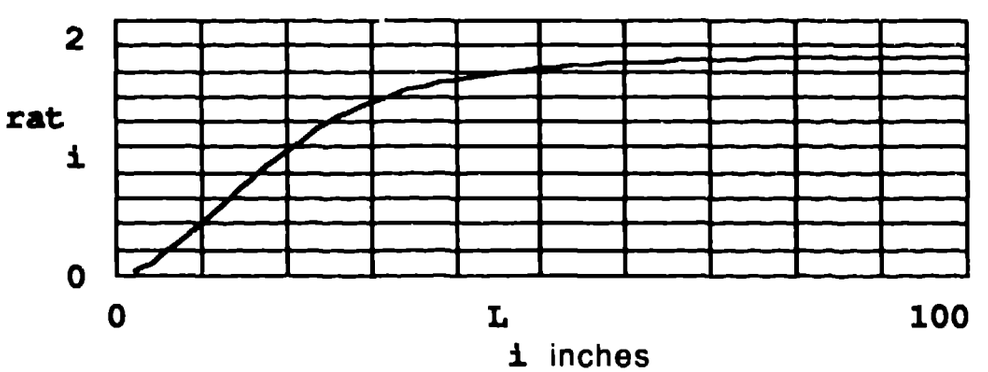

Figure 12. Frequency Ratio for 1.00" dia. X 0.035" wall Tube

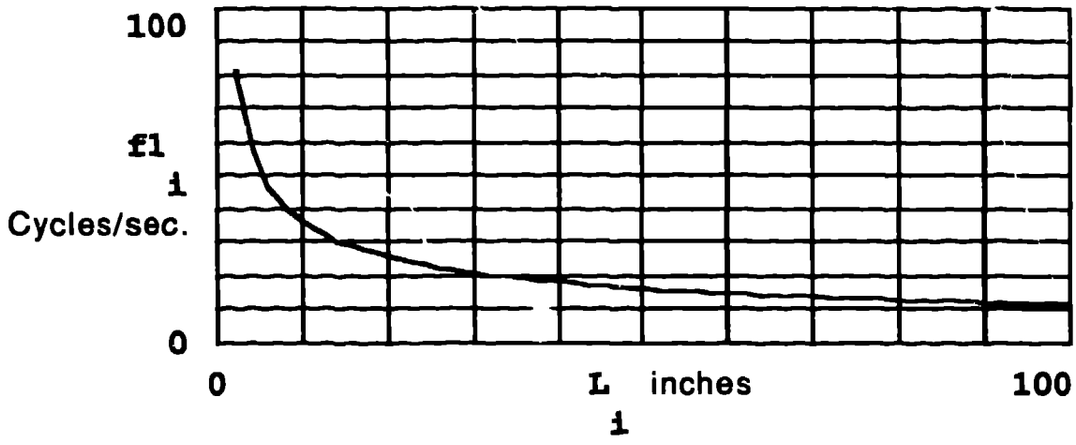

Figure 13. First Natural Frequency for 1/2" dia. X 0.035" wall Tube

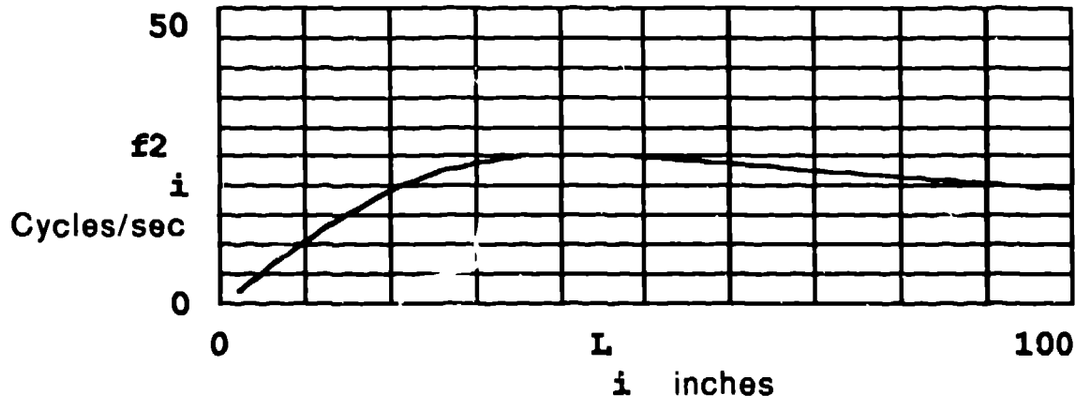

Figure 14. Second Natural Frequency for 1/2" dia. X 0.035" wall Tube

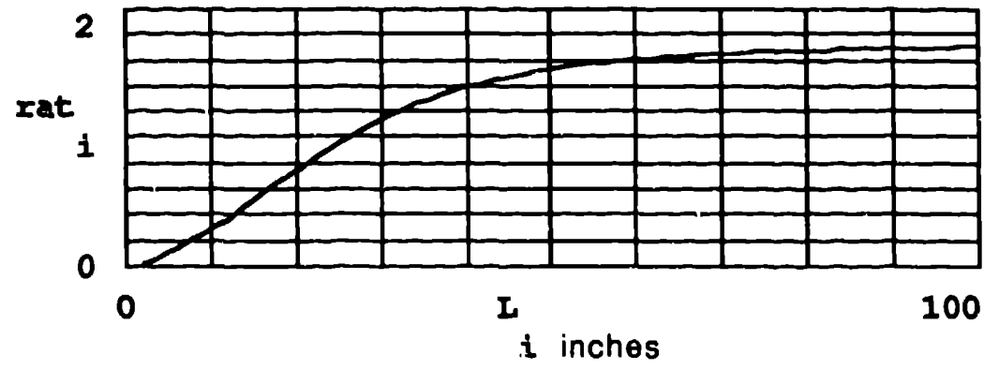

Figure 15. Frequency Ratio for 1/2" dia. X 0.035" wall Tube

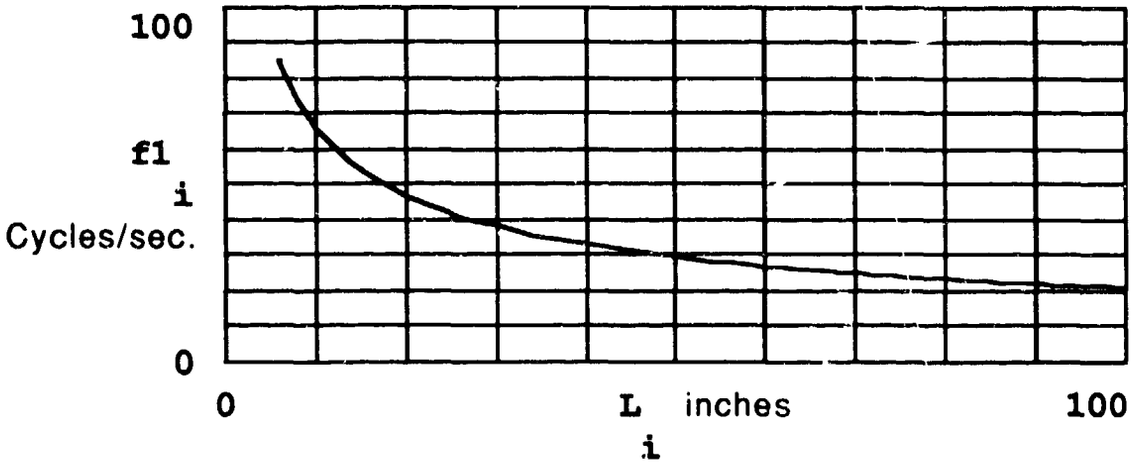

Figure 16. First Natural Frequency for 1/2" dia. X 0.010" wall Tube

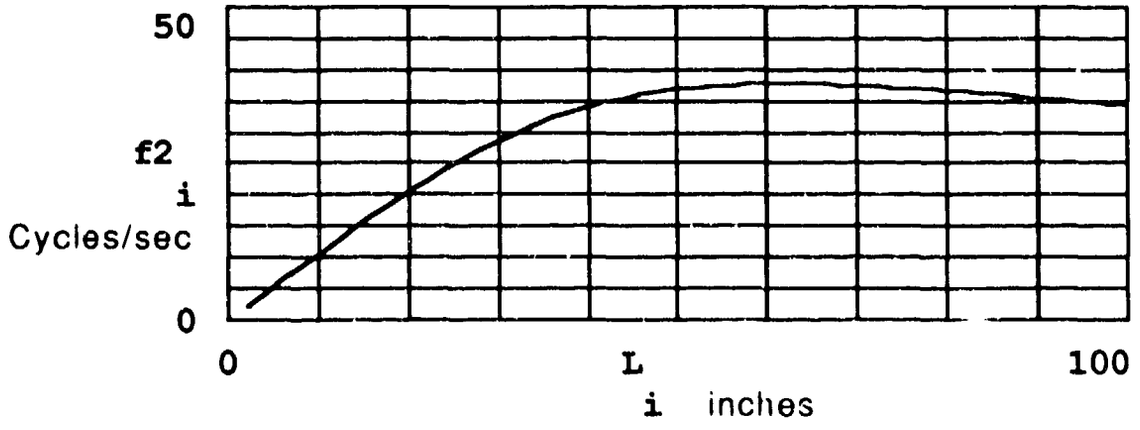

Figure 17. Second Natural Frequency for 1/2" dia. X 0.010" wall Tube

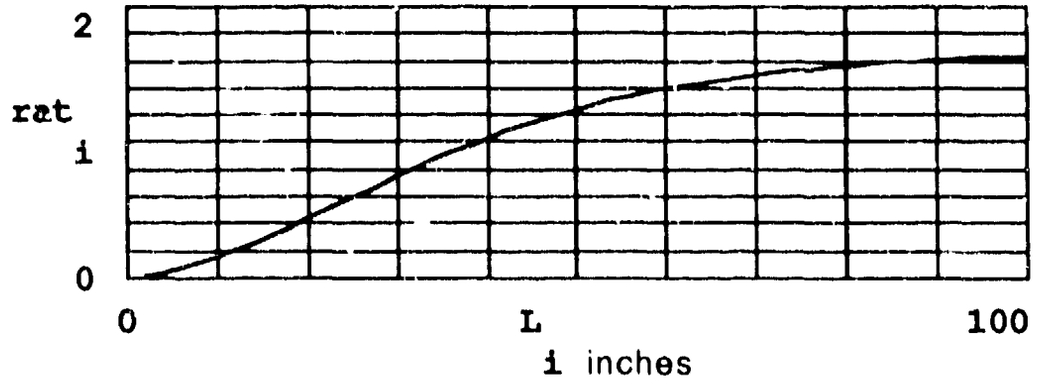

Figure 18. Frequency Ratio for 1/2" dia. X 0.010" wall Tube

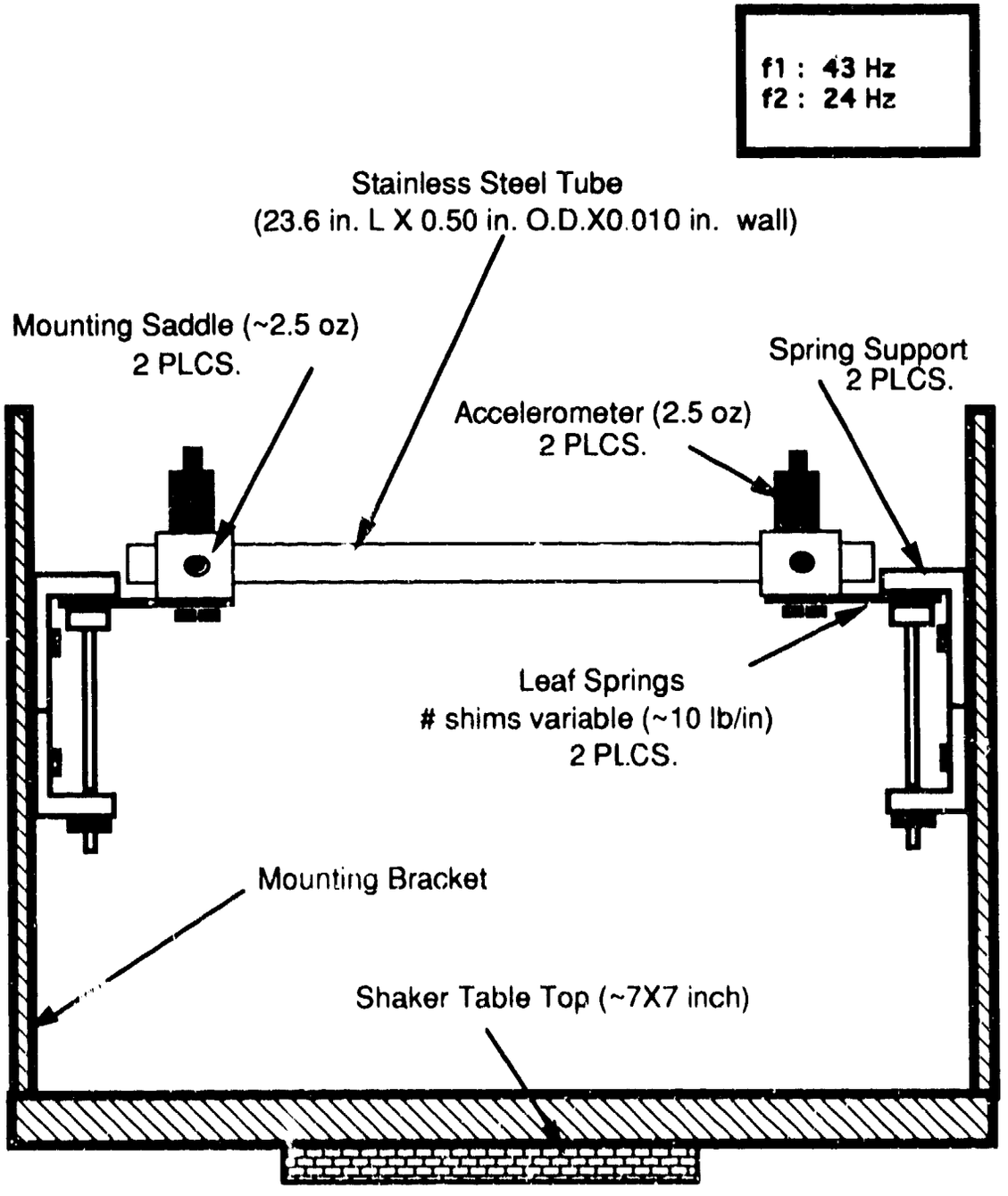

Figure 19 Experimental Set-Up for a Concept Verification Study on the Vibration Response Technique.

Furthermore, there appears to be a second phase shift near 57 Hz; yet, as with the previous figure, the existence of a second natural frequency is not completely evident. The results of the second run, summarized in Figures 22 and 23, more clearly show the two natural frequencies. It is evident that they are about 39 Hz and 53 Hz. The frequency ratio for the baseline system was then approximately 1.4. The predicted frequency ratio was 1.79. The difference between the measured frequency ratio and the predicted frequency ratio may be attributable to differences in the actual and the assumed spring constants. The assumed spring constant was 10 lbs/inch, while the actual spring constant was never determined.

Evident in each of Figures 20 through 23 is a considerable amount of noise. Much of this noise can probably be attributed to torsional oscillations of the tube-springs assembly. Improved spring design and smaller accelerometers should reduce noise. The differences in results between the two runs is interesting. Great care was taken to ensure that the conditi ,ns for the two runs were identical; yet, in the case of the second run, it is possible to precisely determine the second of the first two natural frequencies, while this is not true of the first run. Evidently, the data was not repeatable for this system.

This technique is attractive from the standpoint of being non-destructive and amenable to both low and high temperature heat pipes. In fact, it should be amenable to any rigid heat pipe, not subject to damage as a result of being shaken. Because it is non-destructive, this technique makes it possible to make mass migration neasurements over a series of time intervals. By contrast, destructive methods allow for only one

measurement per heat pipe experiment. The vibration response technique does, however, have several distinct shortcomings. For instance, as stated before, the dummy heat pipe must be the structural equivalent of the actual heat pipe. In practice, this becomes difficult to achieve. Prior to thermal testing, the heat pipes for both the low and high temperature tests must be instrumented with thermocouples. These thermocouples would be either mechanically fastened or welded to the heat pipes. The leads which are a part of these thermocouples would be prone to some shifting of location as a result of handling. While measures could be taken to ensure this situation does not occur, it does add to the cost and complexity of the heat pipe designs and their associated dummy heat pipes. As seen with the method validation experiment, achieving consistency between set-ups is difficult. Making consistency between vibration measurements even more difficult, is the fact that the heat pipes used in the thermal tests will be attached to some form of heat sources, and, in the case of the low temperature heat pipes, will probably be attached to heat sinks as well. To disassemble a heat pipe from its thermal test hardware and fixture it for the shaker table without changing its baseline vibration characteristics would prove difficult. To reassemble a heat pipe into its thermal test hardware without changing its baseline vibration signature or its thermal impedance characteristics between heat source and heat pipe or heat sink and heat pipe would also prove difficult. Furthermore, the risk of damage to a heat pipe increases with the amount of handling it receives.

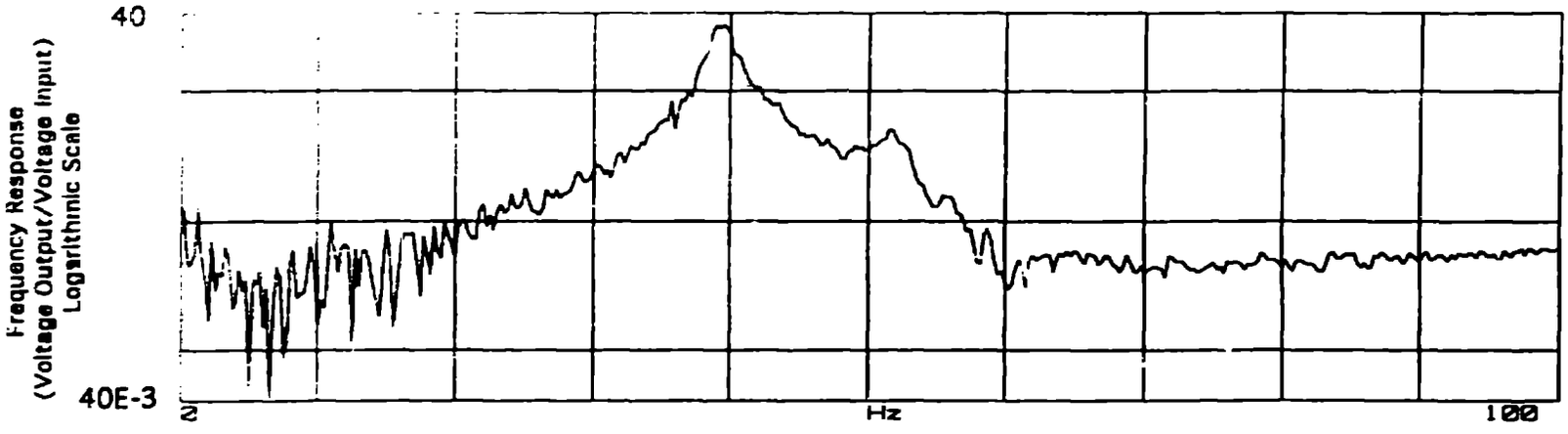

Figure 20. Frequency Response to a Random Driver Signal for the Vibration Technique Qualification Experiment: First Run

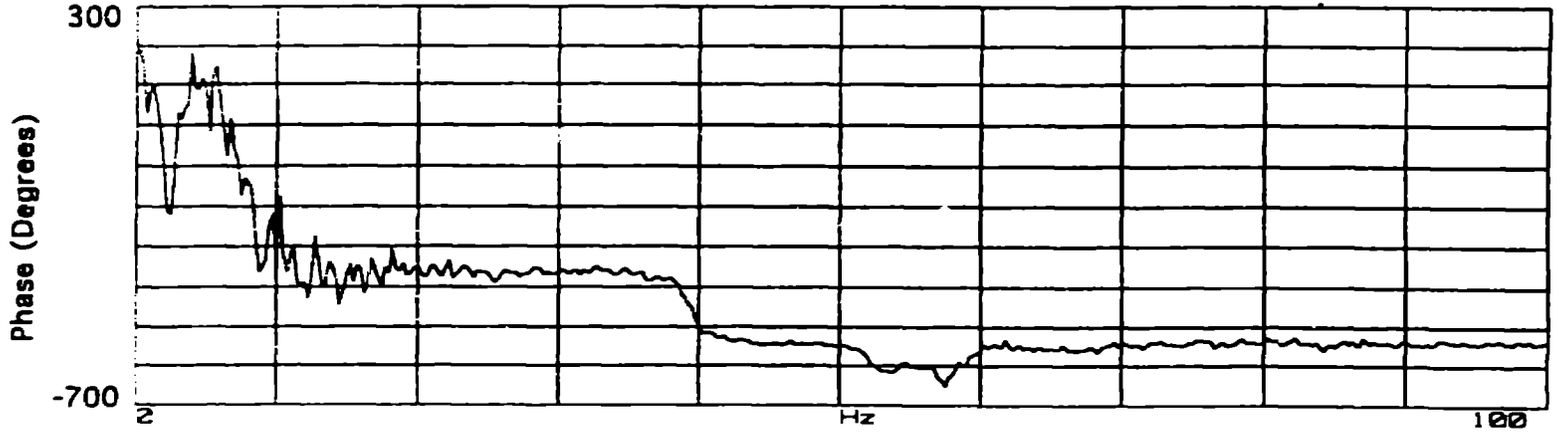

Figure 21. Phase Angle between Driver and Test Unit for the Vibration Technique Qualification Experiment: First Run

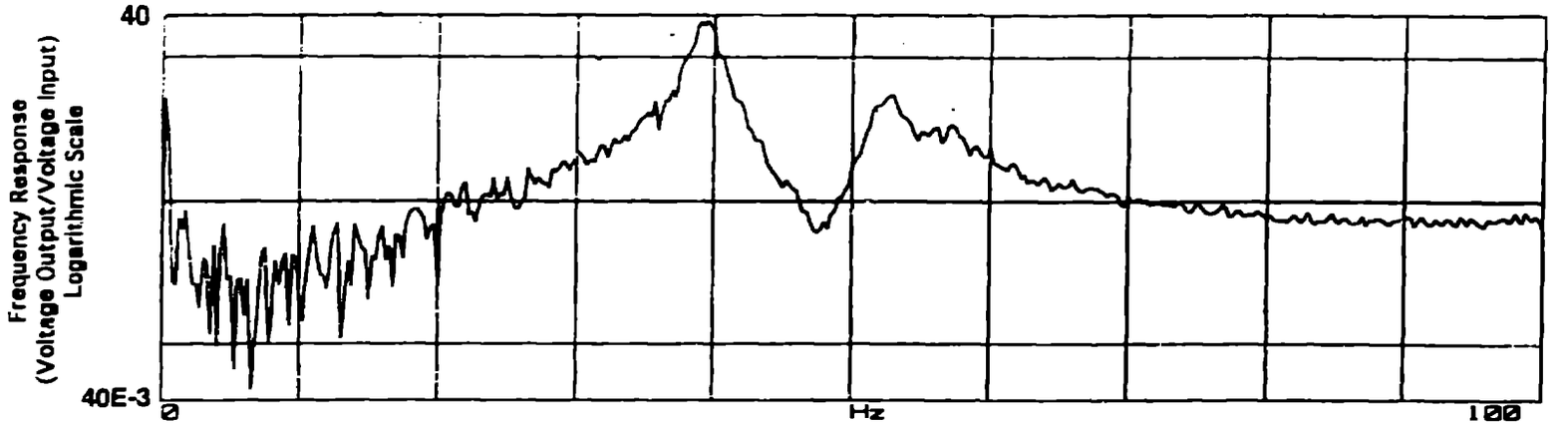

Figure 22. Frequency Response to a Random Driver Signal for the Vibration Technique Qualification Experiment: Second Run

Figure 23. Phase Angle between Driver and Test Unit for the Vibration Technique Qualification Experiment: Second Run

It is conceivable that the technique of Vibration Response to measure mass migration in a heat pipe can be developed. This would require a concerted effort and allocation of funds. The development of this technique was considered beyond the scope of this program and was not pursued.

Measurement of Segment Weights Technique

This, the third alternative is straightforward in principle and in implementation. Essentially the heat pipe is divided into sections, after having first undergone thermal testing. Each section is weighed, and then cleaned of all deposits and weighed again. The difference between weights is a measure of the amount of working fluid deposited at that section. The compilation of this data produces a map of the working fluid distribution in the frozen region.

This method offers the benefit of being able to measure mass distribution rather than just net mass in the frozen region. Unfortunately, this is a destructive method; so only one mass distribution measurement can be made per heat pipe.

For this technique to be successful, it is necessary to ensure that the working fluid deposited in the frozen region is a result of the mass migration phenomena and was not there prior to heat pipe operation. This requires that special care be taken during the heat pipe processing effort. Since this was ultimately the technique selected for the low and high temperature experiments, no discussion is made here on heat pipe

processing techniques; later sections describe all aspects of the heat pipe designs, and their manufacture, including the procedures for processing.

2.2.2 Low Temperature Heat Pipe Working Fluid

Heat pipe failure due to the mass migration phenomena is primarily a concern for high temperature working fluids. Low temperature working fluids invariably have high vapor pressures at their triple points, and as such are not subject to failure by this mode. However, it is expensive and difficult to fabricate and test high temperature heat pipes. There would be several advantages to testing low temperature heat pipes, provided they behaved similar to their high temperature counterparts. The cost of fabrication and test would be reduced, and a low temperature fluid might lend itself to use in a transparent heat pipe design. Selection criteria for low-temperature heat pipe working fluids are listed below.

Useful operating temperature below 200°C to facilitate bench testing by mitigating insulation, instrumentation and handling requirements;

Very low vapor pressure near the triple point such that rarefied flow behavior will exist. The rarefied flow character may be either slip flow and/or free molecular flow Liquid metals typically have vapor pressures on the order of tens to hundreds of microns of mercury at their triple points, and thereby exhibit free molecular flow behavior near their triple points;

Triple point above the dew point to facilitate testing by eliminating condensation of ambient water vapor on the test hardware;

Relatively low saturation vapor pressure at the operating temperature to minimize pressure containment restrictions and their inherent safety concerns;

Chemical compatibility with the materials of construction and processing;

Stability of the fluid's chemical composition and thermophysical properties with successive thermal cycling; and

Low toxicity and hazard potential.

Many candidate fluids were evaluated against this criteria. Some of the more promising candidates are listed in Table 2. Fusion temperatures and boiling temperatures are included along with saturation pressures and their respective reference temperatures when available. Where data could not be located for a given fluid, the entry was left blank. The following discussion pertains to the results shown in this table.

Cesium is a metal, and, as such, presents material compatibility problems. It is corrosive to many containment materials, particularly any transparent materials. Recall that transparency is desired for the low-temperature experiments. Dowtherm A is a proprietary fluid design for single and two phase heat transfer. Fluids which are used in two-phase heat transfer applications, in general, have relatively high vapor

Table 2. Candidate Low Temperature Heat Pipe Working Fluids

Working Fluid	Fusion Temperature (°C)	Boiling Temperature (°C)	Saturation Pressure	Comments
cesium	29	397		Material compatibility problems
Dowtherm A	12	258		probable high saturation pressures
nonadecane	32	330	1 torr @ 133°C	
octadecane	28	317	1 torr @ 120°C	
pentadecane	10	271	1.7 torr @100°C	
methylmyristate	18.5	295	1 torr @ 115°C	
hexadecane	16.7	287.5	$95*10^{-6}$ torr @ 20°C; 1 torr @ 105°C	
lauryl alcohol	24	257		
diphenyl methane	26.5	265	3.5 torr @ 100°C	
diphenyl ether	27	259	1 torr @ 66°C	
anethole	22.5	235	1 torr @ 63°C	
phorone	28	197	1 torr @ 42°C	
methyl palmitate	30.5	196	1 torr @ 135°C	decomposes at elevated temperature
ethyl furoate	34	195	1 torr @ 38°C	
bromoform (tribromo-methane)	8.5	150	20 torr @ 10°C	
phenyl salicylate (salol)	42.5	172.5	1 torr @ 54°C	
polyethylene glycol(PEG-600)	22		$690*10^{-6}$ N/m2 @ 100°C	some decomposing at elevated temp-erature is likely

pressures in order to achieve sufficient vapor flow rates. The decanes are often considered for solar energy storage applications. This is, in part, due to their low vapor pressures, relatively low fusion temperatures and minimal toxicity and hazard potential. These same features make them attractive for application in the low-temperature heat pipe experiments.

Octadecane is particularly attractive, since it has a fusion temperature slightly greater than normal room temperature; thus eliminating the problem of condensation of ambient water vapor on the experiment and minimizing insulation, instrumentation and handling concerns. Polyethylene glycol is similar in many respects to the decanes and is used commercially in the same applications; however, it is a very large molecule (molecular weight of 600) and is prone to fracturing into lighter molecules at elevated temperatures. It would probably be unsuited for use as a heat pipe fluid.

Useful thermophysical properties for octadecane are included in Appendix D. A comparison of select representative property values for octadecane with those for some more conventional heat pipe working fluids are provided in Table 3.

In general, when selecting a working fluid it is desirable to find one with a vapor pressure above 10^4 N/m^2 to avoid excessive vapor losses. Excessive pressures are to be avoided to minimizes pressure containment requirements. Fluids with low values of kinematic viscosity ratios are desirable to minimize vapor losses. For heat pipes which do not benefit from gravity, the wicking height (H) and liquid transport factors (N_l) have the most pronounced effect on heat pipe operation. The heat transport capability is directly proportional to N_l, so this factor should be high consistent with other tradeoffs. In general, the value of N_l reaches a maximum slightly above the normal boiling point then drops off to zero as the critical temperature is approached. The wicking height factor is a measure of how well a wick can support a hydrostatic fluid, and is

important in terrestrial applications or where a composite wick is to be primed.

It is apparent that octadecane has good wicking height and liquid transport characteristics, being comparable to ammonia and water. It appears to be a satisfactory candidate for use in the Low

Table 3. Selected Properties of Various Heat Pipe Working Fluids

Working Fluid	Molec. Wt.	Normal Melting Temp. (K)	Normal Boiling Temp. (K)	Selected Operating Temp, T (K)	Vapor Pressure @T (N/m^2)	kinematic viscosity ratio @ T (υ_v/υ_l)	$H = \sigma/\rho_l g_o$ @T (m^2)	$N_l = \sigma h_{fg}/\upsilon_l$ @T (W/m^2)
Ammonia	17.0	195.5	239.8	300.0	1.06E6	6.12	3.39E-6	1.00E11
Freon 11	137.4	162.2	296.9	350.0	4.87E5	2.47	8.77E-7	9.06E9
Water	18.0	273.2	373.2	400.0	2.45E5	40.7	5.82E-6	5.08E11
Sodium	23.0	371.0	1152.2	700.0	110.6	1.23E5	1.88E-5	2.16E12
Lithium	6.9	453.7	1615.0	1000.0	99.2	3.13E5	6.73E-5	1.23E13
Octa-decane	254.5	301.3	589.5	370.0	37.3	880.0	3.11E-6	9.82E11

H = wicking Height Factor, N_l = Liquid Transport Factor

Temperature Mass Migration Experiments, recognizing that the high kinematic viscosity ratio for octadecane makes it unsuitable for most practical applications.

2.2.3 Qualification Experiments for the Low Temperature Heat Pipe Working Fluid

A heat pipe was designed, built and tested for the purpose of evaluating octadecane as a heat pipe working fluid for the low-temperature experiments. Details of the heat pipe design and qualification experiment, along with the results and conclusions from those experiments are discussed in the following paragraphs.

Heat Pipe Description for Working Fluid Qualification Experiment

Figure 24 illustrates schematically the principle features for the heat pipe design and test layout. The heat pipe was designed to transport approximately 100 Watts at 500 K in a horizontal position. The envelope was 117 cm long and 2.54 cm in inside diameter. It was made of quartz, a transparent material, and thus allowed for the visual inspection of heat pipe operation. Features to be observed included: the presence or absence of boiling in the wick; the occurrence or nonoccurrence of entrainment of condensate; and the occurrence or nonoccurrence of freezing of working fluid in the condenser. The end closures were made of stainless steel and sealed to the quartz tube by means of vacuum O-rings. The wick structure was comprised of 2 wraps of 250 mesh stainless steel screen 89 cm long with one end butted against the evaporator end cap. The wick structure was provided to return condensate to the evaporator and distribute it to the heat source. It also acted to separate the condensate returning to the evaporator from the vapor traveling to the condenser. Separating the vapor flow from the liquid flow mitigates entrainment.

Qualification Experiment: Description and Results

The intent of the preliminary heat pipe tests was to determine whether the selected working fluid would perform satisfactorily in a heat pipe, in particular, to determine whether it would transport sufficient heat, exhibit sufficient wicking capability and not be susceptible to entrainment.

The heat pipe was operated under constant power and allowed to reach steady state at successively greater static lift heights (i.e., condenser lower than evaporator). The temperature profile at each orientation was recorded. Measurements of temperatures were made with chromel-alumel thermocouples (type K) attached along the length of the outside surface of the quartz envelope. A heat pipe performance limit was indicated when the evaporator temperature rose sharply. Such a condition is a result of insufficient fluid circulation. This condition is often termed a capillary limit.

Data from these preliminary tests are shown in Figures 25 and 26. These figures show temperatures along the main axis of the heat pipe for various static lift heights while at a constant power throughputs of 31 and 55 Watts respectively. The heat pipe performance limits are indicated by the "dryout" points. The static lift heights shown in Figures 25 and 26 are dial indicator readings showing the differences in elevation between the furthest spaced ends of the evaporator and condenser along the top surface of the heat pipe. Therefore, these readings are not direct measurements of static lift height, since they do not include the pipe diameter and the influence of the puddle resulting from excess fluid

inventory. The calculated dryout points, once these factors are accounted for, are plotted in Figure 27. The line connecting these points is useful for determining the operating characteristics for this particular combination of heat pipe working fluid and wick structure. It is evident from this figure that this particular combination can achieve in excess of 150 Watts in a horizontal position and can achieve a static lift, with no power throughput, of a little more than 2.0 inches. The heat pipe performed better than expected. It may be concluded that the working fluid, octadecane, is capable of reasonable power throughputs and is not overly sensitive to gravitational effects. Octadecane was, therefore found to be satisfactory for use in the low temperature experiments.

2.2.4 Low Temperature Heat Pipe Experiments

The efforts to design and test heat pipes for the low temperature mass migration experiments, and the results of those experiments are discussed in the following paragraphs.

Experimental Approach

A series of four Low Temperature Heat Pipes (LTHPs), each identical, were to be tested at different power levels and durations according to the matrix in Table 4. The heat pipes were designed about the Measurement of Segment Weights technique as described in Section 2.2.1 Their design and construction are discussed at depth in subsequent paragraphs. Each heat pipe was to be tested using the same experimental approach and set-up. Temperature measurements would be by type K thermocouples. The thermocouples would be attached along the pipe exterior at measured

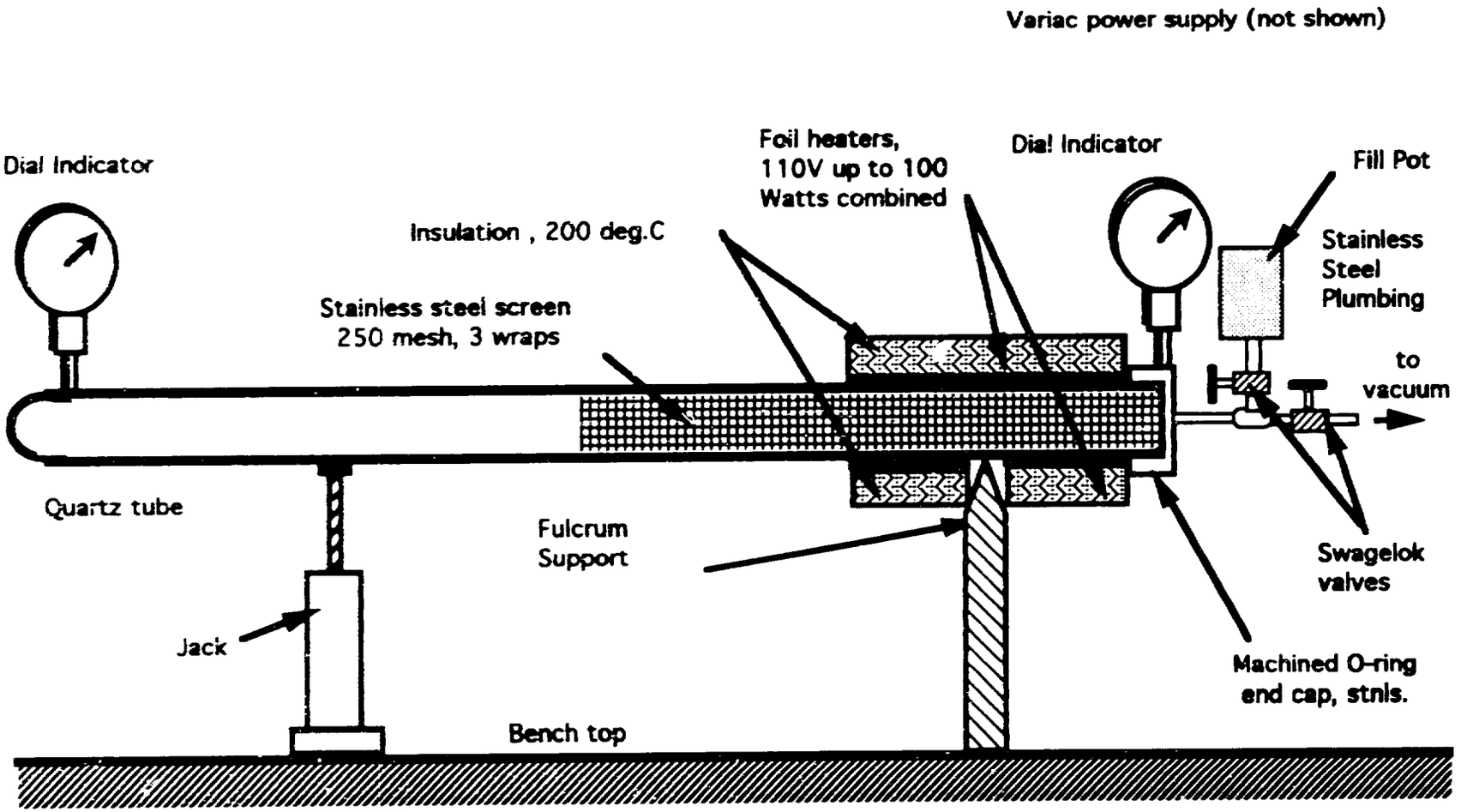

Figure 24. Qualification Heat Pipe Experiment

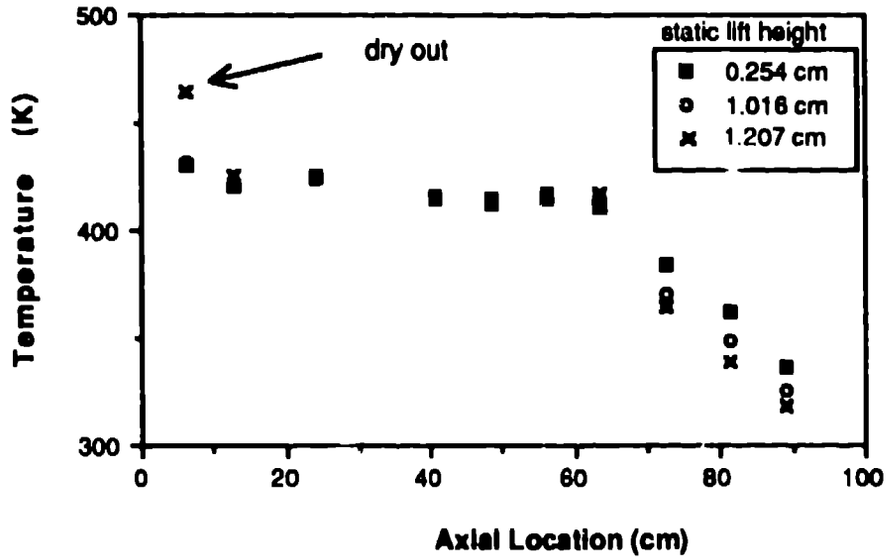

Figure 25. Capillary Performance Limit Test at 31 Watts for an Octadecane/Quartz Heat Pipe with a 250 mesh Homogeneous Stainless Steel Wick.

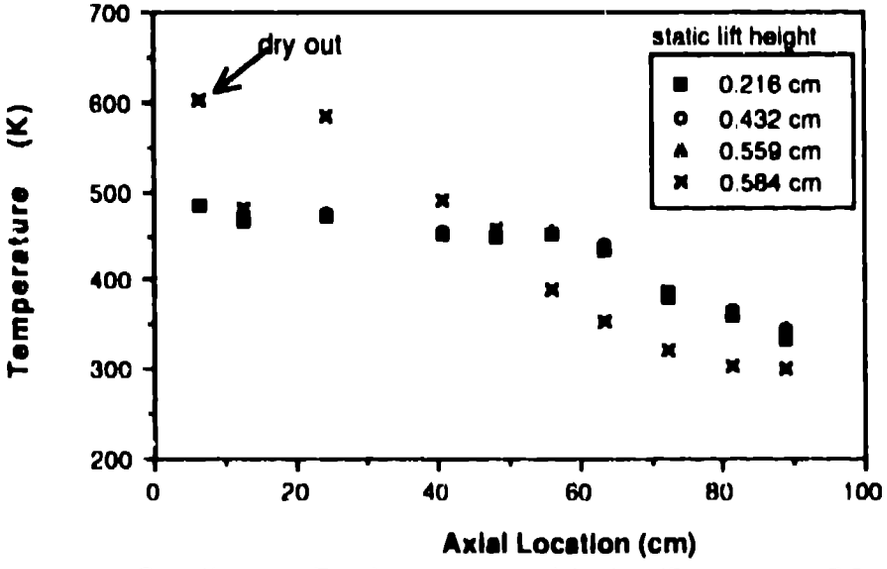

Figure 26. Capillary Performance Limit Test at 55 Watts for an Octadecane/Quartz Heat Pipe with a 250 mesh Homogeneous Stainless Steel Wick.

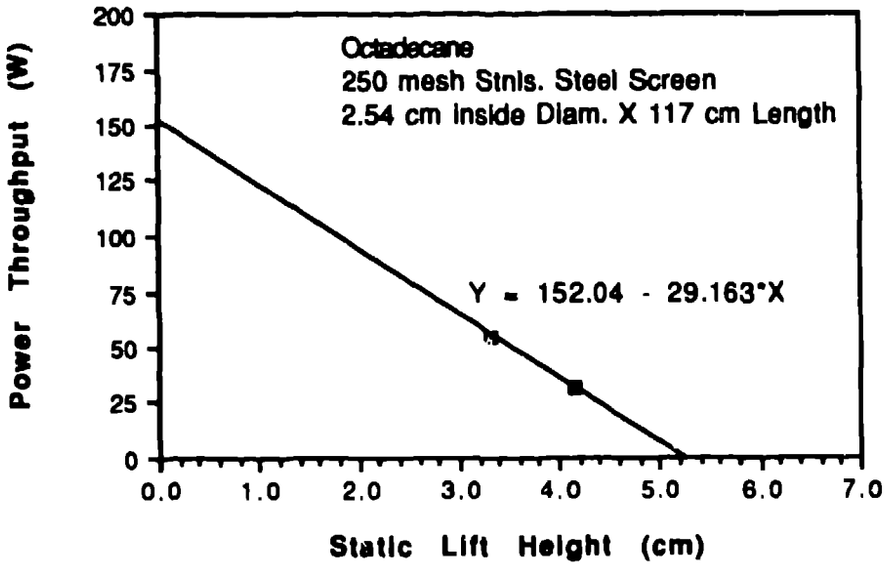

Figure 27. Power Throughput as a Function of Static Lift Height for an Octadecane/Quartz Heat Pipe with a 250 mesh Homogeneous Stainless Steel Wick.

Table 4. Low Temperature Experiments Matrix

	Power Throughput (W)	Test Duration (hours)	Net Watt Hours
LTHP1	15	250	3750
LTHP2	60	75	4500
LTHP3	30	150	3750
LTHP4	30	75	1875

intervals. In addition to the temperatures, the power supplied to the pipe would be measured and recorded. Figure 28 illustrates the experimental layout. In addition to the heat pipe are shown the power supply, the circulating water cooled heat sink and the gas handling system. The

power supply consists of a variable voltage supply, an ammeter and a voltmeter. The heater is a Kapton foil resistance heater, 30 centimeters long, wrapped about the full outside pipe diameter, which allows for uniform heating of the evaporator. The heater is rated for 150 Watts at 115 Volts. The heater is thermally insulated with 7 cm of ceramic blanket. The heat sink consists of a water heater/cooler which circulates a constant flow of constant temperature water to a gas-gap calorimeter fitted over the heat pipe condenser. Temperature control for this system is ±0.2°C with set points ranging from 0°C. to 80°C. The gas handling system consists of an argon supply, a helium supply individual metering valves for controlling gas mixtures and a gas flow meter and display. This system has the capability of supplying either all argon, all helium or a mixture of both to the gas-gap calorimeter. A gas-gap calorimeter is a device which is often used for testing heat pipes where it is necessary to control the thermal resistance between heat pipe and heat sink.[9][10] Helium has a thermal conductivity roughly four times that of argon, allowing for a factor of four range in thermal resistance at the heat sink. The gas occupies the volume or gap between the heat pipe and the heat sink. In this case the gap is an annulus. Figures 29 and 30 illustrate the LTHP design, but also show the gas-gap calorimeter attached.

The experimental procedure included the following steps which were implemented for each LTHP tested.

- Instrument the heat pipe with thermocouples;
- Operate the heat pipe in reverse mode (i.e., run what would normally be the condenser at a higher temperature than the normal evaporator). This is done for several days. The procedure removes all traces of

working fluid from the condenser region. The working fluid which is volatized during this process in moved towards the evaporator section. During this process the condenser is maintained at roughly 70°C while the evaporator is maintained around 20°C to 25°C.

- Operate the heat pipe at roughly two thirds the final power with the condenser raised several centimeters above the evaporator, and check to be sure all equipment is functioning properly.
- Raise the pipe to full power. Stabilize the freeze-front by noting its location visually, and adjusting the thermal resistance at the heat sink. The thermal resistance is adjusted by varying the circulating water temperature and/or the mixture of the gas in the gas-gap calorimeter.
- Once the freeze-front location is stable and the pipe is at steady state, begin taking time, temperature and power throughput data.
- Operate the pipe for the full test duration, taking data at regular intervals.
- At the conclusion of the test duration, shut off power to the heater and allow the pipe to cool to room temperature.
- Disassemble the pipe and measure the mass distribution in the condenser end.

Heat Pipe Design and Fabrication

Figure 29 illustrates the LTHP design with attached calorimeter. The design is based on the Measurement of Segment Weights mass migration measurement technique described in Section 2.2.1. The LTHP design is composed of an outer pyrex envelope, an inner pyrex tube cut into several smaller cylindrical sections and a homogeneous stainless steel wick. The use of pyrex as a containment material makes visual observation of the

mass migration phenomena possible. The sectioned pyrex tube allows for direct measurement of the mass distribution along the pipe.

Figure 30 is an illustration of the condenser end of the heat pipe design. It shows the pyrex sections fitted within the pyrex envelope, and also shows a cross-section view of the gas-gap calorimeter used during testing. The LTHP is a nominal one meter long with the internal sectioned tube a nominal 90 cm long. The evaporator section is 31 cm long and employs a 250 mesh stainless steel screen wick with a nominal thickness of 0.0254 cm. The overall outside diameter is approximately 2.2 cm. The nominal vapor space diameter is 1.5 cm.

The LTHP was designed to operate between 370 K and 430 K evaporator temperature. Figure 31 shows the calculated boiling, sonic and entrainment limits for the LTHP design. The pipe is intended to operate at the sonic limit, thus the temperature of 430 K established as the upper operating temperature corresponds to the point where the sonic and entrainment curves intersect. At temperatures above 430 K the heat pipe will be limited by entrainment, and will not reach sonic conditions at the evaporator exit. Boiling is not expected to be a factor with this design. Figure 32 shows the sonic and entrainment curves on a finer scale. The heat pipe is intended to transport between 11.7 Watts at 373 K and 180 Watts at 430 K.

Figure 33 is a photograph of various LTHP1 components, namely the stainless steel screen prior to its being formed into a wick, the outer pyrex tube used as the pressure containment vessel and the inner sectioned pyrex tube on which the working fluid will accumulate over the

course of an experiment. Figure 34 shows the components as assembled in a partially complete heat pipe.

Preparation of the heat pipe components and assembly of those components into a working heat pipe are accomplished as follows. First, all inner pyrex cylinder sections are numbered sequentially using a diamond tipped scribe. Next, all of the pyrex components, including the envelope, are carefully cleaned in Freon and rinsed in deionized water and ethyl alcohol. The parts are then dried in warm air. Each inner pyrex cylinder is weighed to an accuracy of ± 0.0001 grams. The weights of these sections are logged. A representative cylinder section is 2.0 centimeters long and weighs between 2.9400 and 3.0400 grams. The wick structure is fabricated by wrapping four layers of 400 mesh stainless steel screen around a copper mandrel. The screen wraps are spot welded and the mandrel is etched away using nitric acid to leave a screen tube properly sized to fit snugly within the inner pyrex tube. After the screen is thoroughly rinsed in deionized water and then ethyl alcohol, it is vacuum fired for four or more hours at approximately 700 K. The wick is fitted inside the heat pipe envelope. The cylinder sections are then stacked in numerical sequence inside the envelope. A pyrex nipple section is fused to the end of the envelope and then the whole assembly is heated to approximately 400 K in a vacuum of less than 10^{-5} torr to remove all water. The final steps are to charge the heat pipe with working fluid, evacuate the internal volume of air and seal the end shut by fusing the glass with a torch.

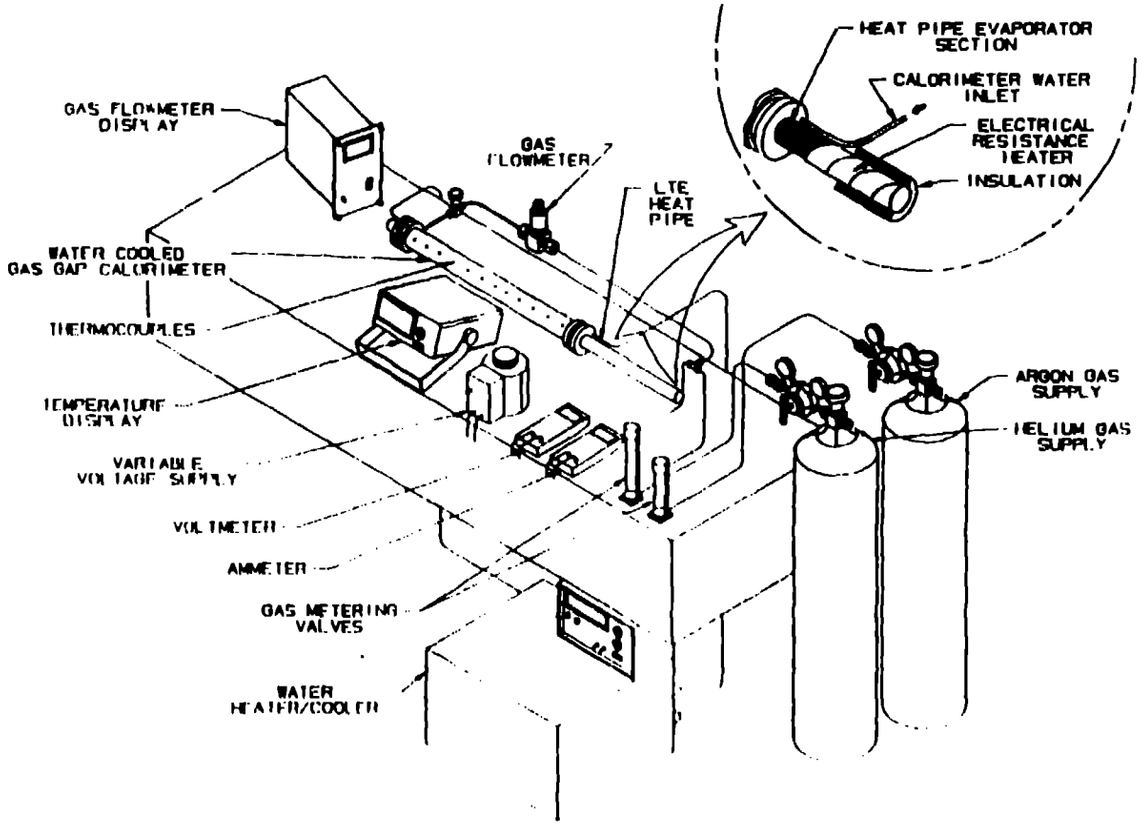

Figure 28. Experimental Layout for the Low Temperature Heat Pipes

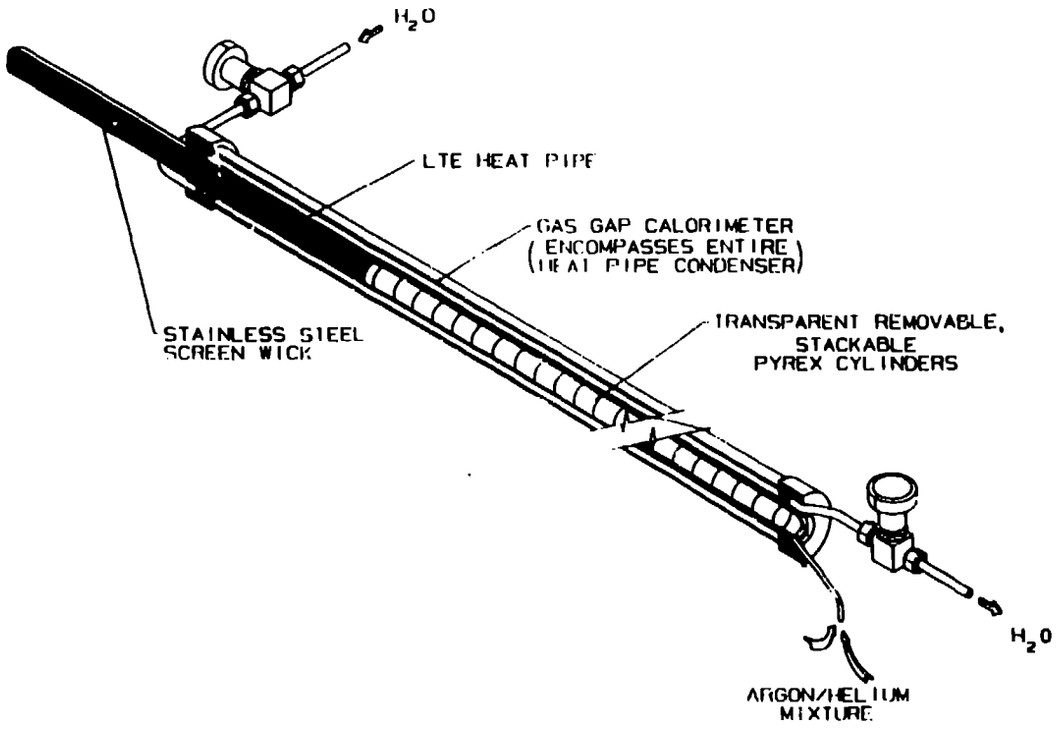

Figure 29. Low Temperature Heat Pipe Design with Calorimeter Attached.

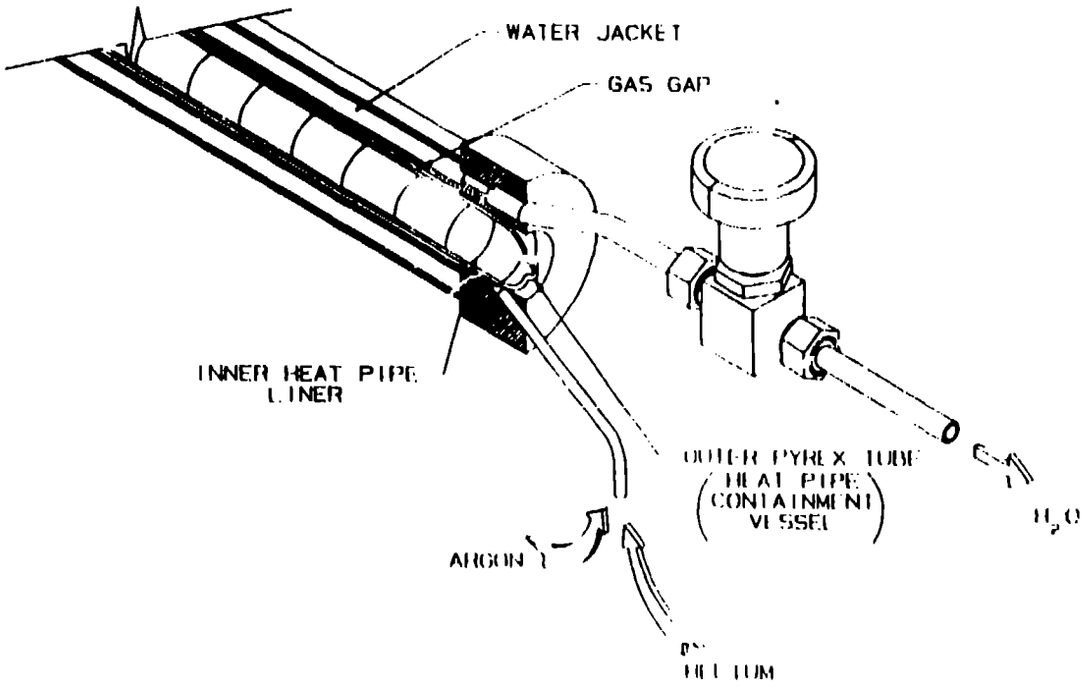

Figure 30. Close-Up View of the Condenser End of the Low Temperature Heat Pipe Design

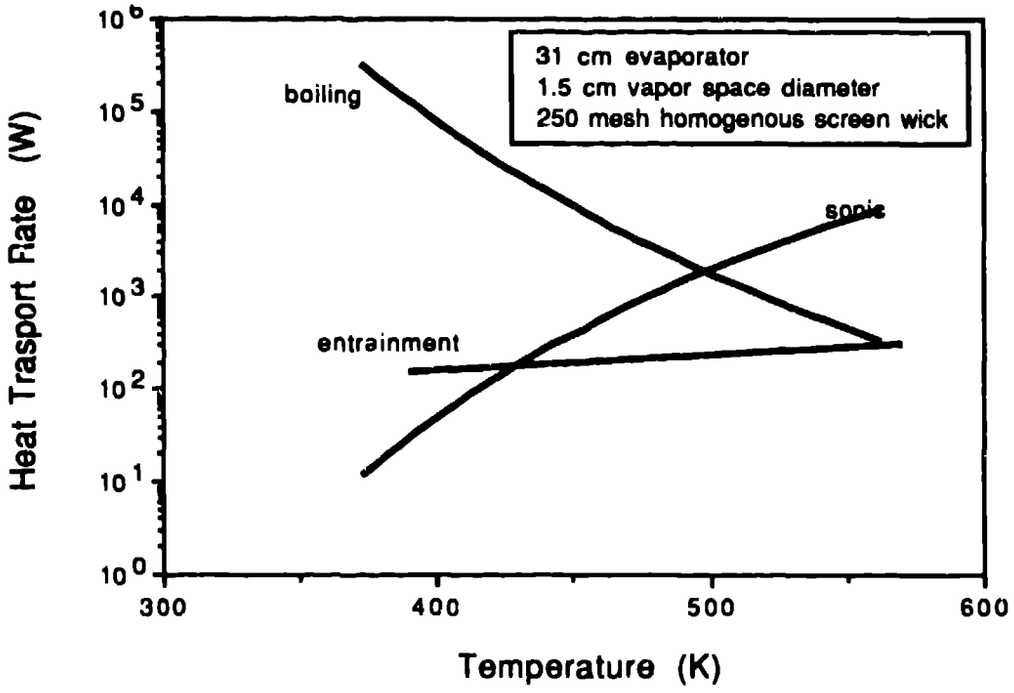

Figure 31. Heat Transport Limits for the LTHPs Design.

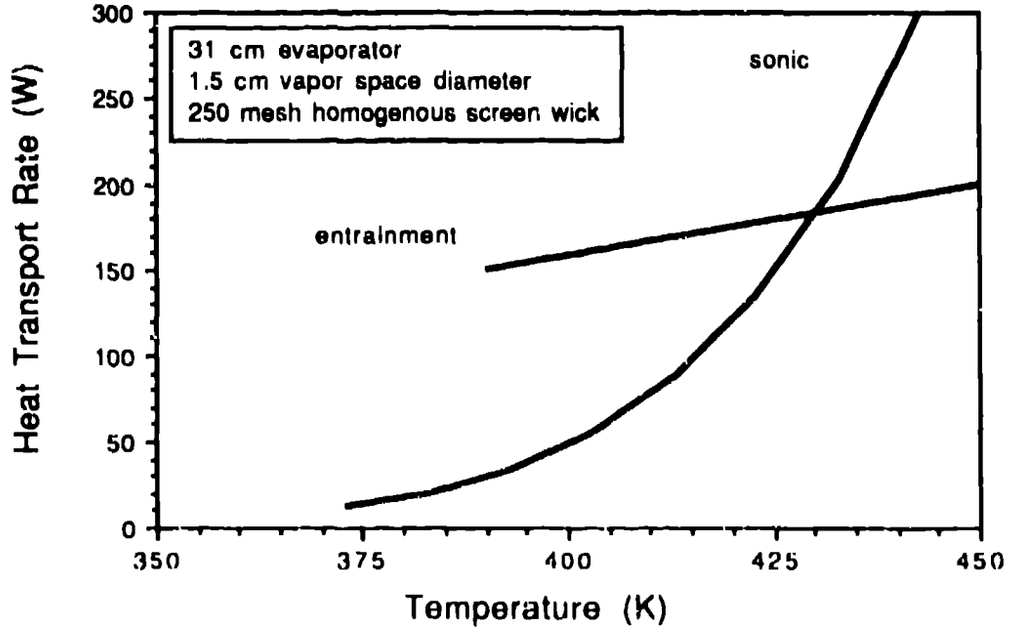

Figure 32. Sonic and Entrainment Limits for the LTHPs Design.

Figure 33 Various Components of the LTHP1 Prior to Assembly

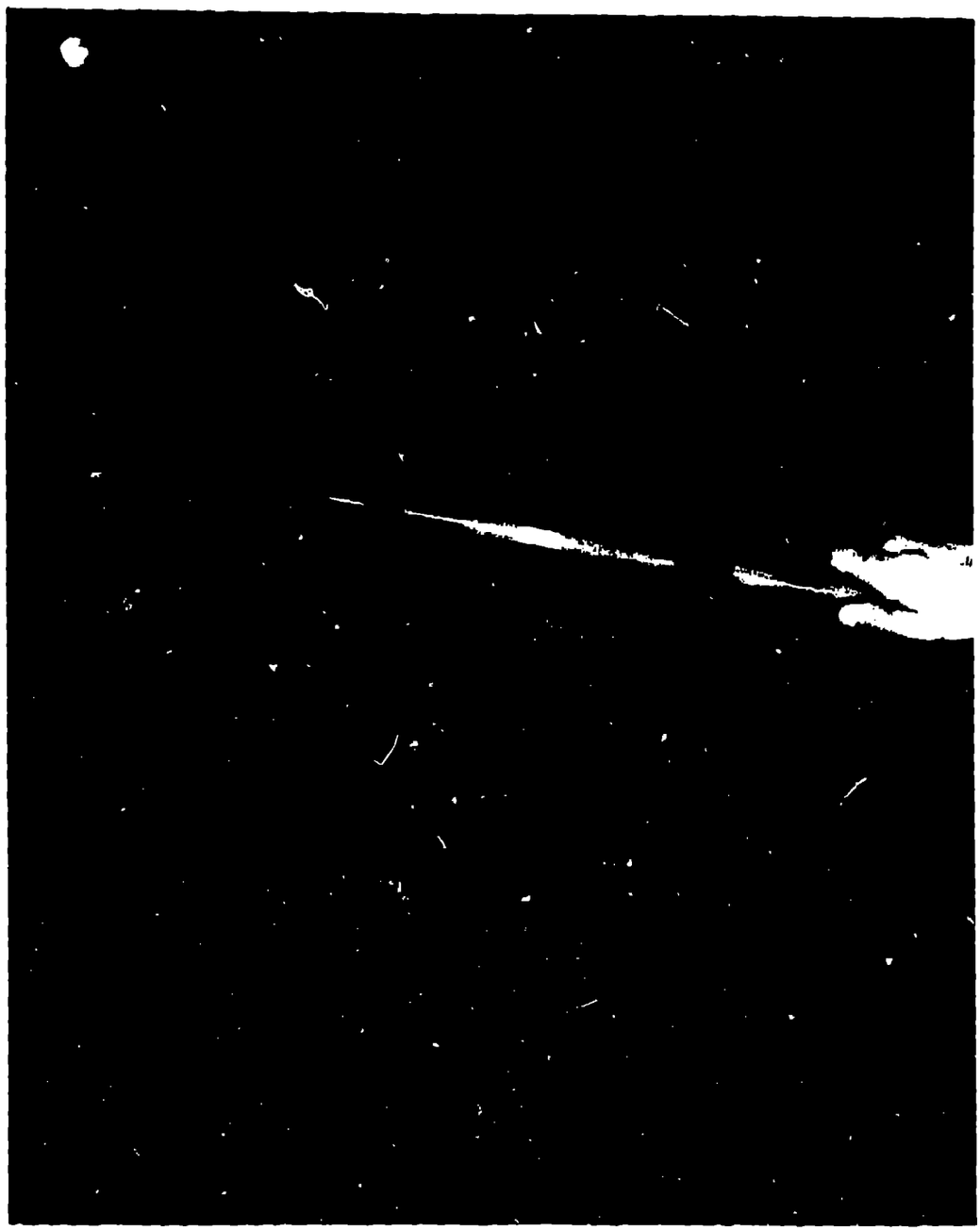

Figure 34. Partially Complete LTHP1 Showing Inner and Outer Pyrex Tubes

2.2.5 High Temperature Heat Pipe Experiments

The efforts to design and test heat pipes for the high temperature mass migration experiments, and the results of those experiments are discussed in the following paragraphs.

Experimental Approach

The planned experimental approach for the High Temperature Heat Pipe (HTHP) is similar in nature to that used for the Low Temperature Heat Pipes (LTHP's). The HTHP was to be operated for a prescribed period of time at a constant power level. At the conclusion of its operation, the pipe was to be sectioned and the working fluid accumulated at each section weighed.

Temperature measurements were to be made using thermocouples, as was the case with the LTHP's. Infrared imaging was also planned for making temperature measurements in the vicinity of the freeze front.

Heat pipe construction, processing and initial performance verification were to be conducted at LANL facilities. The actual testing was planned for AFPL facilities.

Nominal operation specifications were:

- 650 to 710 K stagnation temperature (Sodium working fluid).
- 50 to 300 Watts power throughput.
- 1000 hours of operation time.
- Heat supplied by 110 Volt resistance heaters.

- Cooling by radiation only at a fixed emissivity of about 0.3.

Heat Pipe Design Analyses

The HTHP was designed about the Measurement-of-Segment-Weights technique as described in Section 2.2.1. Stainless steel with either potassium or sodium were the materials considered for the HTHP. Stainless steel was selected for its compatibility with the working fluids, availability, ease of fabrication and, perhaps most importantly, for its low thermal conductivity.. Based on stock sizes of tube available, 9/16 X 0.028 inch wall and 13/16 X 0.035 inch wall tube sizes were selected as representative for design analyses. (A size of 3/4 inc by 0.016 inch wall was later selected for actual use. This is a stock size with a notably thin wall.)

A listing of the physical characteristics and important design parameters used in the performance analyses are included as Table 5. It should be noted that, while the length of the heat pipe was specified as one meter the active condenser length for analyses purposes is that which remains above the fusion temperature of the working fluid. It is, for a pipe operating at its sonic limit, a function of the heat rejection characteristics. For this analyses, that is for a thermal syphon operating at the sonic limit, the condenser length is arbitrary, provided it is sufficient to reject the heat load. The choice of a 250 mesh screen was based on its ready availability and its ability to provide sufficient wicking fluid distribution.

Performance curves generated from the figures in Table 5 are shown in Figure 35. These results are for both the 9/16 and 13/16 inch tube sizes using potassium as the working fluid and for the 13/16 inch tube size using sodium as the working fluid. It is apparent that the potassium and sodium will operate similarly (i.e., at nominally the same power levels over about the same size of temperature range). The sodium operates about a 100 K hotter than the potassium.

A potassium heat pipe will satisfy the design criteria for temperatures in the range of 560 to 620 K. At approximately 620 K entrainment may occur. Entrainment would be deleterious to the experiment, since any working fluid which is deposited into the frozen region of the heat pipe by a mechanism other than evaporation-condensation would obfuscate the

Table 5. Partial Listing of Design Parameters

PARAMETERS	VALUES
Container Material	Stainless Steel
Thermal Conductivity	0.16 W/cm/K
Evaporator Wick Material	Stainless Steel 250 Mesh Screen
Heat Pipe Length	39 inches (1 meter)
Evaporator Length	6 inches (15 cm)
Condenser Length	33 inches (84 cm)
Pipe Inside Radii (accounting for 0.004 inch thick wick in evaporator)	0.249 inch (0.633 cm) and 0.367 inch (0.933 cm)
working fluid and operating temperature range	Potassium, 560 K to 660 K and Sodium, 650 K to 750 K
tilt angle	20 degrees above horizontal (condenser above evaporator)

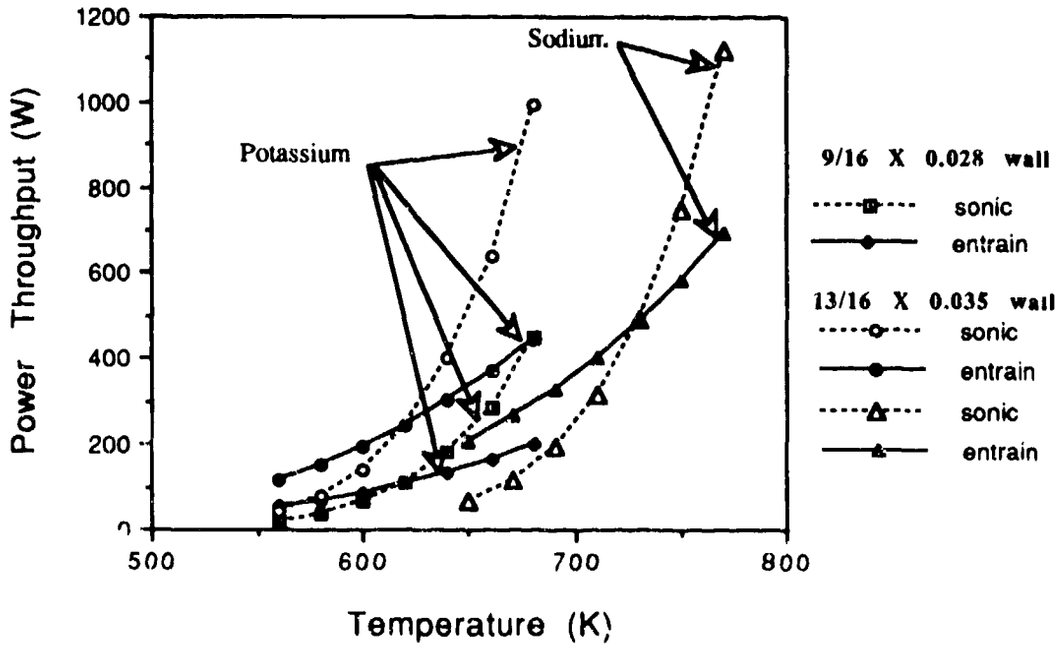

Figure 35. Performance Curves for Potassium/Stainless Steel and Sodium/Stainless Steel Heat Pipe Material Combinations

results. Therefore, a more conservative operating temperature limit would be 600 K.

A sodium heat pipe will also satisfy the design criteria, and would have a useful operating temperature range of approximately 650 to 710 K.

Figure 36 compares the heat rejection rates via radiation to the heat transport limits for potassium and sodium in the 13/16 inch diameter heat pipe concept. It is evident that to operate the potassium heat pipe at its sonic limit would require the pipe be specially coated to give it a high emissivity (i.e., an emissivity of 0.6 or greater). The sodium heat pipe,

however, with its higher operating temperature should have sufficient heat rejection capability to allow it to operate at its sonic limit without the need for an enhanced emissivity. The emissivity for cleaned or lightly oxidized stainless steel is in the range of 0.15 to 0.3.

Based on the results presented in Figures 35 and 36, sodium with a stainless steel containment vessel appears better suited for the HTHP design. The sodium/stainless steel concept does not require any treatments to enhance its emissivity and has a slightly broader range of operating temperatures than that for potassium.

The effect of wall thickness as it relates to axial heat conduction and heat pipe performance was analyzed.

The data from a heat pipe developed for a prior, unrelated program[1] but operated in a manner similar to that planned for the HTHP was reviewed. This data was presented earlier in the Introduction as Figure 2. It served as a baseline for the HTHP design analyses, and established a set of boundary conditions for the appropriate heat conduction problem The heat pipe for which the data in Figure 2 applies was constructed of niobium with potassium as the working fluid.. Its wall thickness was approximately 0.028 inch. The power throughput at the evaporator exit was estimated at 70 Watts, a power similar to that intended for the HTHP. Observe in Figure 2 that the rate of temperature decline is about 100 °K or less per every 20 centimeters of heat pipe length. Less than one half of one watt is the corresponding heat conduction rate along the wall in the region of most rapid temperature decline. This temperature decay rate in

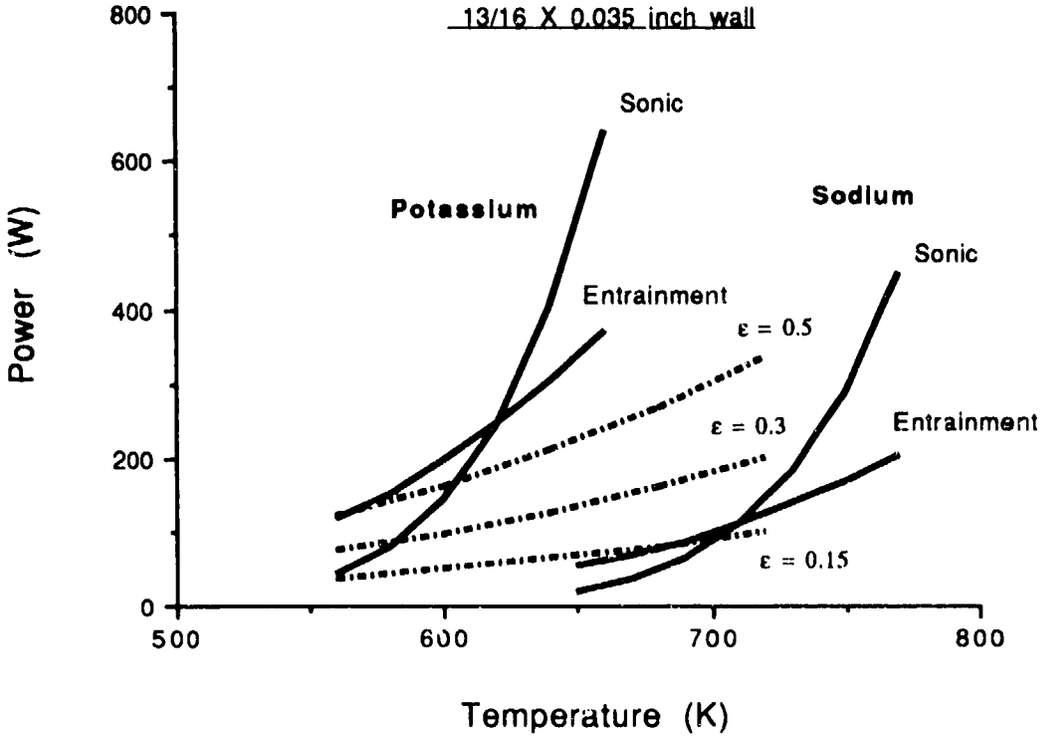

Figure 36. Performance Limits Compared With Maximum Radiant Heat Rejection Rates for Potassium/Stainless Steel and Sodium Stainless Steel Heat Pipes. The Maximum Heat Rejection Rate Assumes the Full Condenser Length is at the Evaporator Exit Temperature.

effect defines the boundary conditions for the heat conduction problem. Having thus defined the problem in this manner, a parametric analysis was conducted to determine the effect of wall thickness on heat conduction rate and to determine the sensitivity of freeze-front location to variations in heat conduction rate.

Even small fluctuations in the axial heat conduction rate at or near the freeze-front may result in the thawing of frozen working fluid. This would obscure the the test rosults. Anticipated working fluid migration rates will be the heat transfer equivalent of less than 0.01 Watts. This

owing to the very low vapor density and high latent heat for the working fluid. Control of heat conduction rates should be at least on the same order (i.e., <0.01 Watts). Obviously wall thickness will strongly influence heat conduction rates as will heat input and output (i.e., the boundary conditions).

The effect wall thickness has on heat conduction rate is illustrated in Figure 37. The material is stainless steel. Temperature drops of 100 and 200 °K occurring over lengths of 1, 2 and 10 centimeters are shown. Inspection of Figure 37 reveals that heat conduction varies linearly with wall thickness, and the boundary conditions (i.e., temperature decay as a function of axial location.) have a strong influence on heat conduction rate. It is evident from this figure that as long as temperature decay rates remain similar in size to that of the test data in Figure 2 and wall thicknesses are on the order of 0.010 to 0.020 inches, the axial heat conduction rate will be on the order of 0.5 Watts or less.

These low axial heat conduction rates for a thin walled pipe indicate that the freeze-front location may be determined with reasonable accuracy by means of temperatures along the exterior of the pipe. Maintaining the location of this front means the heat input at the evaporator and heat output at the condenser must be held constant.

For the condenser, it is not difficult to maintain a constant heat rejection rate provided the heat pipe temperature remains constant. Emissivity, sink temperature and the view factor are the only remaining variables. The view factor is determined by the experimental set-up and may be held

constant. The sink temperature will be ambient temperature. While it will vary, as long as it remains constant to about ± 10 K the variation will have negligible effect on heat transfer rates.

Changes in the emissivity, however, will strongly effect heat transfer rates. The heat pipe surface will be kept free of contaminants and will only be operated in vacuum. This will ensure that the surface emissivity remains constant.

Control of the heat input rate at the evaporator will be accomplished primarily by employing a large thermal capacitance heat source. This heater made of stainless steel is designed to have a large thermal time constant (i.e., low thermal diffusivity) so that it is insensitive to small fluctuations in input power. To achieve a heat pipe temperature change of 1.0 K at an operating temperature of 700 K, the heater would require a voltage change in excess of 2 Volts for greater than 10 seconds. The power supply controller will maintain a more constant voltage on a time averaged basis, so the heater will provide a satisfactorily constant input power and thus maintain a constant heat pipe operating temperature. An operating temperature which is constant to ± 0.1 K is expected. Changes in contact resistance can also affect operating temperature. The contact resistance is expected to change as the heat pipe is brought up to operating temperature due to shifting of parts under thermal expansion. However, once operating temperature is reached the contact resistance should remain constant. Table 5 is included to help quantify the affect of changes in contact resistance, or alternatively contact conductance, on operating temperature.

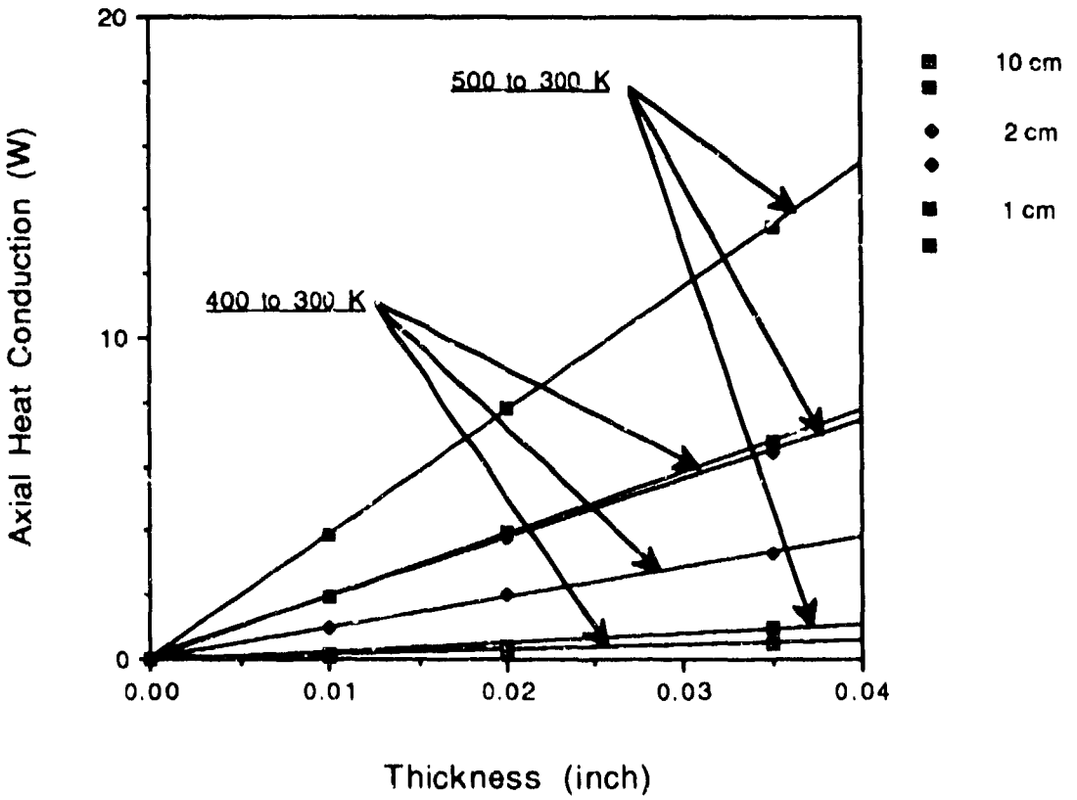

Figure 37. Axial Heat Conduction Along the Wall for Various Wall Thicknesses. Curves Represent a Fixed Temperature Drop of 100 K or 200 K Occurring Over a Prescribed Length of 1, 2 or 10 Centimeters.

Table 6. Effect of Thermal Conductance Changes on Operating Temperature.

Baseline Thermal Conductance, (W/cm/K)	Heater Inside Surface Temperature (K)	Change in Thermal Conductance over Baseline	Resulting Change in Heat Pipe Wall Temperature (K)
0.10	700.02	+100%	+0.01
		-100%	-0.03
0.01	700.24	+100%	+0.12
		-100%	-0.24

HTHP Design Description

The HTHP is one meter long and 1.91 centimeters (3/4 inch) in diameter by 0.041 centimeter (0.016 inch) wall thickness. The evaporator is a nominal 15 centimeters in length. The condenser is a nominal 85 centimeters long and is scored every 2 centimeters to facilitate the sectioning process following the completion of heat pipe operation. The wick, whose sole purpose is to distribute the working fluid to the heat source, is comprised of 2 wraps of 250 mesh stainless steel screen. A valve is located at the evaporator end for the purpose of evacuation and filling. The filling process is described later.

The heater is 7.0 centimeters (2.75 inch) in diameter 15 centimeters long. It contains three 0.95cm (3/8 inch) diameter cartridge heaters, spaced uniformly about the circumference on a common radius. The heater is a clam-shell style, made of two, mating stainless steel sections mechanically fastened about the heat pipe to form a cylinder.

The heat pipe was constructed as follows. Each separate heat pipe component was mechanically cleaned and solvent degreased. Following assembly, the uncharged heat pipe was heated under vacuum to a temperature of 1000 K to remove adsorbed gases. Following the cleaning operations, the heat pipe was evacuated, and then charged with 10 grams of sodium. The fillig operation was done be vacuum distillation. After sealing the pipe, the entire heat pipe length was heated to 800 K and allowed to wet-in. Details of the vacuum distillation and high temperature heat pipe processing procedures and equipment can be found in the literature [1],[14].

As with the LTHP experiments, it is necessary that all working fluid at the beginning of the HTHP operation be located precisely in the evaporator. The condenser must be devoid of working fluid. To achieve this, after wet-in, the condenser section was heated to a temperature of approximately 800 K while the evaporator section was cooled to room temperature. The heat pipe was operated in this reverse mode for an extended period of time in order to drive all of the working fluid into the evaporator section. Afterwards, the heat pipe was cooled to room temperature, thus freezing the working fluid in place. The pipe was then instrumented with thermocouples, fitted with the heater and positioned within a vacuum chamber. It was then ready for the high temperature experiment. A schematic for the HTHP experiment layout is presented as Figure 38. This was the layout used for the initial warm-up tests conducted at LANL. The actual HTHP experiment which was conducted at AFPL used the exact same layout, with the exception that the quartz vacuum chamber was removed, and the entire heater, heat pipe and end closure assembly was fixtured within a larger diameter, stainless steel vacuum chamber. Schematically, there was no difference.

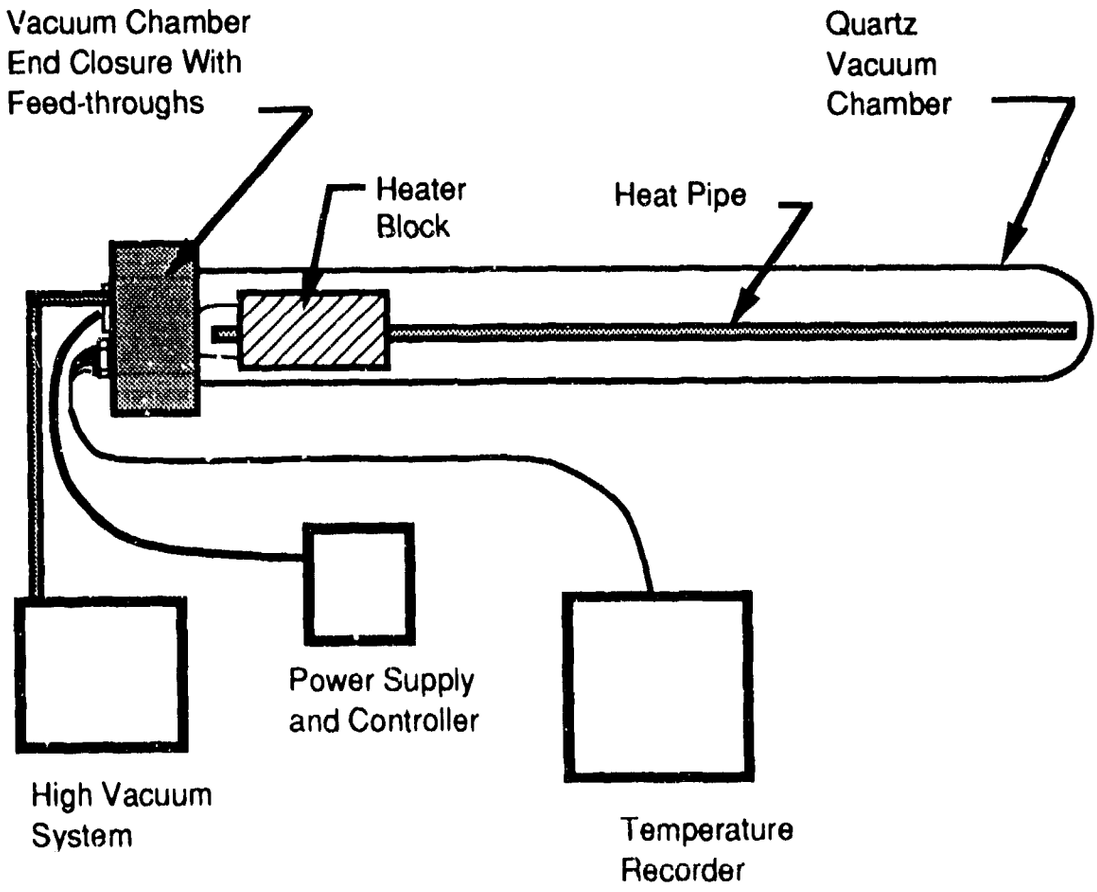

Figure 38. HTHP Experimental Layout Schematic

3 Results and Discussion

3.1 Experimental Results for the Low Temperature Heat Pipes

The results from the tests of the four low temperature heat pipe tests, LTHP1 through LTHP4, are discussed separately below.

Low Temperature Heat Pipe #1 (LTHP1)

Fabrication and testing of LTHP1 was done in accordance with the procedures discussed in the previous section. However, the pipe was not sealed after charging with the working fluid. The heat pipe was actively pumped for the duration of the thermal test by a vacuum system attached to the condenser end. The closure process for sealing the heat pipe was still being developed at the time LTHP1 was tested. It was deemed prudent not to attempt the closure process on LTHP1 and risk damaging the pipe until the procedure was perfected. So the test was done with the vacuum system attached. Figure 39 illustrates the thermocouple placement for LTHP1. Figure 40 shows the temperature profile for the heat pipe in operation. The temperature profile was seen to be constant with time. The heat pipe was operated at 19.0 ±0.4 Watts for a duration of 220 hours and resulted in the accumulation of 5.3825 grams of frozen working fluid in the condenser. The net Watt-hours was 4182.35. Figure 41 shows the mass distribution of working fluid along the heat pipe condenser. The accumulation to the right of the freeze-front was frozen. The accumulation to the left was liquid while the heat pipe was in operation, and so was not included when determining the frozen mass accumulation. It is evident that the majority of mass accumulates near

the freeze-front. For this heat pipe, little or no mass traveled to the furthest reaches of the condenser. Figure 42 is a photograph of LTHP1 showing several sections of the condenser as they looked at the completion of the heat pipe operation. The accumulated mass on the various sections is discernible.

Low Temperature Heat Pipe #2 (LTHP2)

This heat pipe was fabricated and tested in the same manner as for LTHP1. It too was not sealed, but instead actively pumped by the vacuum system. Figure 43 shows the thermocouple placements. The

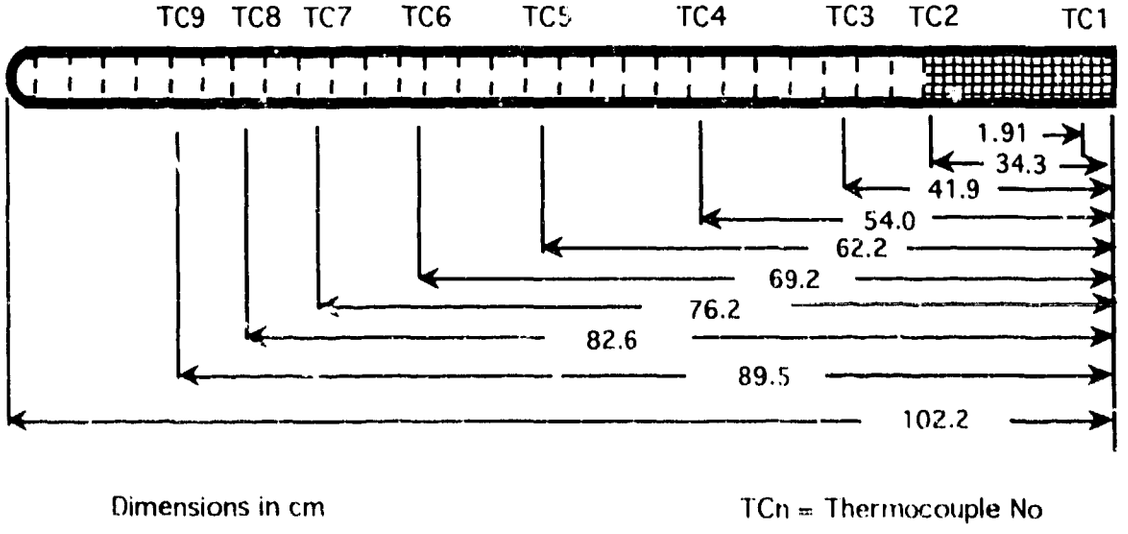

Figure 39. Schematic of Thermocouple Placements for LTHP1

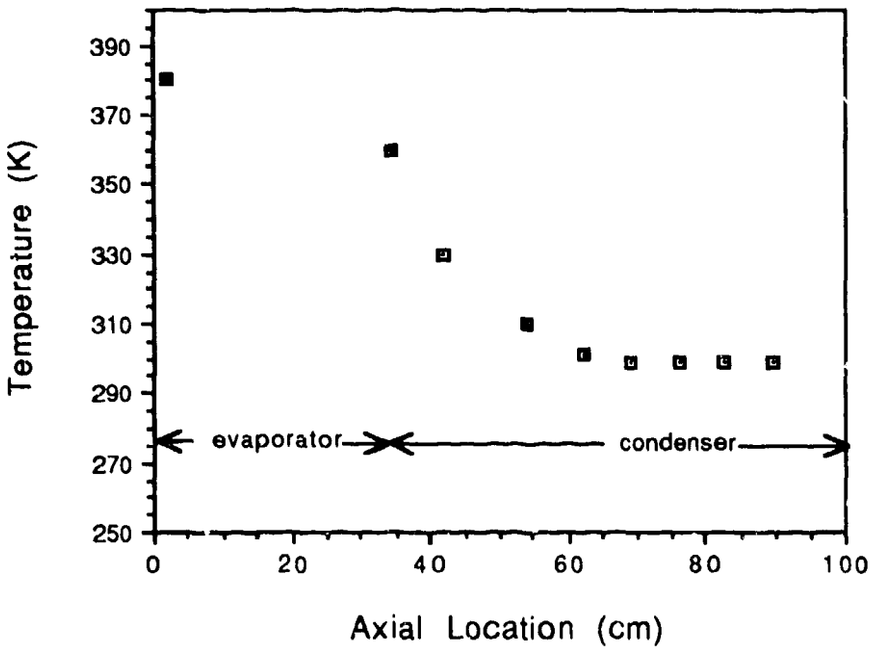

Figure 40. Temperature Profile for LTHP1

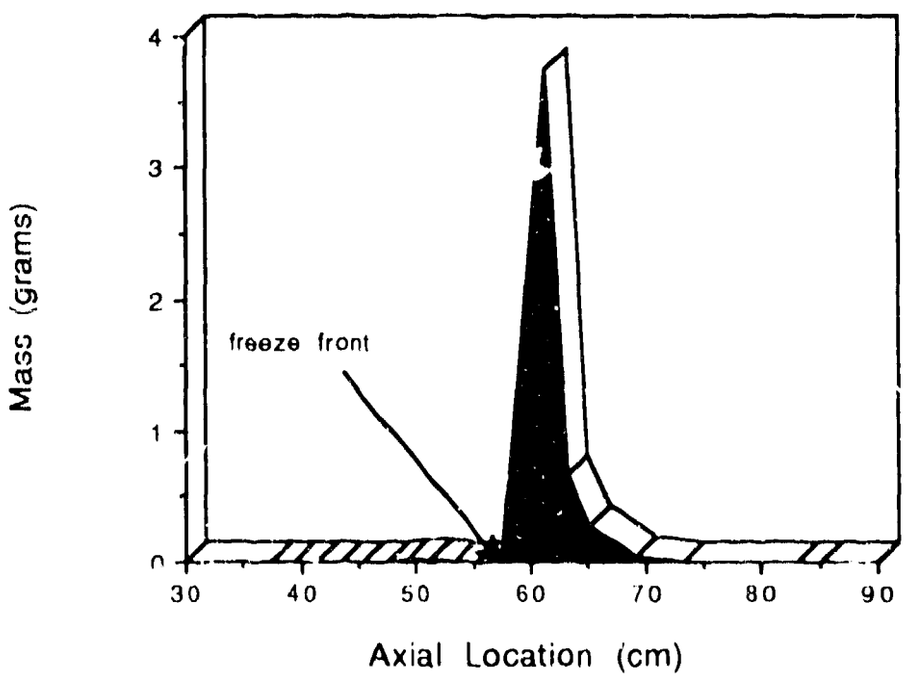

Figure 41. Mass Accumulation Distribution for LTHP1

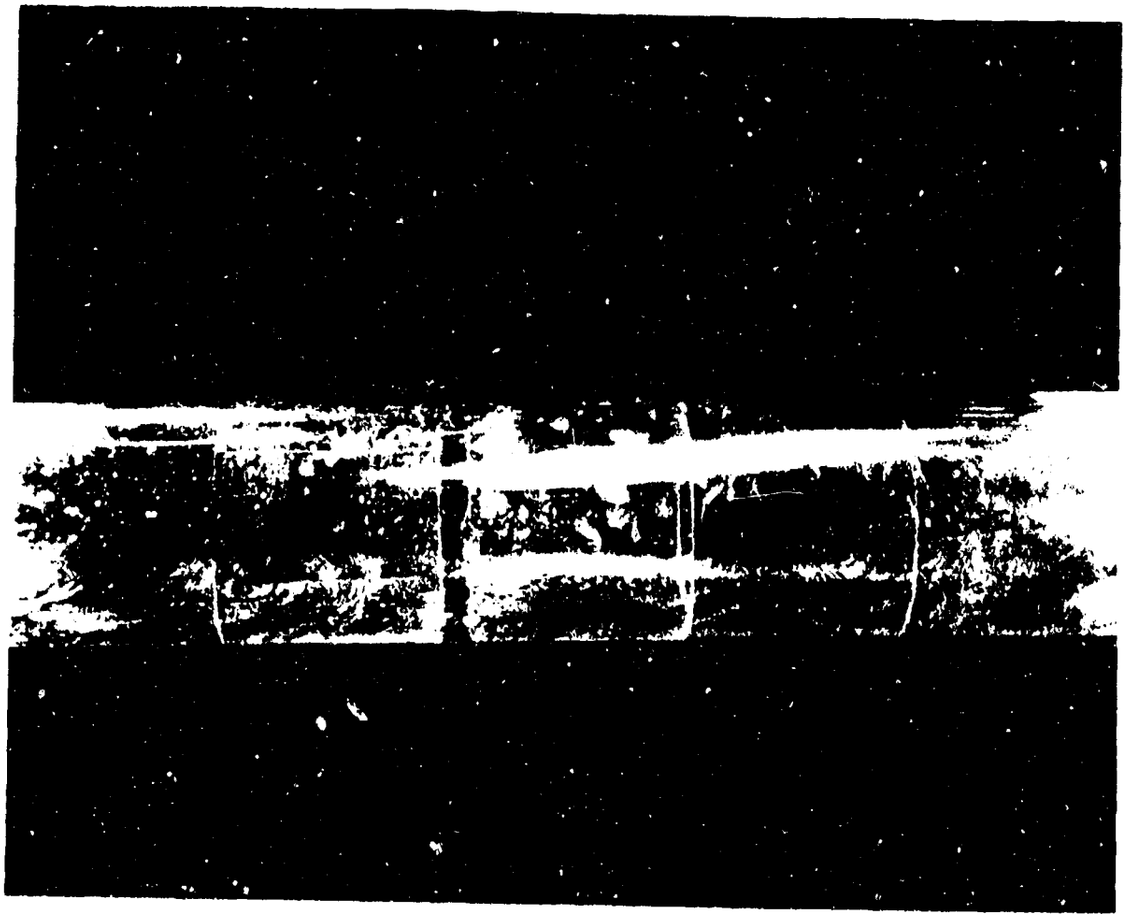

Figure 42. Sections of the Condenser of LTHP1 at the Conclusion of the Experiment Showing the Accumulation of Mass

heat pipe was operated with a power throughput of 65 ±3 Watts. Figure 44 shows the temperature profile during heat pipe operation. The pipe did not operate as expected, having an excessive evaporator temperature and exhibiting no mass accumulation in the condenser. The pressure at the

condenser end nearest the vacuum system was excessive, reading approximately 20 μm Hg where it snould have read less than 1.0 μm Hg. to determine the cause of the high pressures, the vacuum system was isolated from the heat pipe. The pressure at the condenser rose at a rate of 5 μm Hg per minute, eventually exceeding 1.0 mm Hg, the limit of the gauge. The pressures in the heat pipe were a strong indication that the working fluid had partially decomposed into lighter, more volatile components. This was all the more likely given the temperatures in the evaporator. The heat pipe was then removed from the test layout, disassembled and inspected. It was found that the wick was badly damaged. The damage appeared to have occurred during the working fluid charging process. In effect the wick was crumpled up and was occupying a significant portion of the vapor space, instead of being fixed tightly against the wall lining the vapor space. Heat had to conduct through the space between the wall and wick before it reached the working fluid. The temperature differential across the gap was high. In this situation the temperature measurements taken at the heat pipe wall were not indicative of vapor temperatures. The vapor temperature at which working fluid decomposition occurred could not be determined from this experiment.

During the refitting of a new wick, the pipe was accidentally dropped and was destroyed. No useful mass accumulation data was ever produced during the test of LTHP2. A decision was made not to test any of the remaining pipes above 30 Watts to minimize the possibility of decomposing the working fluid.

Low Temperature Heat Pipe #3 (LTHP3)

A different test facility from that used for LTHP1 and LTHP2 was used to conduct the thermal test of LTHP3. The facilities for testing LTHP3 were essentially identical to those used previously with the exception of the vacuum system. The facilities were located at the Air Force Phillips Laboratory and at the time did not include a vacuum system, so it was necessary to employ the glass seal closure technique described in Section 2.2.4. Figure 45 illustrates the thermocouple placement for LTHP3. Figure 46 shows the temperature profile for the heat pipe during operation. As with LTHP2 there was no mass accumulation in the

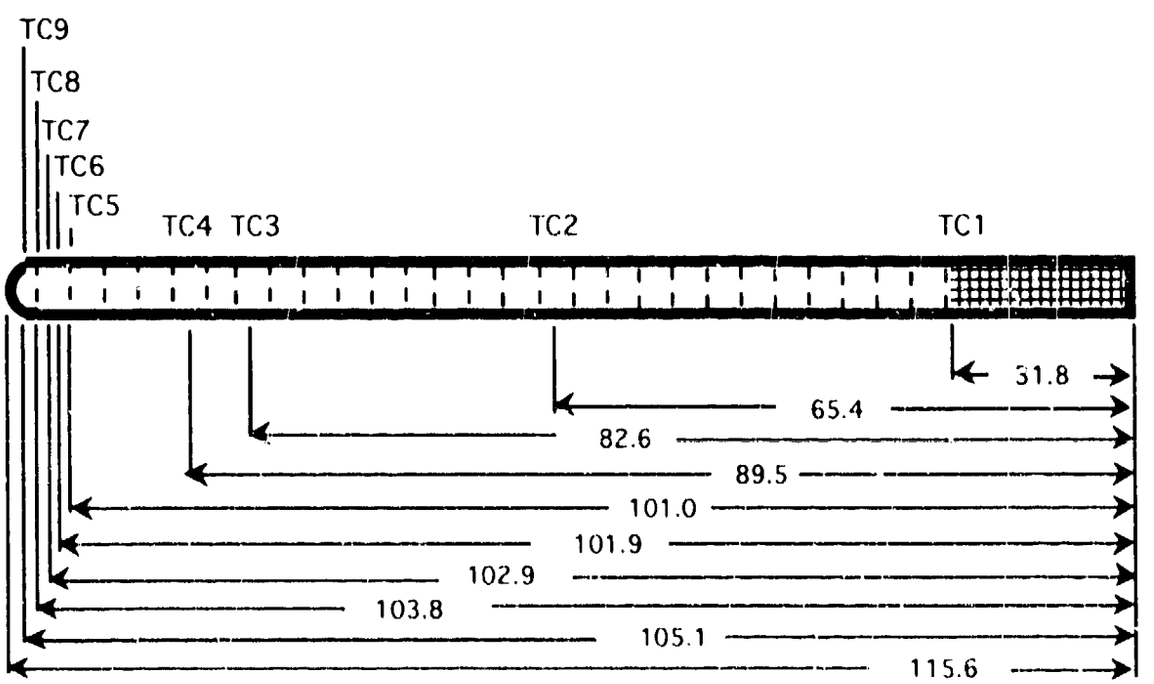

Figure 43. Schematic of Thermocouple Placements for LTHP2

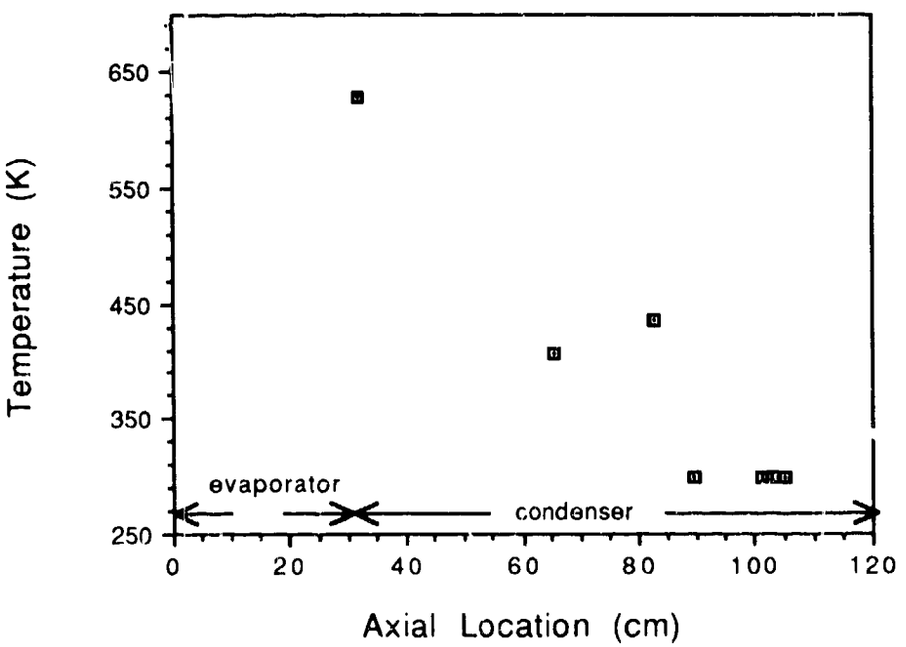

Figure 44. Temperature Profile for LTHP2

condenser. The cause was suspected to be volatile, non-condensable gases in the condenser which were produced by the decomposition of the working fluid in the evaporator. It was believed that the problems which occurred to a high degree in LTHP2 may occur to some degree in all the pipes even when tested at lower temperatures. The solution would be to test with an active pumping system attached to the condenser as was done with LTHP1. Thermal testing of LTHP4 was occurring at the LANL facilities in conjunction with the testing of LTHP3. The results of the LTHP4 tests were similar to those of LTHP3, namely no mass accumulation was occurring in the condenser. Experiments were conducted with LTHP4 to determine precisely the cause of the inadequate performance. These experiments are described in the paragraphs which follow for LTHP4. At

the conclusion of those tests, it was decided to ship LTHP3 back to LANL and fit it with a nipple to which a vacuum system could be attached. The heat pipe was damaged beyond repair during shipping, so it was never properly tested. No mass accumulation data was gathered for LTHP3.

Low Temperature Heat Pipe #4 (LTHP4)

The testing of LTHP4 was done in conjunction with LTHP3. It was tested at the LANL facilities while LTHP3 was tested at the Air Force Phillips Laboratory. Figure 47 shows the location of the thermocouples. As with LTHP3, this heat pipe was sealed and, therefore, not operated while attached to a vacuum system as with LTHP1. It too showed no mass accumulation during initial tests, probably as a result of excessive pressures in the condenser. The source of this pressure was believed to be volatile hydrocarbons, the result of thermal decomposition of the working fluid. To verify this, experiments were run to analyze the heat pipe vapors. First the heat pipe was removed from the test assembly, then it was disassembled and fitted with a glass to metal nipple which could be attached to a gas analyzer system. The pipe was reassembled, charged with working fluid, processed and fitted to the gas analyzer system. The gas analyzer was a Quadrex 200 residual gas analyzer manufactured by Inficon Leybold-Heraeus Inc. It measures between 1 and 200 AMU at pressures between 5 $x10^{-11}$ torr and 10^{-5} torr using a Faraday cup detector and is capable of detecting to 10 ppm. The heat pipe was operated as before, and a series of gas analyses were made. The heat pipe was first brought to steady-state operation while being valved off from the analyzer. The background readings for the analyzer were recorded. Next the heat pipe was opened to the analyzer and a second set of readings

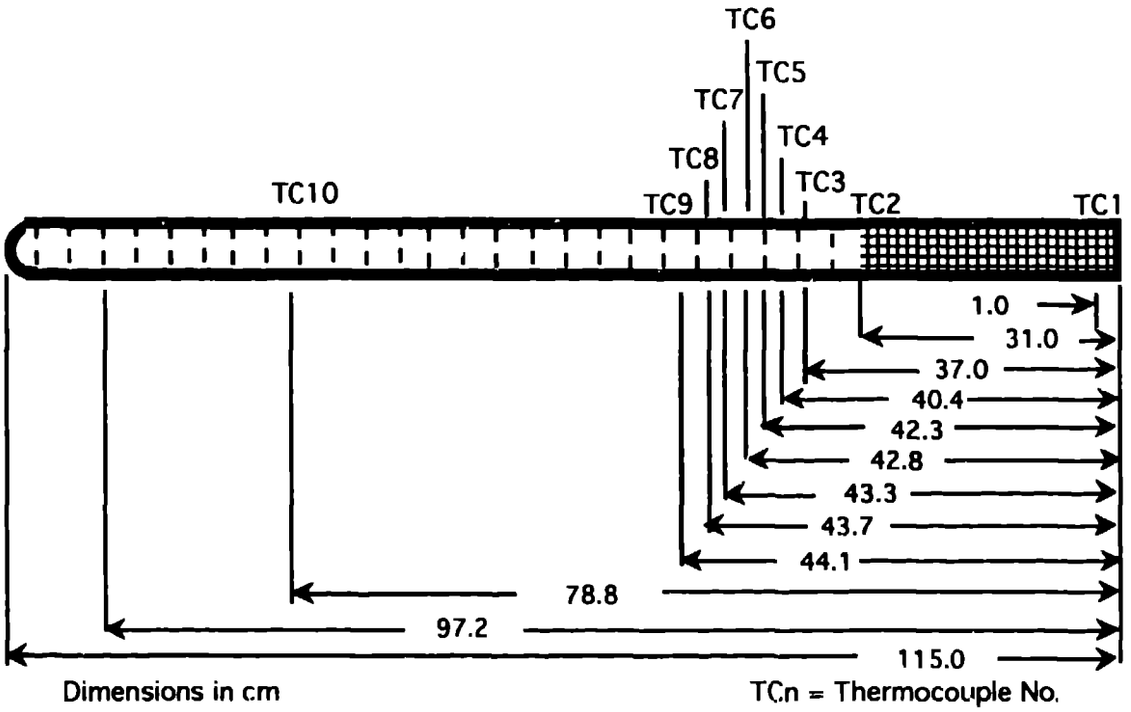

Figure 45. Schematic of Thermocouple Placements for LTHP3

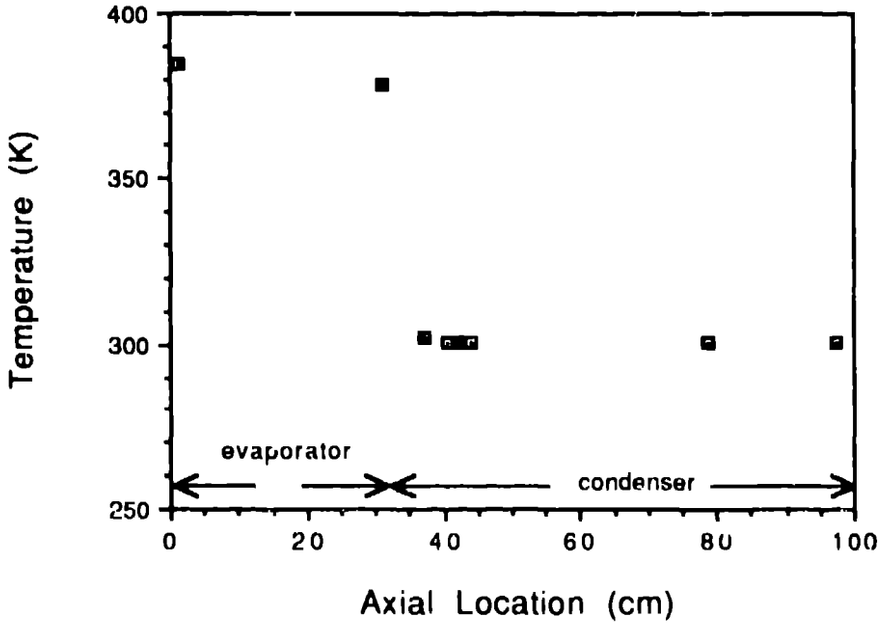

Figure 46. Temperature Profile for LTHP3

taken. The heat pipe operation was continued for several hours while remaining to be open to the gas analyzer system. Readings were taken periodically to observe any changes in constituent concentrations with time. The vapor constituents were found to be mostly diatomic hydrogen, water, carbon monoxide and carbon dioxide. Traces of heavier hydrocarbons were detected, and measurable quantities of Argon were found in the background readings for the analyzer. Table 5 displays the results in terms of partial pressures for a representative gas analysis run. The concentration of each constituent was found to exceed the background readings once the valve between the heat pipe and analyzer was opened. The heat pipe clearly contained volatiles. It is evident that water was present within the pipe which accounts for the oxygen in the carbon monoxide and carbon dioxide. The source of carbon was almost certainly the working fluid. The last set of readings in Table 5 which were taken after running the heat pipe open to the gas analyzer system for approximately 96 hours are close to the background readings for the analyzer. This indicates that continuos pumping on the heat pipe during operation does remove the volatile vapors and thus maintains the heat pipe condenser at a satisfactory pressure. It was noted that during these tests, there was an accumulation of frozen working fluid in the condenser.

The LTHP4 was operated while being actively pumped by a vacuum system in the same manner in which the LTHP1 was tested. Figure 48 shows the temperature profile for the heat pipe in operation. The heat pipe was operated at 24.3 ±0.4 Watts for a duration of 76.25 hours and resulted in the accumulation of 4.7211 grams of frozen working fluid in the condenser. The net Watt-hours was 1854.6. Figure 49 shows the mass

distribution of working fluid along the heat pipe condenser. Figure 50 is a photograph of the condenser sections of LTHP4 at the conclusion of the mass accumulation experiment and during the disassembly of the heat pipe. Figure 51 shows the first four sections of the condenser as they appeared during the post test weighing. Nearly all the accumulated mass in the condenser was on these four sections.

Table 7. Partial Pressures of Volatile Vapors in LTHP4

	Hydrogen	Water	Carbon Monoxide	Carbon Dioxide
RGA Background	1.9×10^{-6} torr	1.0×10^{-6} torr	3.2×10^{-6} torr	0.56×10^{-6} torr
Initial Values	3.3×10^{-6} torr	2.5×10^{-6} torr	6.2×10^{-6} torr	1.1×10^{-6} torr
After Steady Operation for 96 hours	2.8×10^{-6} torr	0.73×10^{-6} torr	5.5×10^{-6} torr	0.19×10^{-6} torr

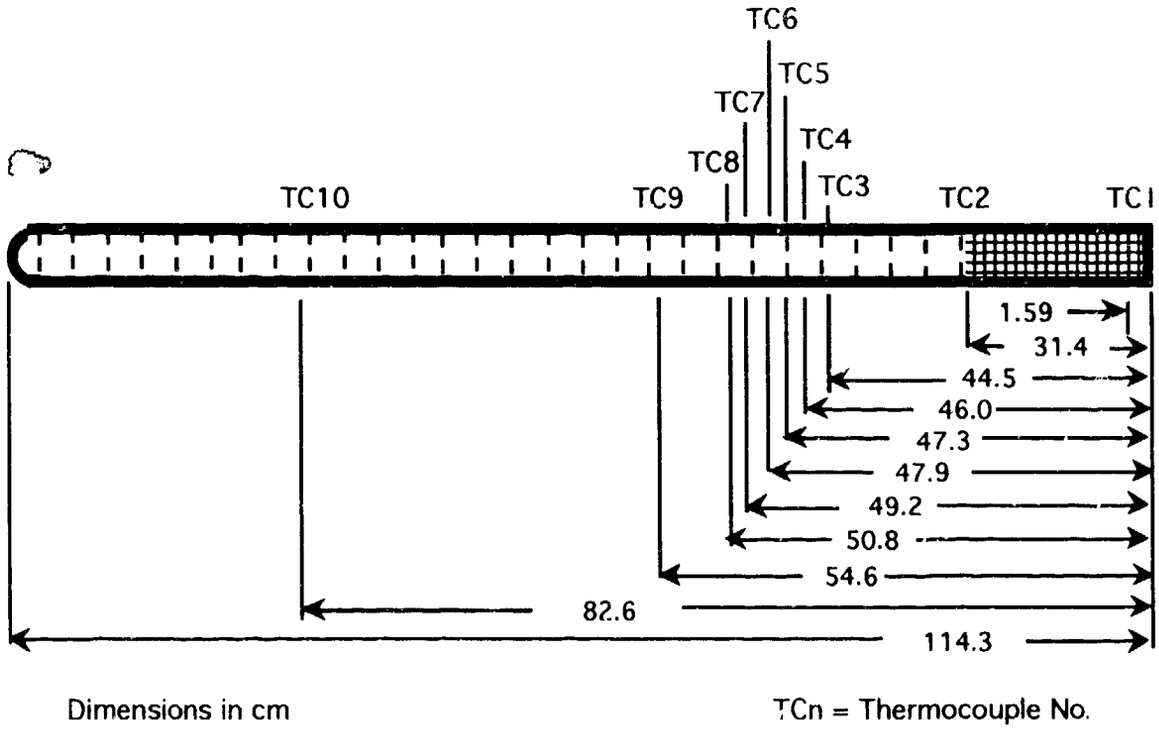

Figure 47. Schematic of Thermocouple Placements for LTHP4

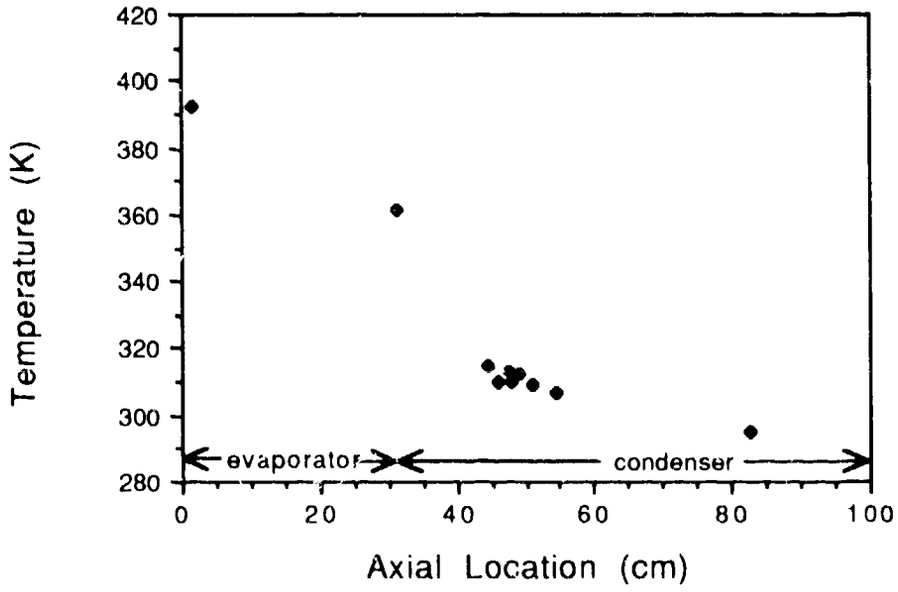

Figure 48. Temperature Profile for LTHP4

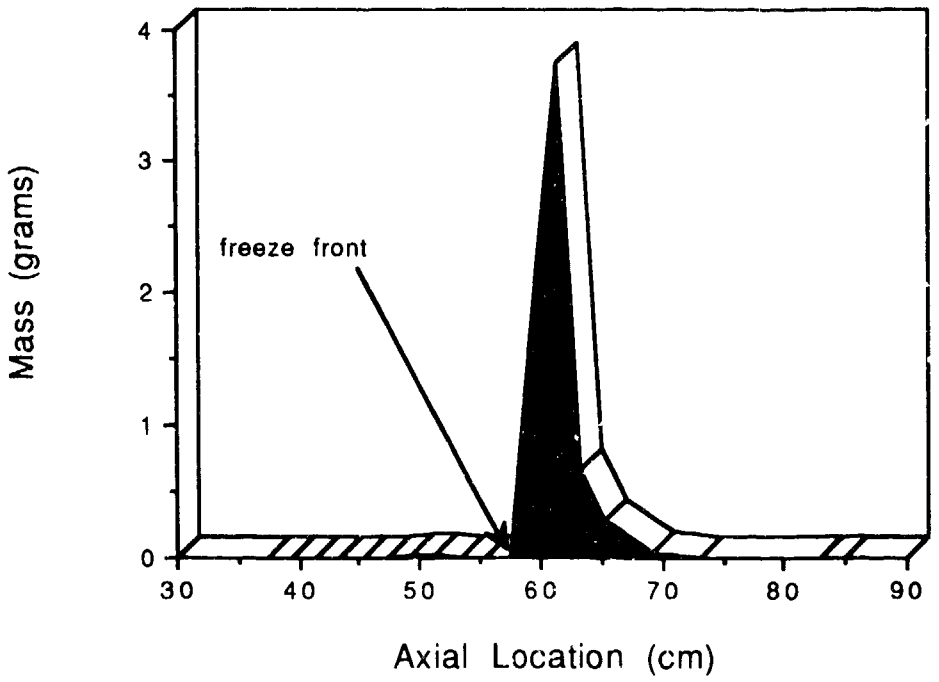

Figure 49. Mass Accumulation Distribution for LTHP4

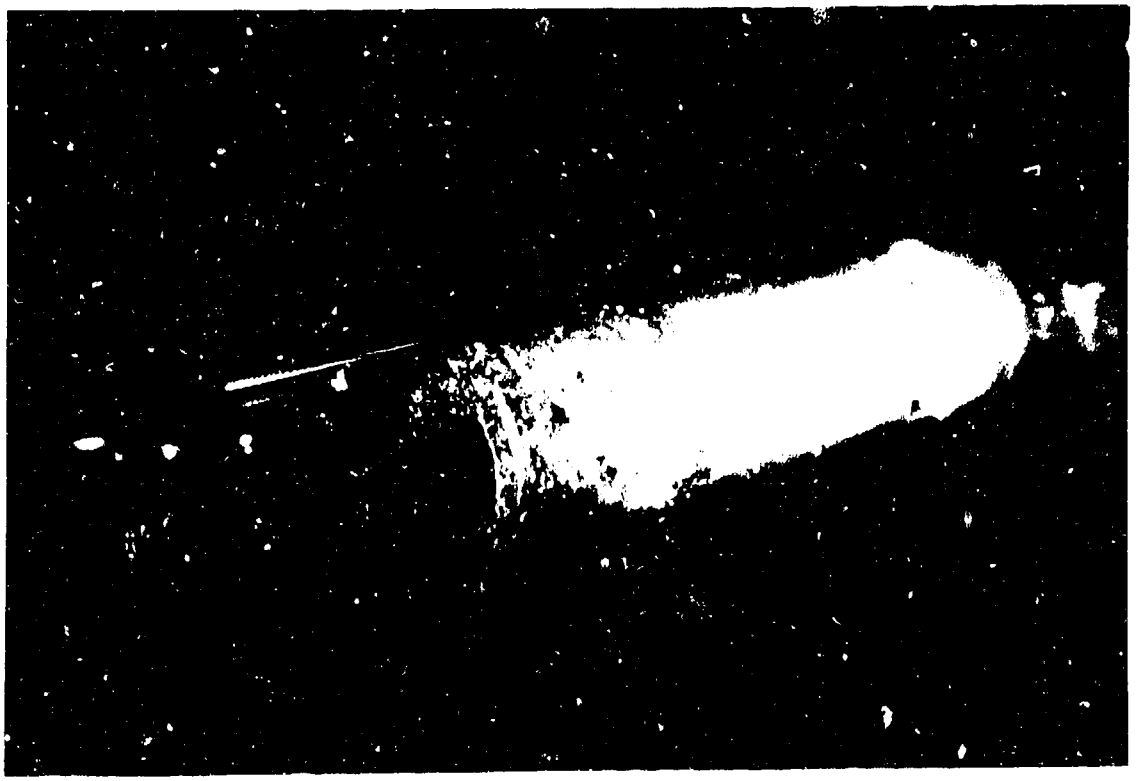

Figure 50. Condenser of the LTHP4 Following the Mass Accumulation Experiment

Figure 51. The First Four Sections of the Condenser of LTHP4 as They Appeared at the Time of Post-Test Weighing

3.2 Experimental Results for the High Temperature Heat Pipes

The HTHP was tested at the AFPL vacuum test facility. The heat pipe was brought up slowly to steady-state. After reaching steady-state the heat pipe was then run continuously at 91.8 W for a period of 598 hours. The net Watt-hours for the test was 54900. Temperatures were recorded at regular intervals for the duration of the test. Temperatures as a function of time at each location along the heat pipe are shown in Figure 52. The temperature profiles at the start and end of the test run are shown in Figure 53.

The heat pipe was shipped to LANL where it was disected and the mass distribution of the working fluid was measured. The mass distribution along the condenser is plotted in Figure 54. The net accumulation of mass in the frozen region was 0.0045 gms ±0.0008 gms. The accumulation to the left of the freeze front was liquid while the heat pipe was in operation, and so was not included when determining the frozen mass accumulation.

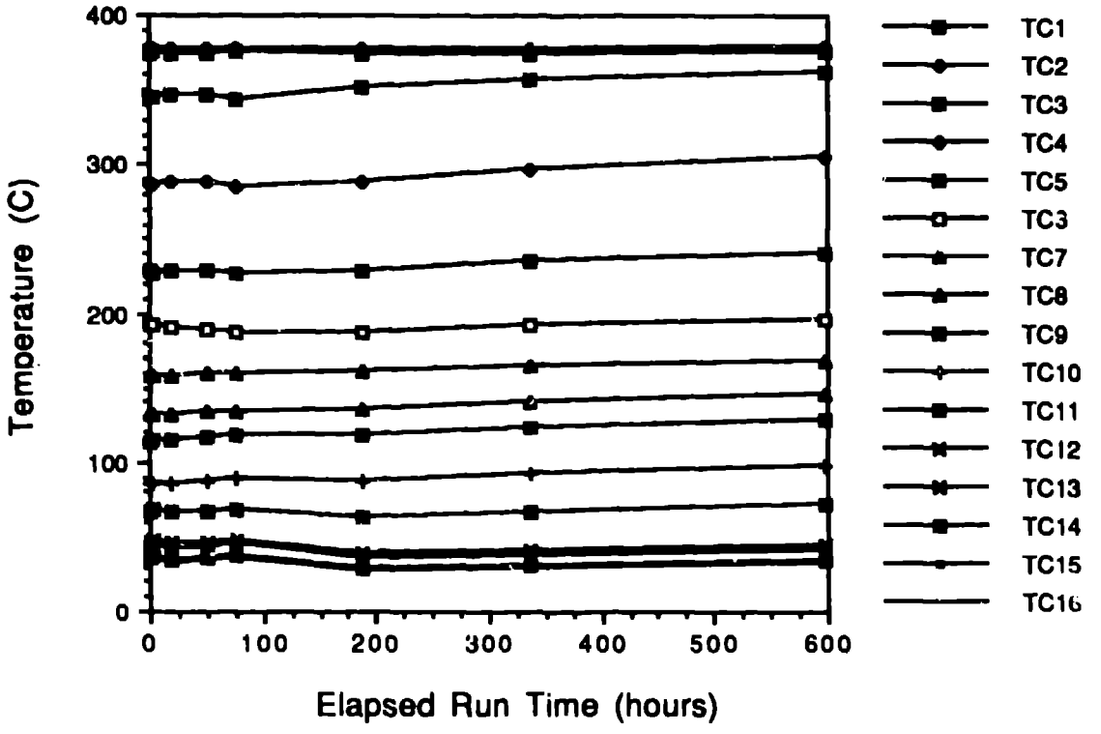

Figure 52. Temperatures for The HTHP Experiment

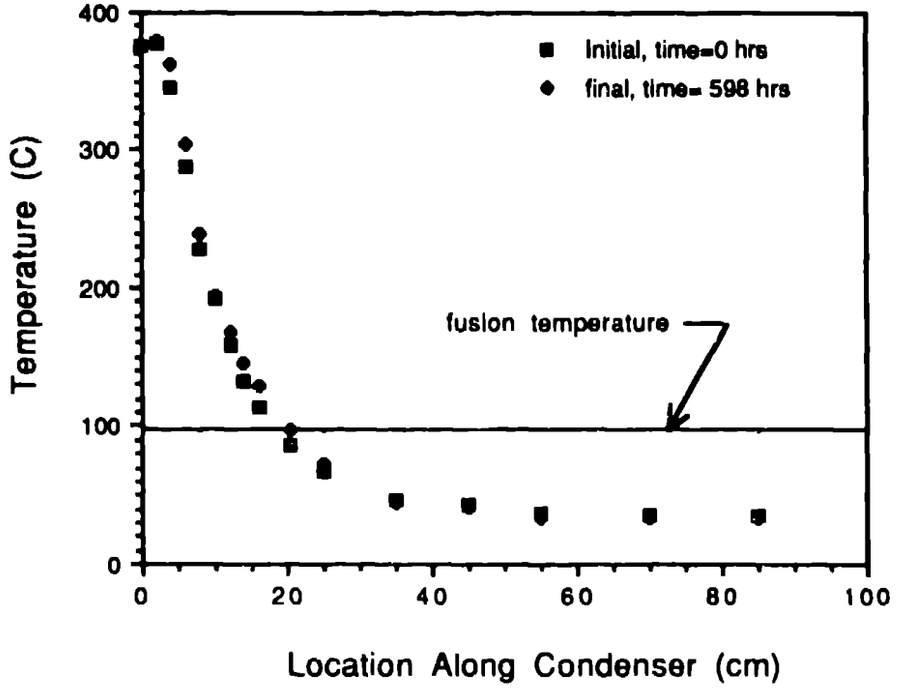

Figure 53. Temperature Profiles for the HTHP Experiment

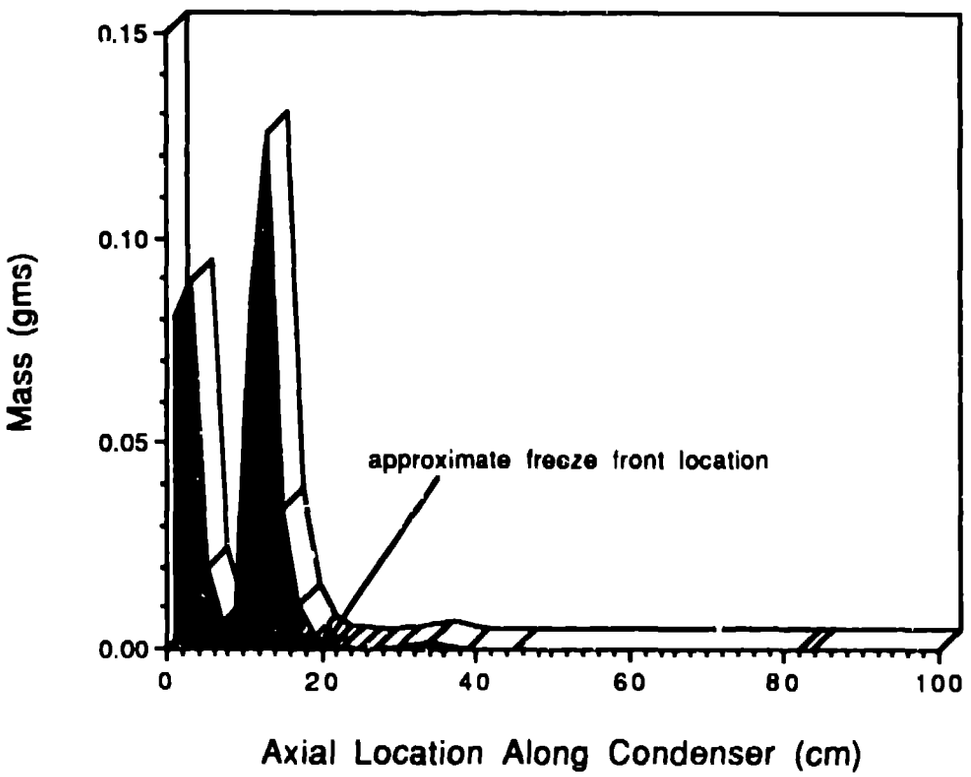

Figure 54. Mass Distribution For the HTHP

3.3 Correlation of Data with Model Predictions

The computer model, the development of which was described in Section 2.1, was used to predict the performance of LTHP1 and LTHP4. The model was used primarily to predict local temperatures and mass throughputs. The geometry and operating environment inputs to the code for each low temperature heat pipe are summarized in Table 6.

Table 6. Inputs to the Computer Code for LTHP Experiments

	outside diameter (cm)	inside diameter (cm)	stagnation temperature (K)	sink temperature (K)
LTHP1	2.21	1.57	379	299
LTHP4	2.21	1.50	386	300

Subroutines for the various thermophysical properties of the working fluid were also introduced to the code. These subroutines calculated the viscosity, latent heat of vaporization, density and saturation pressure of the working fluid as functions of temperature. The average value for heat transfer coefficient was also input. The heat transfer coefficient was assumed to remain constant at the average value over the length of the heat pipe condenser. The actual value of heat transfer coefficient used to predict performance for a given heat pipe was determined by best fit to experimental data. Recall the stagnation temperature, sink temperature and heat transfer coefficient were the parameters in the semi-analytical model. The stagnation temperature and sink temperature are readily measured in experiment. The heat transfer coefficient cannot be directly measured. It must be either determined by existing emperical

relationships or by experiment. It carries a greater uncertainty than the temperature measurements. The effect heat transfer coefficient has on the predicted temperature profile for a given heat pipe is shown graphically in Figure 56. The results shown in Figure 56 are for an octadecane heat pipe with the same nominal dimensions and operation environment as the LTHPs. The stagnation temperature was 362 K. The vapor space diameter was 1.5 cm, and the sink temperature was 295 K. The heat transfer coefficient was varied from 25 $W/cm^2/K$ to 60 $W/cm^2/K$.

Figures 57 and 58 compare model predictions with data for LTHP1 at several values for average heat transfer coefficient. The fusion

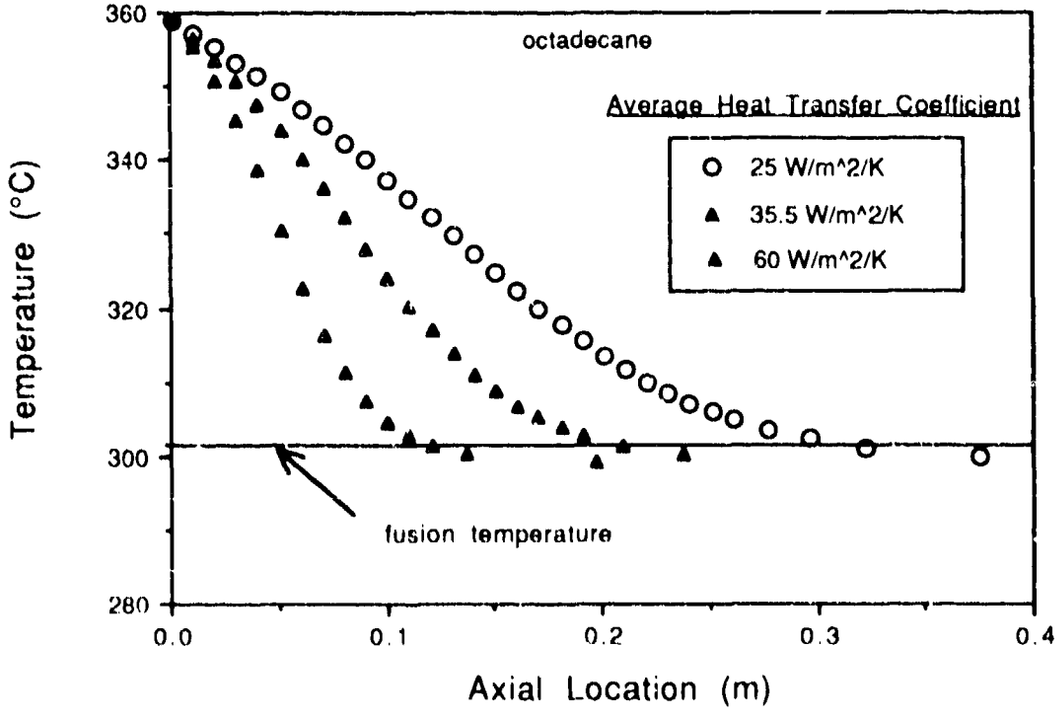

Figure 56. The Effects of Average Heat Transfer Coefficient Values on the Model Predictions for Temperature Profile at a Stagnation Temperature of 362 K.

temperature and freeze front are indicated. The freeze front was determined by visual inspection during testing. From Figure 58 it can be seen that the value for heat transfer coefficient that best fits the experimental data is between 31.1 and 31.7 W/m^2/K. The mean of these values is 31.4 W/m^2/K and was the value used in the model for predicting the performance of LTHP1.

Figures 59 and 60 compare the LTHP4 data with model predictions at various values of average heat transfer coefficient. The freeze front location shown in these figures was also determined by visual inspection. The best fit heat transfer coefficient derived from these results is 34.3 W/m^2/K and was the value used for modeling the performance of LTHP4.

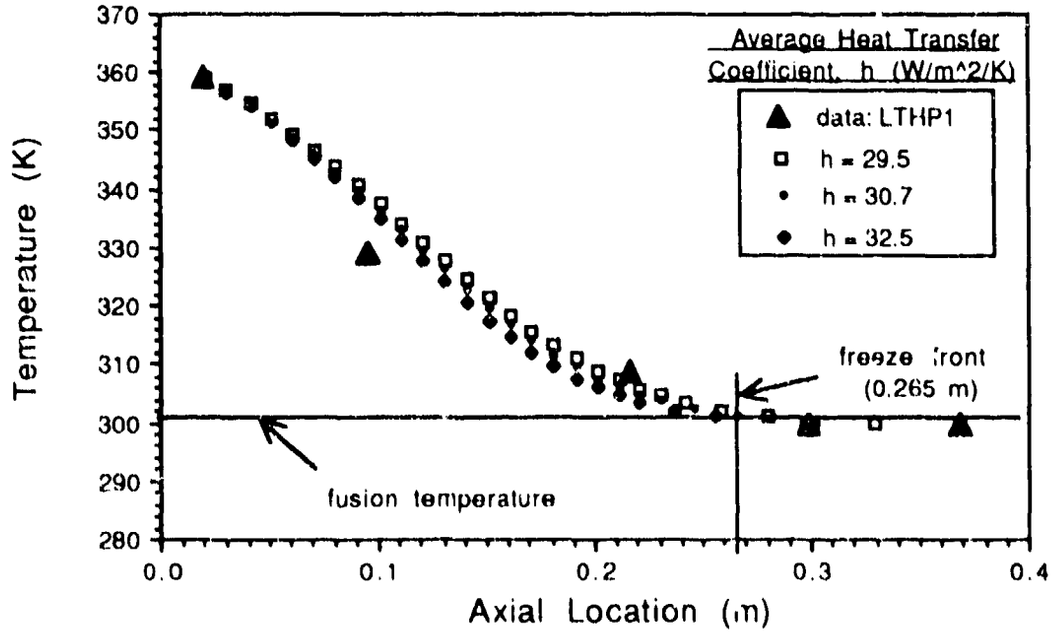

Figure 57. LTHP1 Data Compared with Model Predictions at Various Values for Average Heat Transfer Coefficient.

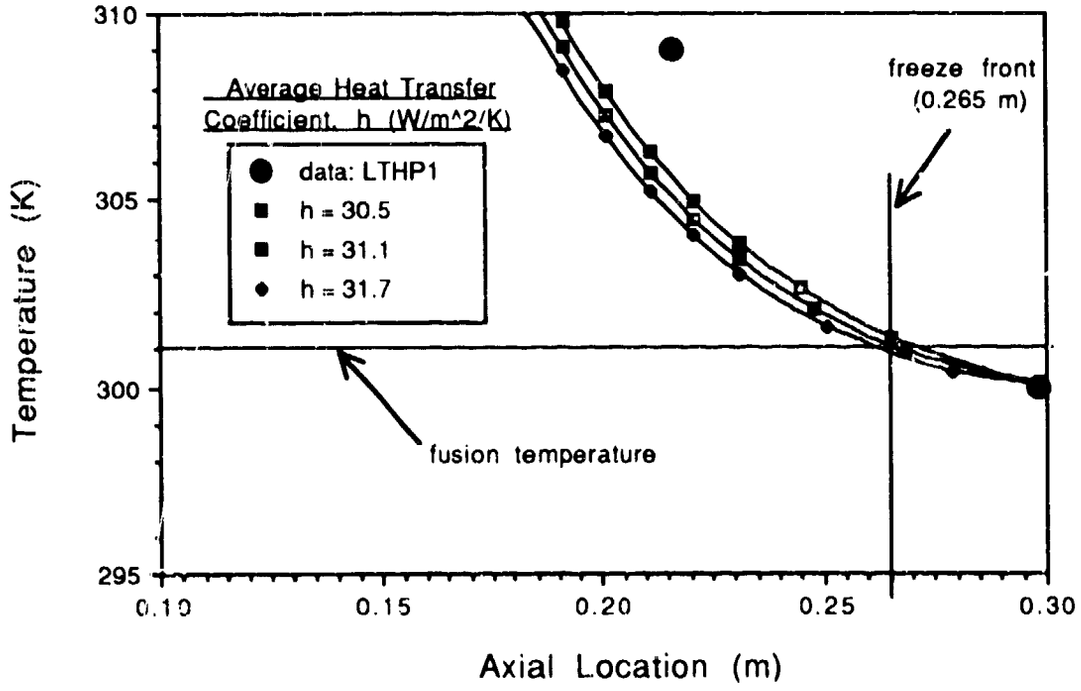

Figure 58. LTHP1 Data Compared with Model Predictions at Various Values for Average Heat Transfer Coefficient: A Closer View.

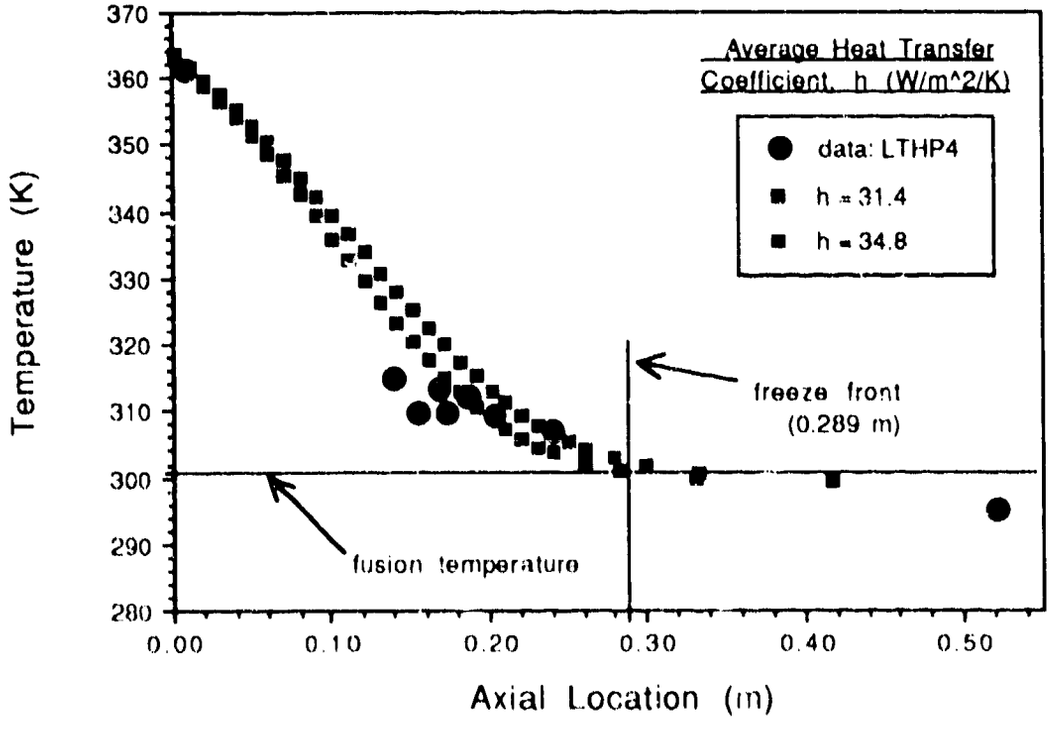

Figure 59. LTHP4 Data Compared with Model Predictions at Various Values for Average Heat Transfer Coefficient

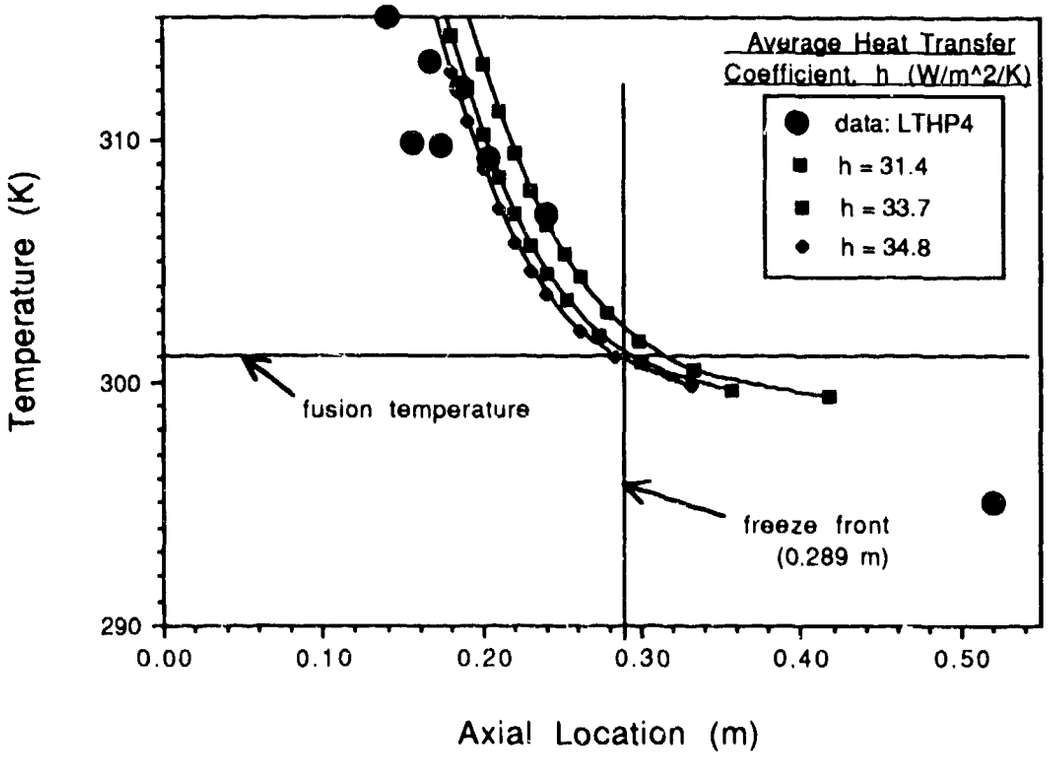

Figure 60. LTHP4 Data Compared with Model Predictions at Various Values for Average Heat Transfer Coefficient: A Closer View.

The respective values for heat transfer coefficient for LTHP1 and LTHP4 were input to the computer model, and the results shown in Figures 61 through 68 were generated. Figures 61 and 65 compare the predicted temperature profiles with the actual data. Observe, that for these figures, the point x=0.0 on the x-axis is located at the evaporator exit. Included are the fusion temperature and the location of the freeze front. Figures 62 and 66 show the temperature decline and pressure decline along the heat pipe condenser normalized with respect to the conditions at the evaporator exit. The pressures fall rapidly at the beginning of the condensers and then less rapidly as the respective heat transfer rates

decline along the condenser lengths. The temperatures also fall dramatically at first, and then approach the sink temperature asymptotically. The normalized densities and mass throughput rates are shown in Figures 63 and 67. The density, by virtue of the ideal gas equation of state, should and does behave the same as the pressure, falling rapidly at first, then approaching a small yet finite value in an asymptotic fashion. The mass throughputs also behave the same way. They fall rapidly at first, owing to the high heat transfer rates at the beginning of the condenser. They then approach a limiting value in an asymptotic fashion as the vapor temperature approaches the fusion temperature. The predicted mass throughputs at the freeze fronts are 16.7% and 14.5% of the evaporator exit values for LTHP1 and LTHP4 respectively. Alternatively these values are 9.45 μgm/s and 11.61 μgm/s. The actual values determined by experiment were 6.80 μgm/s and 17.20 μgm/s respectively for LTHP1 and LTHP4. LTHP1 operated for 220 hours and accumulated 5.3825 gm of frozen material. Based on the model predictions, this same amount of mass would have accumulated in 158.2 hours, a difference of 61.8 hours or 28%. Similarly, LTHP4 accumulated 4.7211 gm of frozen material in 76.25 hours. The model predicted this same accumulation in 109.04 hours, a difference of -32.75 hours or -43%.

Figures 64 and 68 show the flow character as defined by the flow characterization parameter and the local Mach number. The flow characterization parameter is useful for determining the nature of the flow, that is whether it is continuum, transition of free molecular. It is similar to the Knudsen number, and is defined as [2]

$$X = \frac{2\mu}{PD\sqrt{\frac{g_c}{RT}}}$$

where X = flow characterization parameter
- < 0.013, continuum flow
- > 0.013 and < 1.0, transition flow
- > 1.0, free molecular flow

μ = vapor viscosity
P = vapor pressure
D = diameter
g_c = gravitational constant
R = gas constant
T = Temperature

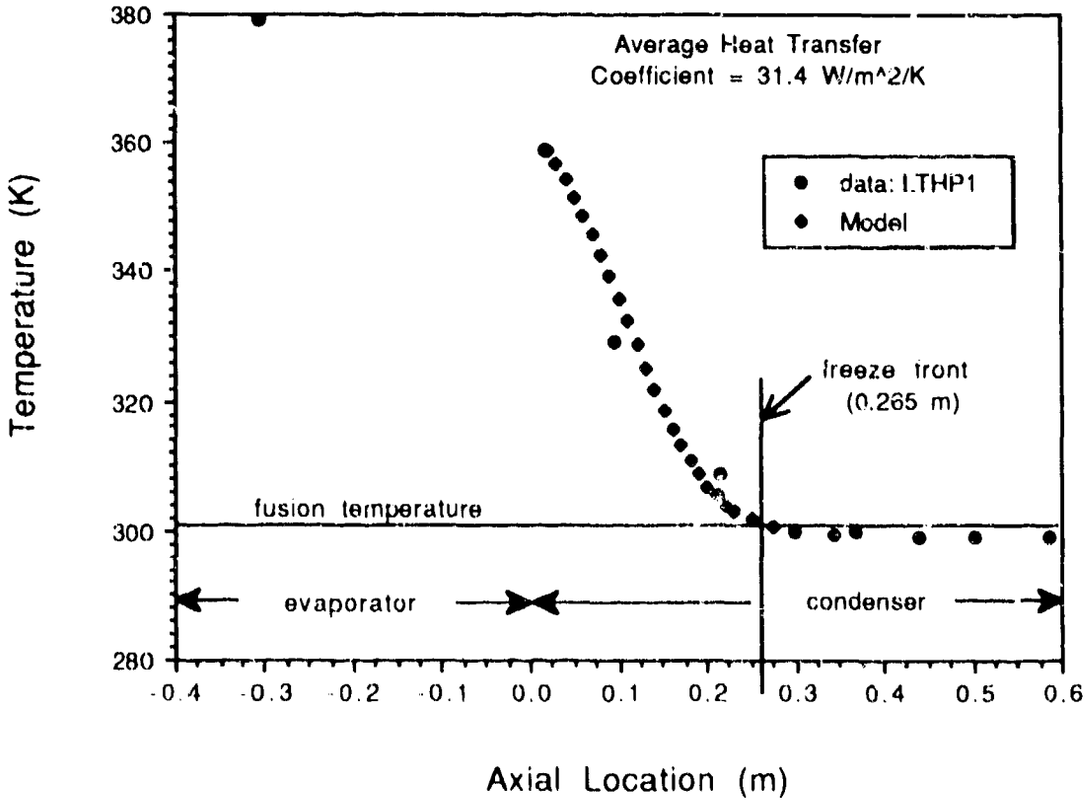

Figure 61. Predicted Temperature Profile and Temperature Profile Data for LTHP1

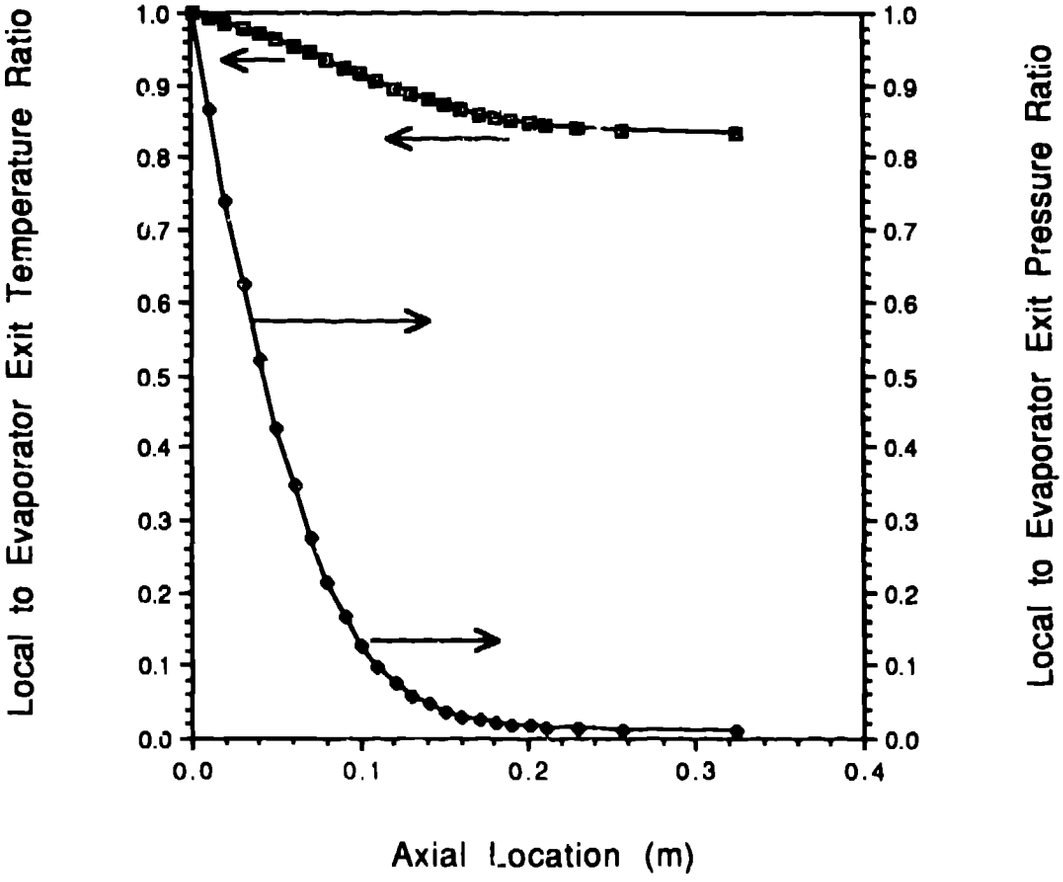

Figure 62. Temperature and Pressure Results for LTHP1 Model Predictions

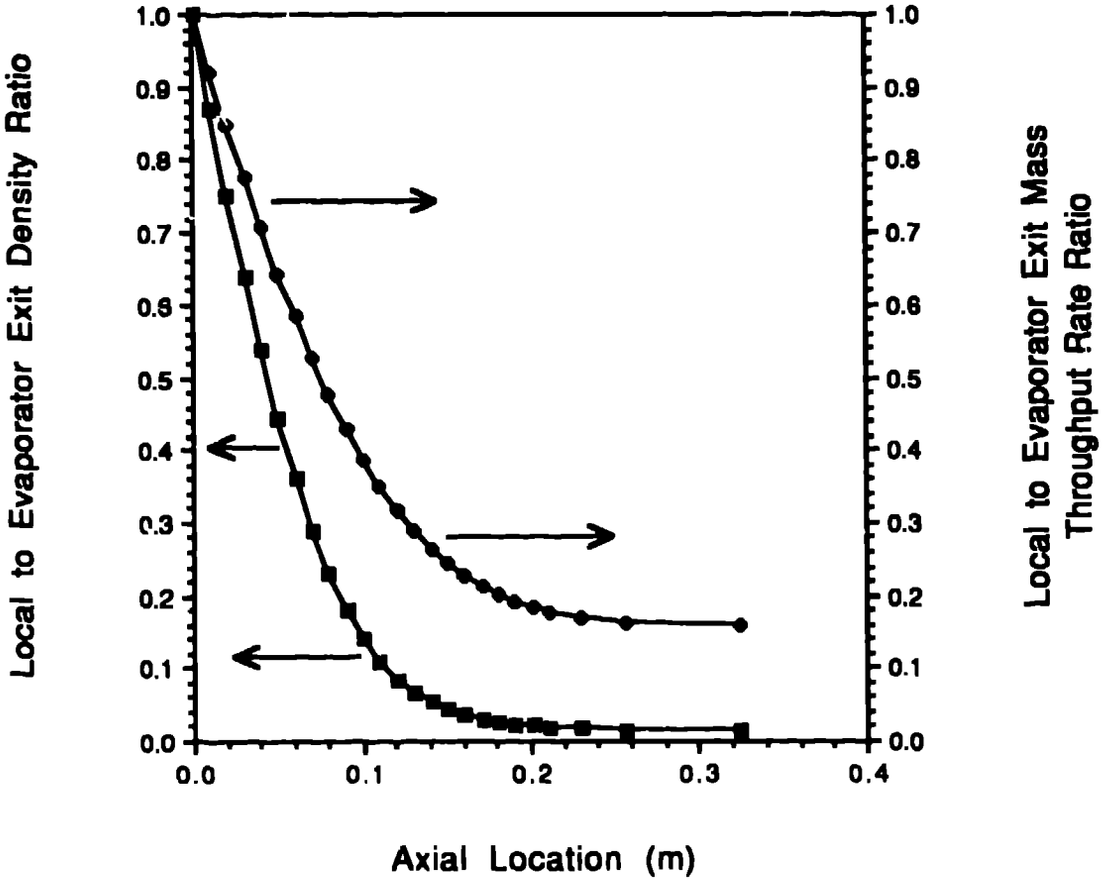

Figure 63. Density and Mass Throughput Rate Results for LTHP1 Model Predictions

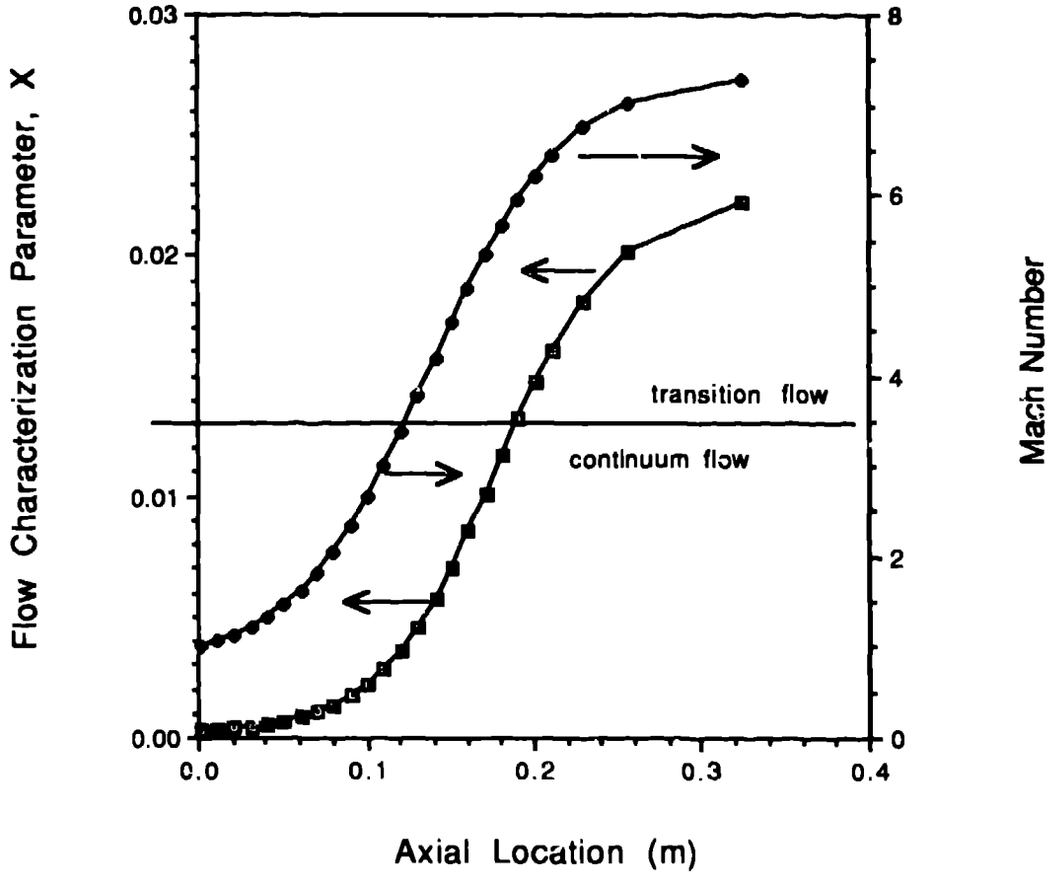

Figure 64 Model Predictions for the Flow Characterization Parameter and Mach Number for LTHP1

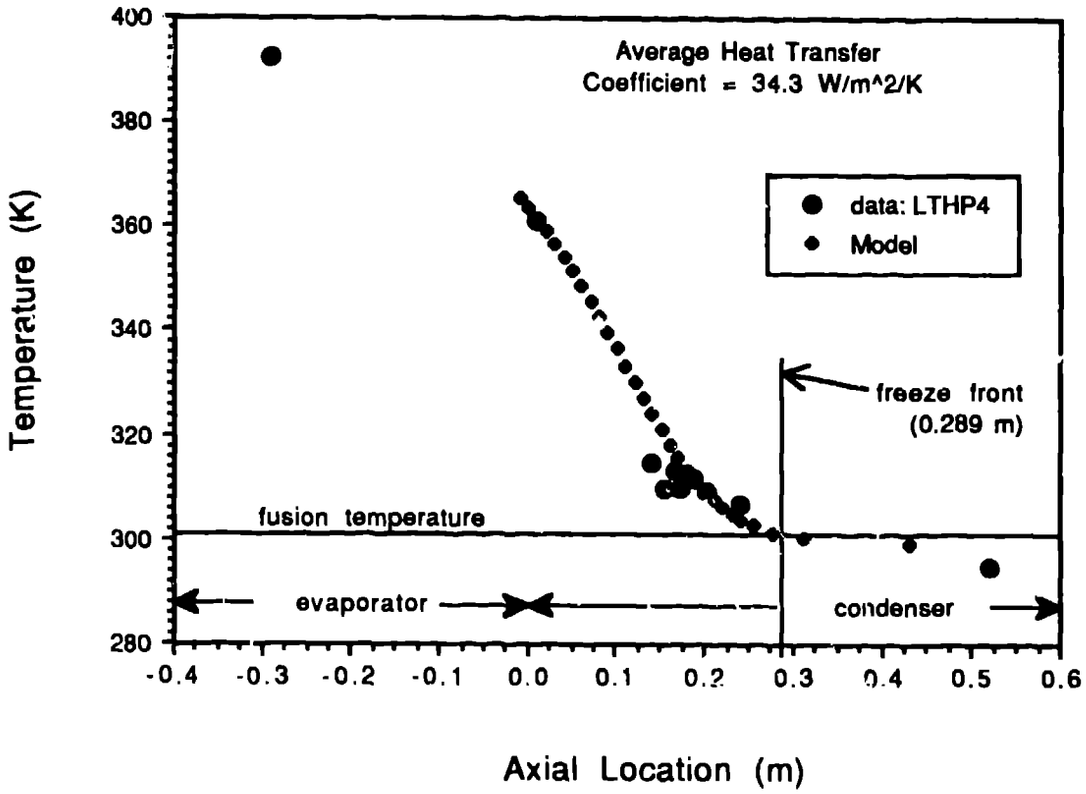

Figure 65. Predicted Temperature Profile and Temperature Profile Data for LTHP4

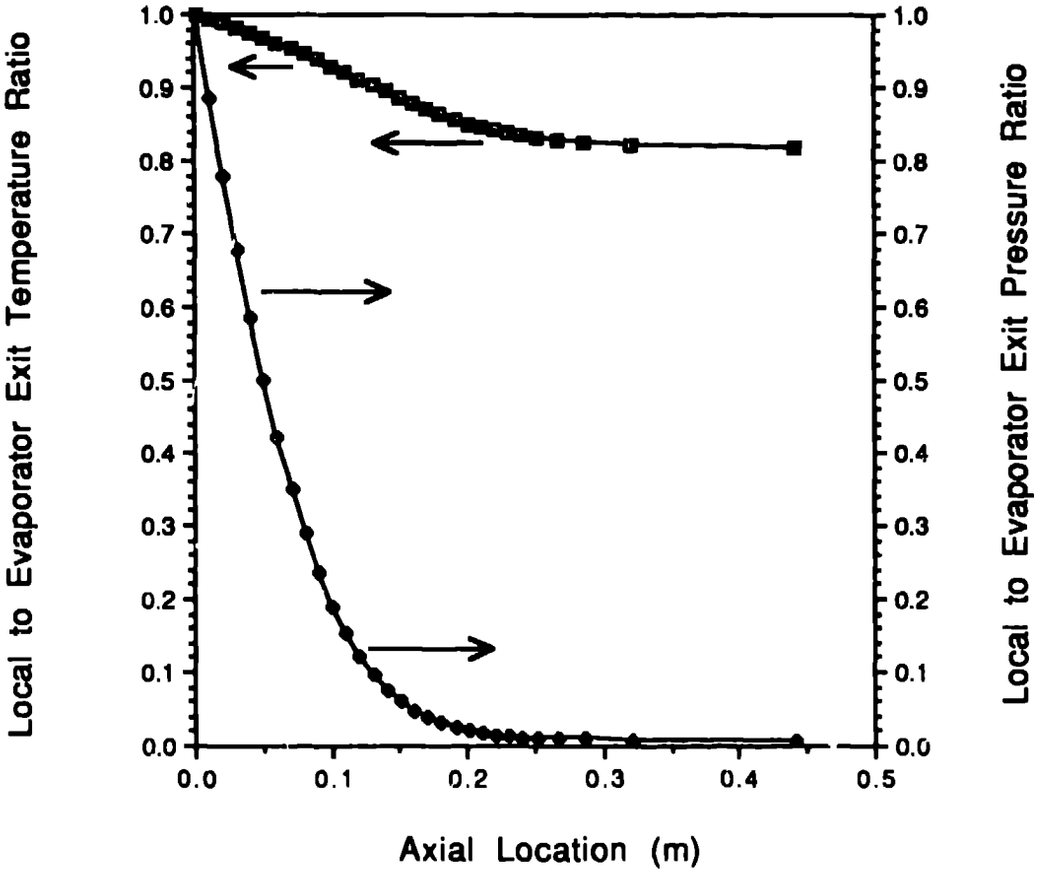

Figure 66 Temperature and Pressure Results for LTHP4 Model Predictions

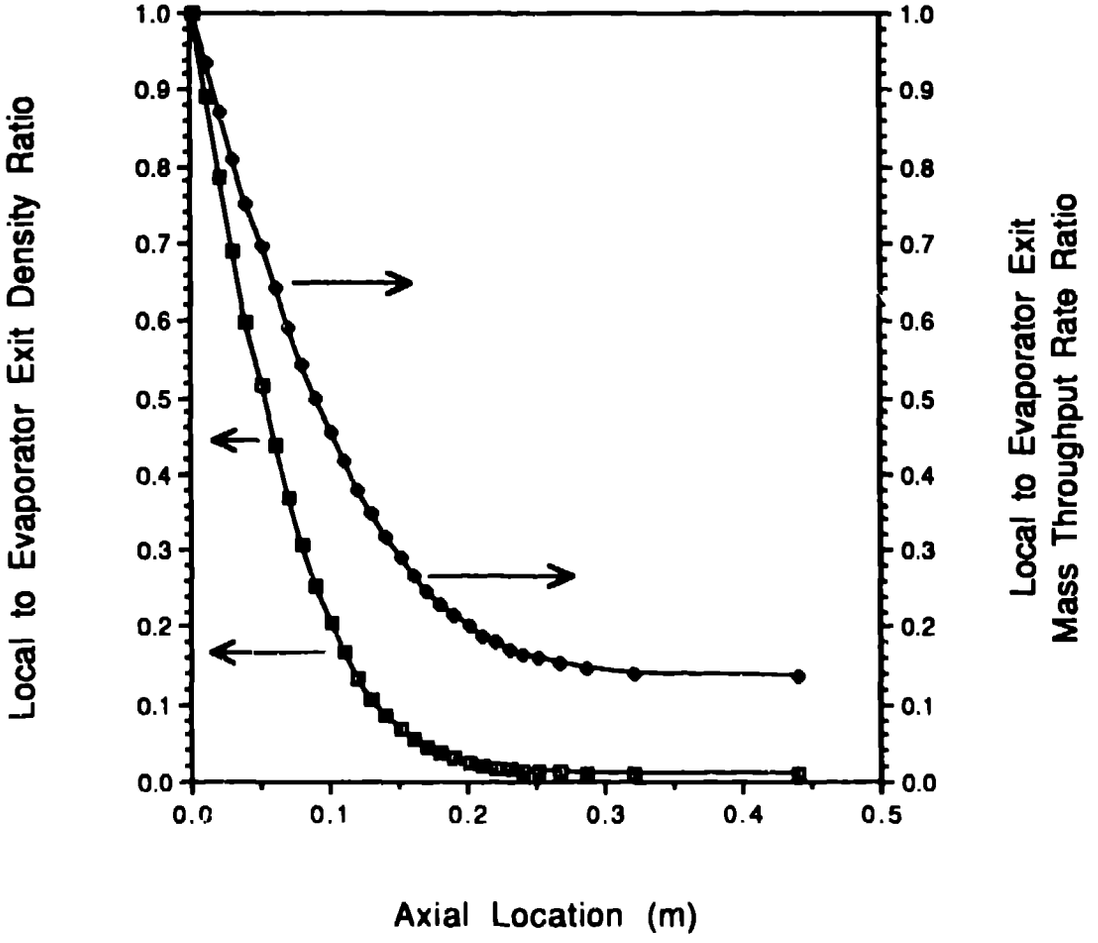

Figure 67 Density and Mass Throughput Rate Results for LTHP4 Model Predictions

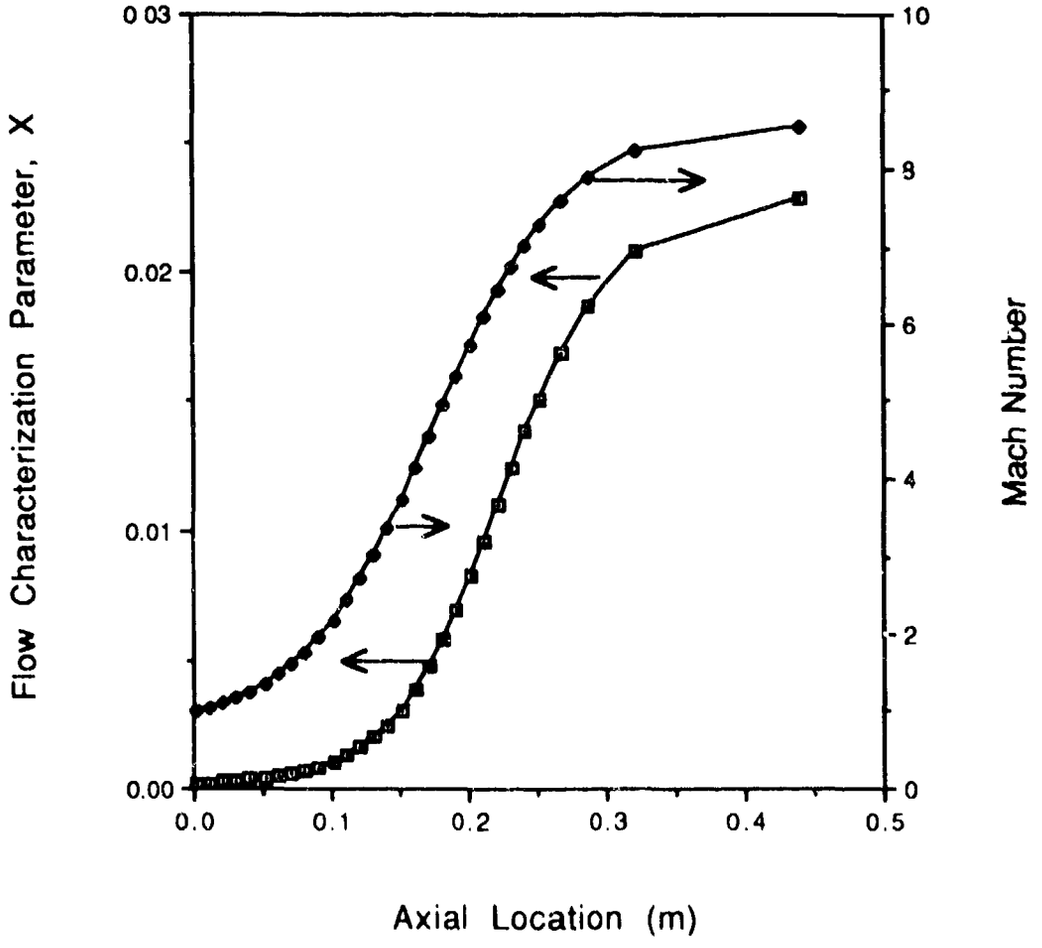

Figure 68. Model Predictions for the Flow Characterization Parameter and Mach Number for LTHP1

Figure 69 compares the predicted temperature profile to the data for the high temperature heat pipe. The predicted freeze front occurs at approximately 19.5 cm along the condenser as measured from the evaporator. The temperature data for HTHP shows the freeze front to occur at approximatly 20 cm from the evaporator exit. The predicted mass migration rate is 5.0E-8 kg/s, while the measured value is 2E-12 kg/s (7 μgm/hr).

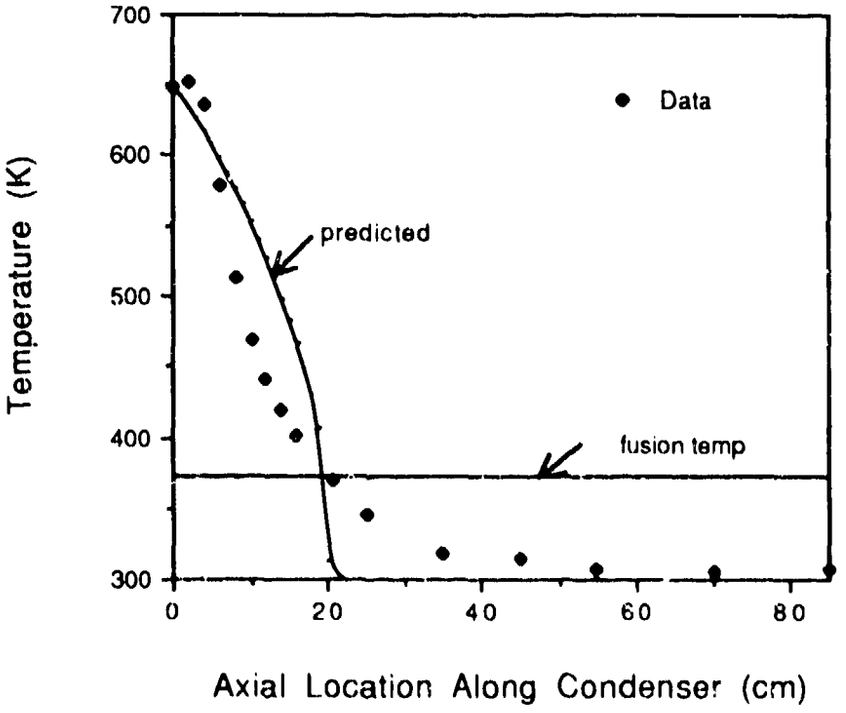

Figure 69. Predicted and Measured Temperature Profiles for HTHP

3.4 Conclusions

The experiments were successful in producing useful temperature profile data and mass accumulation data for both the low and high temperature heat pipes.

The model was able to satisfactorily predict temperature profiles for the low temperature heat pipes provided sufficient empirical data was available to input the appropriate average heat transfer coefficient. The temperature predictions are limited by the users estimate of the heat transfer coefficient. In the cases of LTHP1 and LTHP4, experimental data was available, and thus curve fit values for heat transfer coefficients could be determined. The predicted temperature profiles for LTHP1 and LTHP4 were good approximations to the actual profiles. The predicted mass migration rates into the frozen region exceeded the rates determined by experiment by 28% in the case of LTHP1 and under-predicted the rate by 48% in the case of LTHP4.

The performance limits for heat pipes are often influenced by a variety of factors, including the working fluid and structural materials, wick geometry and surface and wetting characteristics as well as the fabrication procedures and processing techniques. For these reasons, the calculation of boiling incipience, entrainment limitations, etc. are highly empirical. Often times there is no single equation or set of equations which can be used to predict a heat pipe's performance when operated in a given regime. This becomes particularly evident in reviews of some of the texts on heat pipe design and analysis.[11][12][13]

As more data on long-duration heat pipe operation in the low power regime becomes available, improvements to the analytical model should be possible, thus improving the models accuracy and utility as a design tool. Where order of magnitude estimates are needed and rough comparisons of designs are desired, this model should prove satisfactory.

The model was less satisfactory for predicting the temperature profiles and mass migration rates for the high temperature heat pipes. The model does approximately predict the temperature profile and location of freeze front, However, the model's predicted mass migration rate was several orders of magnitude higher than that measured experimentally. The predicted mass flow rate was 0.17 gm/hr, while the measured mass flow rate was 7 μgm/hr.

The difference in agreement between the low and high temperature mass flow predictions and there respective data is believed to be a result of the variations in the flow character for each. In the case of the low temperature heat pipes, the flow is largley in the slip or transition regime. Vapor flow in the high temperature heat pipe is largely free molecular. As flows become increasingly more rarified , as is the case between the high temperature and low temperature heat pipes, the flow dynamics become increasingly more difficult to model. For continuum flows, averages can be used to describe the various flow properties. For transition flows, it is still possible to use continuum flow relations with some modifications. The model was able to still successfully predict the flow properties for the low temperature heat pipes. However, it appears

that a one dimensional approach is insufficient for modeling the high temperature heat pipes which are characterized largely by free molecular flow. A more sophisticated, multi-dimesional model which accounts for nonlinearities in the velocity profile and the corresponding pressure and temperature gradients should prove more accurate and may be satisfactory.

The HTHP was designed to be nominally representative of actual space born heat pipe radiators. It was indicitive of the physical size and thermal capacity which would likely be employed on long mission duration spacecraft. Based on the measured mass migration rate for HTHP, a spacecraft radiator heat pipe might be expected to lose about 1 gm of working fluid to the frozen region every 5 to 20 years. The actual values will vary widely depending upon actual circumstances.

Long mission duration spacecraft radiators should be designed to account for mass migration rates on the order of those measured for the high temperature, sodium heat pipe used in this program. When possible, sufficient excess working fluid should be included in the design to offset any losses due to migration. Spacecraft radiator designs may also make use of vapor flow directors which may mitigate the migration of mass by directing the vapor radially towards the heat pipe walls, thus ncreasing the condensation rates near the warmer end of condenser. An alternative may be to change the operating strategy and occasionally heat the entire length of heat pipe, thus allowing frozen working fluid to thaw and wick back to the evaporator.

Appendix A

A One-Dimensional, Compressible Flow Analysis of Heat Pipe Vapor Dynamics in the Evaporator Section

Nomenclature

A	cross sectional area of vapor passage
c	sonic velocity
C_v	vapor specific heat at constant volume
C_p	vapor specific heat at constant pressure
f	friction factor
h	specific enthalpy of vapor
h_l	specific enthalpy of liquid
h_g	specific enthalpy of saturated vapor
h_f	specific enthalpy of saturated liquid
h_{fg}	enthalpy of vaporization (latent heat of vaporization)
k	ratio of vapor specific heats
M	Mach number
p	static pressure
Q	heat transfer rate
R	gas constant
T	absolute temperature
V	vapor velocity
V_l	liquid velocity
W	molecular weight
w	mass flow rate of vapor
w_l	liquid mass flow rate
z	axial coordinate
ρ	vapor density

Subscripts and Superscripts

0	evaporator upstream section, stagnation point
1	evaporator downstream section, evaporator exit
*	sonic conditions, M=1
s	saturation condition

Pressure, Temperature and Density Ratios

Consider the control volume shown schematically in Figure A.1. The control surface is considered to be the vapor side of the vapor-liquid

interface in the evaporator section. The cross sectional area is considered to be constant. The evaporator pressure ratio P_0/P_1 can be determined by a force-momentum balance over the control volume. For relatively high evaporation rates, frictional effects can be neglected, since inertial effects will dominate. The net force in the z-direction is $(P_0 - P_1)A$. The momentum transport in the z-direction at the upstream end (section 0) is zero, and at the downstream end (section 1) is $(\rho_1 A V_1)V_1$. The evaporated liquid entering the control volume does so radially and has no z-component of momentum. Balancing the force and momentum yields

$$(P_0 - P_1)A = (\rho_1 A V_1)V_1$$

or

$$P_0 - P_1 = \rho_1 V_1^2 \tag{A1}$$

Assuming the vapor behaves as an ideal gas with the equation of state

$$P = \rho RT \tag{A2}$$

and

$$C_p - C_v = R \tag{A3}$$

The velocity of sound in an ideal gas is given by

$$c = \sqrt{kRT} \tag{A4}$$

The Mach number defined as

$$M = \frac{V}{c} \tag{A5}$$

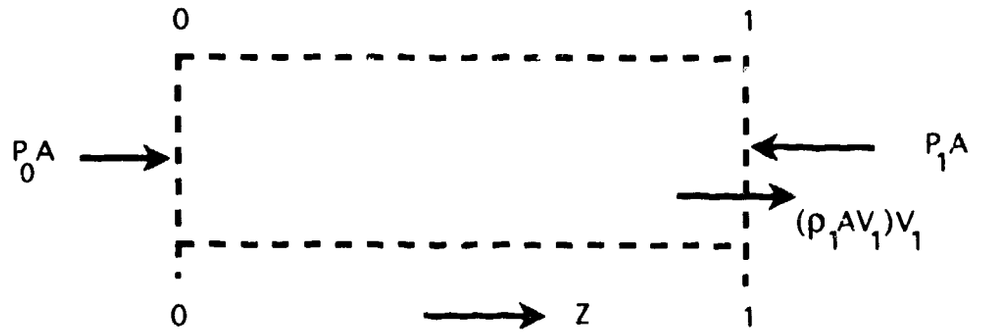

Figure A.1. Evaporator Control Volume for Force-Momentum Balance

Using equations (A2), (A4) and (A5), equation (A1) can be written as

$$\frac{P_0}{P_1} - 1 = \frac{\rho_1 V_1^2}{P_1} = \frac{M_1^2 kRT_1}{RT_1} = kM_1^2$$

or

$$\frac{P_0}{P_1} = 1 + kM_1^2 \qquad \text{(A6)}$$

The maximum velocity which can be developed at the evaporator exit is the sonic velocity (M_1=1) which occurs when the flow rate is a maximum (choked). The maximum evaporator pressure ratio occurs at this condition and is

$$\frac{P_0}{P_1^*} = 1 + k \qquad \text{(A7)}$$

If k is evaluated at the evaporator exit condition (T_1), then equations (A6) and (A7) are valid regardless whether k changes values at other locations along the evaporator.

Assume no shear work, no conduction or radiation of heat to the control volume, and that the kinetic energy of the mass entering the control

volume by evaporation can be neglected when compared with the enthalpy of the evaporated liquid. Further assume that the evaporated liquid enters the control volume at the upstream temperature of the main flow (T_0). Then for constant specific heat, the energy transport rate due to evaporated liquid is $w(C_pT_0)$. The energy transport rate at section 0 is zero, and the energy transport rate at section 1 is $w(C_pT_1 + V_1^2/2)$, which is the enthalpy transport plus the kinetic energy transport. These energy flows are depicted in Figure A.2.

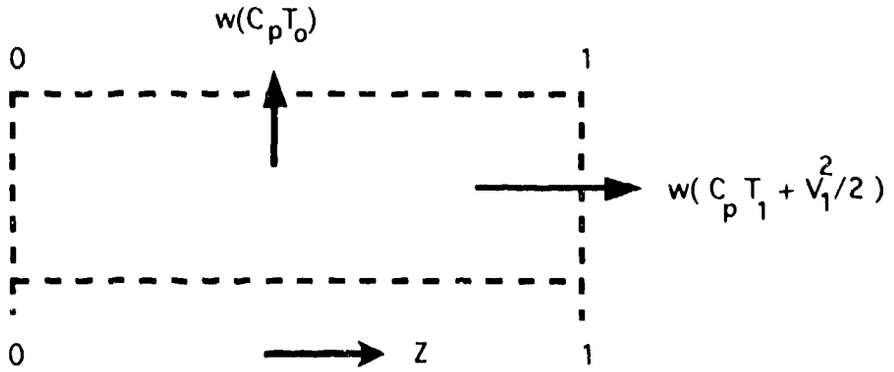

Figure A.2. Evaporator Control Volume for Energy Balance

At steady-state the energy balance becomes

$$w(C_pT_0) = w\left(C_pT_1 + \frac{V_1^2}{2}\right)$$

which can be rearranged as

$$\frac{T_0}{T_1} = 1 + \frac{V_1^2}{2C_pT_1} \qquad \text{(A8)}$$

Using equations (A3), (A4) and (A5) evaluated at section 1, equation (A8) may be modified to yield

$$\frac{T_0}{T_1} = 1 + \frac{M_1^2 kRT_1}{2C_pT_1} = 1 + \frac{M_1^2 k(C_p - C_v)}{2C_p}$$

or

$$\frac{T_0}{T_1} = 1 + \frac{k-1}{2} M_1^2 \qquad \text{(A9)}$$

The maximum evaporator temperature ratio corresponding to the choked flow condition ($M_1=1$) is

$$\frac{T_0}{T_1^*} = 1 + \frac{k-1}{2} = \frac{k+1}{2} \qquad \text{(A10)}$$

The assumption of constant C_p for an ideal gas implies that C_v, and thus k, W, and R are also constant. The evaporator density ratio can be determined from equation (A2).

$$\frac{\rho_0}{\rho_1} = \frac{P_0}{P_1}\frac{T_1}{T_0}$$

Substitution from equations (A6) and (A9) results in

$$\frac{\rho_0}{\rho_1} = \frac{1 + k M_1^2}{1 + \frac{k-1}{2} M_1^2} \qquad \text{(A11)}$$

At the choked flow condition

$$\frac{\rho_0}{\rho_1^*} = 2 \qquad \text{(A12)}$$

The density ratio is independent of k.

Note that the above property ratios correspond to those in Shapiro[8] found in Table 8.3, p.239 of vol. I headed 'Gas injection only, y=0, dA=0, dT_0=0, f=0'. This heading implies the following conditions and assumptions:

- y=0, gas injection normal to the main flow, no axial velocity component
- dA=0, constant cross section area normal to the flow
- dT_0=0, constant stagnation temperature and neglect kinetic energy of the gas entering the main stream
- f=0, neglect friction effects.

These are identical to the assumptions made in the preceding derivation.

When considering the properties temperature, pressure and density, only the pressure will be nearly uniform across the cross-section area. The temperature and density at section 1 as determined using equation (A9) and (A11) should be regarded as approximations of the averages existing at that point. Stagnation conditions exist at section 0, so the stagnation temperature, T_0, is known. One may proceed to determine downstream conditions by taking P_0 and P_1 to be the saturation pressures corresponding to T_0s and T_1s. The Mach number, M_1, and estimates of the average vapor temperature and density at the evaporator exit may then be calculated from equations (A6), (A9), and (A11), respectively. In equation (A11) ρ_0 is taken as the saturation density corresponding to T_0. For sonic flow at the evaporator exit, equations (A7), (A10) and (A12) apply.

Heat Transfer Rate

Heat transfer at the evaporator section can be evaluated by use of a control volume enclosing the entire evaporator including the vapor space, the liquid and wick structure and the envelope. The control volume is shown schematically in Figure A.3.

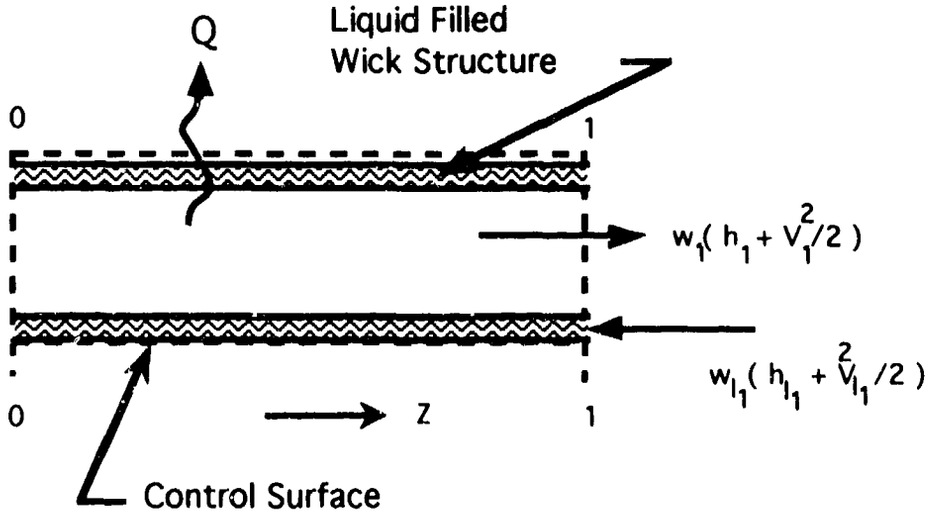

Figure A.3. Control Volume for Heat Transfer Rates

Neglecting axial conduction in the vapor, liquid filled wick structure and envelope, the steady-state energy balance can be written as

$$Q = w_1\left(h_1 + \frac{V_1^2}{2}\right) - w_{l_1}\left(h_{l_1} + \frac{V_{l_1}^2}{2}\right)$$

By conservation of mass

$$w_1 = w_{l_1}, \quad \text{and} \quad w_1 = \rho_1 A V_1$$

So the heat balance equation becomes

$$Q = \rho_1 A V_i \left[(h_1 - h_{l_1}) + \frac{V_1^2}{2} - \frac{V_{l_1}^2}{2} \right]$$

The difference between kinetic energy for the vapor and liquid is negligible. Furthermore, the specific enthalpy for the vapor is equal to the saturation enthalpy because the vapor is in equilibrium with the liquid at the vapor-liquid enthalpy interface. Because there is some radial conduction through the liquid, the vapor will be superheated at points away from the vapor-liquid interface. However this amount of superheat is negligible in relation to the latent heat. The heat throughput in terms of the evaporator exit conditions becomes

$$Q = \rho_1 A V_1 \, (h_{g_1} - h_{f_1}) \; = \; (\rho_1 A V_1) \, h_{fg_1} \qquad \text{(A13)}$$

Introducing the Mach number into equation (A13) results in

$$Q = \rho_1 A M_1 \sqrt{kRT_1} \; h_{fg}$$

where the subscript is omitted from the latent heat of vaporization, h_{fg}, since it is a weak function of temperature. However it should be noted that the latent heat should be evaluated at the saturation temperature corresponding to station 1. Utilizing the expressions (A9) and (A11) for T_1 and ρ_1 respectively in equation (A13) results in

$$Q = M_1 \frac{\sqrt{1 + \frac{k-1}{2} M_1^2}}{1 + k M_1^2} \rho_0 A \sqrt{kRT_0} \; h_{fg} \qquad \text{(A14)}$$

Solving equation (A6) for M_1 and substituting in equation (A14) results in

$$Q = \left(\frac{P_0}{P_1}\right)^{-1} \sqrt{\frac{1}{k}\left(\frac{P_0}{P_1} - 1\right)\left[1 + \frac{k-1}{2k}\left(\frac{P_0}{P_1} - 1\right)\right]}\ \rho_0 A \sqrt{kRT_0}\ h_{fg}$$

for the heat throughput in terms of the stagnation conditions (upstream end of the evaporator) and the evaporator pressure ratio.

For sonic conditions at the evaporator exit ($M_1 = 1$), the heat throughput rate becomes

$$Q^* = \frac{\rho_0 A \sqrt{kRT_0}\ h_{fg}}{\sqrt{2(k+1)}} \qquad \text{(A16)}$$

Appendix B

Listing of the Computer Code for the Mass Migration Model

```
REM  *11massmig,  040893                          04/08/93
REM  %%%%%%  additional remarks at end of program listing  %%%%%%
REM       **************     MAIN  PROGRAM     *****************

REM #Note: Output is best if SHOW OUTPUT is activated prior to running code.

REM  Initialization of variables
DEFINT i-j : DEFINT n: DEFDBL a-h : DEFDBL k-m: DEFDBL o-z
OPTION BASE 0
index=2001
DIM  t(index),  z(index),hfg(index),v(index),p(index),rho(index)
DIM  muu(index),mach(index),mdot(index),q(index),tsat(index)
DIM  bigx(index), delmdot(index), delq(index)

REM                  %%%%%%%%%  CONSTANTS  %%%%%%%%%
g=9.81  : rbar=8314 ' accel. of gravity (m/s^2) & univ. gas const.(J/kg-mol °K)
pi=3.14159:  qsum=0: mtot=0
REM            convergance criteria, counters, and No. of elements
epps1=.0001# :epps2 = .0000001#: epps3=.0003 : ncount=0: n=2000
i=0 : iflag=0:epps = .000001#: limmach=10000!
nprint = 10' print increment
slip= .014: molec=1! ' slip flow and molecular flow conditions
delz=.001' length of an element [m]
di=.62*.0254 : do=.87*.0254 '  inside and outside diameters [m]

tsink=27+273.13'        sink temperature [K]
emiss=.45'               pipe emissivity
hbar=2.9*.018/(.06*.0254)' equivalent heat transfer coeff. [W/m^2/K]

w1$="Tsink [K]" : w2$="Outside Diam. [in]": w3$="Inside Diam. [in]"
w4$="Eff.heat trns. coeff. [W/m^2/K]" : w5$="Stag. Temp. [K]"
w7$="Qsonic  [W]":w8$="Qtot"

REM CONSTANTS PECULIAR TO WORKING FLUID, FLUID$
fluid$="octadecane"
```

```
tc=745 : tb=590 : tfus=301 '  critical, boiling & fusion temperatures (K)
k=1.1114 : mw=254.502 ' ratio of spec. heats, molecular weight
rg=rbar/mw ' gas const.  (J/kg K)
adum  =.5*(k-1!)

FOR ii=1 TO 4
LOCATE 5, 2
PRINT "Be sure the fluid properties are correct for the working fluid, ";
PRINT fluid$ :CLS
NEXT ii
LOCATE 10, 2
PRINT "Be sure the fluid properties are correct for the working fluid, ";
PRINT  fluid$
PRINT""
PRINT" To continue hit RETURN.  Otherwise, pull up the listing and check properties."
   executor:
INPUT"",ss$

              OPEN "zdat" FOR OUTPUT AS #1
              OPEN "mdotdat" FOR OUTPUT AS #2
              OPEN "tdat" FOR OUTPUT AS #3
              OPEN "pdat" FOR OUTPUT AS #4
              OPEN "rhodat" FOR OUTPUT AS #5
              OPEN "machdat" FOR OUTPUT AS #6
              OPEN "bigxdat" FOR OUTPUT AS #7
               OPEN "titlesdat" FOR OUTPUT AS #8
              OPEN "miscdat" FOR OUTPUT AS #9
                OPEN "t-profile" FOR OUTPUT AS #10
              OPEN "tmach" FOR OUTPUT AS #11


REM  ************        SOLUTION        ****************
   solution:
i=0 : jcount=0
INPUT" Enter stagnation temperature, [K]",t(0)
  tsat(0) = t(0)
```

```
GOSUB satpress
rho0=p0/rg/tsat(i) '            [kg/m^3]
p(i+1)=p0/(1+k)   '  Evaporator exit pressure @ sonic limit [N/m^2]
 t(i+1)=2!*t(0)/(k+1!)   '  Evap.  exit temperature @ sonic limit [K]
i=1
CALL  sattemp(p(i),t(0),tsat(i))
GOSUB latheat
hfg(0)=hfg(1)

REM                    *** Sonic Power Limit ****
CALL  sonic(t(0),hfg(1),q(1))

REM  %%  initialization of evaporator exit quantities used in
REM                  stepwise calculations. %%%

          tsat(i)=tsat(i)
         delq(i)=0
           mdot(i)=q(i)/hfg(i)
           mach(i)=1! :mach(i-1)=0!
            rho(i)=p(i)/rg/tsat(i)
         z(0)=0
 PRINT " q(1), mdot(1) , P(1)";
 PRINT USING" ##.#####^^^^     ";  q(1), mdot(1),p(1)

REM      *******          ELEMENT SOLUTIONS  *****
    FOR i=1 TO n
IF  (tsat(i-1)-tsat(i))/tsat(i) < epps3  THEN  delz=2!*delz
IF  i=1  THEN  z(i)=0
z(i)=z(i-1)+delz
asurf=pi*do*delz
REM  hbar=emiss*.0000000567#*(tsat(i)+tsink)*(tsat(i)^2+tsink^2)'    ##  REM  this  line
REM                                                FOR convection B.C. ###
delq(i)=-1*hbar*(tsat(i)-tsink)*asurf
GOSUB viscos
REM GOSUB latheat
hfg(i)=hfg(1)
```

```
q(i+1)=q(i)+delq(i)
  delmdot(i) = -1!*delq(i)/hfg(i)
 mdot(i+1) = mdot(i) - delmdot(i)
IF mdot(i+1) < 0! THEN GOTO endroutine
lmach=mach(i-1)
wdum = mdot(i+1)/mdot(i)
IF mach(i)>limmach THEN mach(i+1)=mach(i): GOTO downstre
CALL mach2((i), (delmdot(i)),(mach(i)),mach(i+1))

 downstre:
REM                %%%  Downstream Properties %%%
REM t(i+1) = t(i)*((1! + adum*mach(i)^2)/(1! +adum*mach(i+1)^2))
p(i+1) = p(i)*wdum*(mach(i)/mach(i+1))*SQR((1! + adum*mach(i)^2)/(1!
+adum*mach(i+1)^2))
CALL sattemp(p(i+1),(tsat(i)),tsat(i+1))
tsat(i+1)=tsat(i+1)-beta
rho(i+1)=p(i+1)/rg/tsat(i+1)

REM      ************    Determination of flow character    ***********
rho1=(rg*tsat(i)/g)^-1  :  pmean=(p(i+1)+p(i))/2
bigx(i)=2*muu(i)/(pmean*di*SQR(rho1*g))
mtot=ABS(mtot+delmdot(i))
qsum=qsum-delq(i)

REM %%%%%%%  Routine Stoppage Criteria  %%%%%%%%%%%

IF ABS(mtot-mdot(1)) <= (mdot(1)*.0001#) OR mtot > mdot(1) THEN PRINT" All mass
removed ":GOTO endroutine
IF tsat(i)<=tsink THEN PRINT" T at or below sink temperature ",tsat(i): GOTO endroutine
IF bigx(i)< slip THEN GOTO nextelem
IF bigx(i) >= slip AND bigx(i) < molec THEN GOTO 100
IF bigx(i) >= molec AND iflag < 2 THEN PRINT"MOLECULAR FLOW ",bigx(i): iflag=2!
GOTO nextelem
100 :  IF iflag < 1 THEN PRINT"SLIP FLOW ",bigx(i) : PRINT" @ z - ",z(i)
       iflag=1!
           v2=mach(i+1)^2*k*rg*tsat(i+1)
```

```
                f=(do/2#/rho(i+1)/v2)*(p(i)-p(i+1))/deiz
PRINT" f @ i = "; f,i
  nextelem:
    nn=i
    ncount=0
   NEXT i

      nn=i-1
  endroutine:

REM                    ******* Output Routines ***********
   PRINT" DONE AND DONE AT i =",i:PRINT "Qsonic = ", q(1)," Qtot = ", qsum
   INPUT" hit RETURN ";DUMMY

   FOR i = 1 TO nn STEP nprint
WRITE #1, CSNG(z(i))
WRITE #2, CSNG(mdot(i)/mdot(1))
WRITE #3, CSNG(tsat(i)/tsat(1))
WRITE #4, CSNG(p(i)/p(1))
WRITE #5, CSNG(rho(i)/rho(1))
WRITE #6,CSNG(mach(i)/mach(1))
WRITE #7, CSNG(bigx(i))
WRITE #10, CSNG(tsat(i))
WRITE #11, CSNG(t(i))

NEXT i
WRITE #8,w1$:WRITE #8,w2$:WRITE #8,w3$:WRITE #8,w4$:WRITE #8,w5$
WRITE #8,w7$:WRITE #8, w8$:WRITE #8,fluid$
WRITE #9, tsink:WRITE #9,do/.0254:WRITE #9,di/.0254:WRITE #9,hbar
WRITE #9,t(0):WRITE #9,q(1):WRITE #9,qsum

CLOSE #1:CLOSE #2: CLOSE #3: CLOSE #4: CLOSE #5: CLOSE #6: CLOSE #7
CLOSE #8: CLOSE #9:CLOSE #10:CLOSE #11

nprint=4*nprint
qsum=0:pinc=nprint:PRINT" nn = ",nn
```

```
PRINT"   Z(m)   T(K)      hfg(J/kg)       dq(W)      q(W)        X      Mach No."
FOR i=1 TO nn
qsum=qsum+delq(i)
IF i=1 THEN GOTO table
IF i=pinc OR i=nn THEN GOTO table
GOTO looper
  table:
 pinc=nprint+pinc
   PRINT USING" #.###";z(i);
   PRINT USING"   ###.##"; tsat(i);: PRINT USING"   #.####^^^^"; hfg(i), q(i);
   PRINT USING"   ###.###";qsum;
   PRINT USING"     #.#####"; bigx(i),mach(i)
  looper:
 NEXT i
END

REM                  ************  SUBROUTINES ****************
REM                      ++++++++++++++++++++++++++++++++++++++++++

REM                          ++++++++++++++++++++++++++++++++++++
REM  calculate temperature along saturation curve, tsat(i) corresponding
REM  to p(i)
 SUB sattemp( p,t0,ts) STATIC
SHARED epps2
ts=t0  :ncount=0
GOTO tloop
  tcont3:
PRINT" max. iteration count critera (100), exceeded"
PRINT" continue with relaxed convergance critera ?"
INPUT" enter new value(negative #=stop)";epps2
IF epps2 <=0! THEN STOP

ncount = 0
   tloop:
ncount=ncount + 1
GOTO pcode
```

```
 tcont2:
tsnew=ts-(p0-p)/p0prime
IF ABS((tsnew-ts)/ts)<epps2 THEN GOTO tcont1
IF ncount>100 THEN GOTO tcont3
ts=tsnew
GOTO tloop
   REM   working fluid = n-octadecane
 pcode:
         p0=7.8617#-2644.1#*(1/ts)-173690#*(1/ts)^2
     p0=132.89#*10^p0 '     [N/m^2]
         p0prime=LOG(10#)*(2644.1#/ts^2+2#*173690#/ts^3)*p0
GOTO tcont2
  tcont1:
   ts=tsnew
END SUB

REM                              ++++++++++++++++++++++++++++++++
REM calculate sonic limit and mass throughput at the evaporator exit

SUB sonic(temp,latheat,qsonic) STATIC
SHARED rho0,k,rg,pi,di
qovera=rho0*SQR(k*rg*temp)*latheat/SQR(2*(k+1))
ac=pi*di^2/4
qsonic=ac*qovera
END SUB

REM                              ++++++++++++++++++++++++++++
REM finds M2 using incremental search and bisection method
SUB mach2(j,dm,M1,M2) STATIC
SHARED k,pi,mdot(),muu(),adum, wdum,delz,do,epps,lmach,limmach,f
dm=dm/delz : Mfix=M1
Rey=4!*mdot(j)/muu(j)/pi/do
PRINT "Re No.",Rey
 IF Rey < 10^5 THEN GOTO 302
301 : f=.0791/Rey^(1/4) :GOTO 303
302 : f=SQR((3.6*LOG(Rey/7))^-1)
```

```
REM  friction factor routine :Prandtl's Eqn. 'fixed pt. iteration scheme
303 :  fstar=f*Rey
bdum=fstar*muu(j)*pi*k/dm
cdum = (1! +adum)/(2!*adum +bdum)
ddum = (1!-bdum)/(2!*adum + bdum)
edum=wdum*M1
edum=edum*(1!+adum*M1^2)^(-1!*cdum)

REM                    Incremental search routine
ncount2=1
jj = 0
mg=M1
 GOTO machfunc
  it3cont1:
ncount2=ncount2+1
jj = 1
xsav=xdum
M2=M1+(M1-Imach)
mg=M2 : GOTO machfunc
  it3cont2:
IF (xsav * xdum) < 0! THEN GOTO bisect
M1=M2 : GOTO it3cont1

REM          Bisection Routine
  bisect:
jj = jj + 1
mlo = M1 : mhi = M2
  itloop1:
mg = (mhi+mlo)*.5
jjj = 0
GOTO machfunc
   it1cont1:
jj = jj + 1
IF ABS(xdum) < epps GOTO endloop3
jjj = 1
msave = mg
```

```
xsav = xdum
mg = mlo : GOTO machfunc
   it1cont2:
IF xsav*xdum < 0! THEN mhi = msave ELSE mlo = msave
IF jj>50 THEN PRINT" max. iteration stop criteria, jj = "; jj
IF jj>50 THEN PRINT"M2, msave :"; mg, msave
IF jj>50 THEN PRINT"continue ? ":STOP
GOTO itloop1

REM  function for implicitly defining downstream Mach No. in terms of
REM  upstream Mach No. and mass removal rate.

  machfunc:
IF mg > limmach THEN GOTO endloop2
IF (2!-bdum*mg^2)/(2!-bdum*Mfix^2) < 0 THEN STOP
xdum  =  mg*(1!+adum*mg^2)^(-1!*cdum)*((2!-bdum*mg^2)/(2!-bdum*Mfix^2))^ddum
xdum =xdum - edum
IF jj=0 GOTO it3cont1
IF jj=1 GOTO it3cont2
IF jj>1 AND jjj= 0 GOTO it1cont1
IF jj>1 AND jjj= 1 GOTO it1cont2
  endloop2:
PRINT" Solution becoming asymptotic !"
PRINT" Upstream Mach No.(M1) and downstream search interval [a,b] for M2"
PRINT USING"########.#      ";Mfix,m1,m2
PRINT"Continue ?  M2 and all subsequent mach numbers will be set "
INPUT"at INPUT value.  (negative number = NO )"; mg
IF mg < 0 THEN STOP
  endloop3:
M2 = mg
END SUB


   REM  working fluid = octadecane
   REM  calculates saturation pressure (stagnation pressure for stagnation
   REM  temperature)
```

```
SATPRESS:
        p0=7.8617-2644.1*(1/tsat(i))-173690#*(1/tsat(i))^2
    p0=132.89*10^p0 '    [N/m^2]
  RETURN

   REM  working fluid = octadecane
   REM  calculates the latent heat of fusion as a function of temperature
LATHEAT:
     tr=tsat(i)/tc
        hfg(i)=(10481*(1-tr)^.354+12805*(1-tr)^.456)*4184/MW'        [J/kg]
  RETURN

   REM  working fluid = octadecane
   REM  calculates the vapor absolute viscosity at atmospheric pressure and
   REM   temperature t(i).
VISCOS:
    aa=1.16145:  bb=.14874:  cc=.52487:  dd=.7732:  ee=2.16178: ff=2.43787
      tfict=.001451*tsat(i)
       muu(i)=aa/tfict^bb+cc/EXP(dd*tfict)+ee/EXP(ff*tfict)
       muu(i)=.0000005187#*SQR(tsat(i)/muu(i))  '    [kg/m/s]
  RETURN
```

```
REM          ###########   Program Description   #############
REM  Mass migration within a heat pipe. The heat pipe is operating under
REM  sonic conditions at some heat load and corresponding sink temperature
REM  significantly lower than its design operating point. The conditions at
REM  the evaporator exit (choke point) are defined. These conditions
REM  form the entrance boundary conditions for the mass migration
REM  model. That is, the mass flowrate, temperature and corresponding
REM  saturation pressure as well as vapor velocity (mach 1.0) are known at
REM   the evaporator exit. The parameters describing the heat sink, once
REM   defined, complete the list of necessary constraints on the model.
```

```
REM  This model requires an input heat sink temperature and an equivalent
REM  heat transfer coefficent (hbar). Hbar may be a constant or a function
REM  of one or more variables.

REM  The temperature of each element is assumed to equal the exit temper-
REM  ature of the previous element ( e.g., T1=T evap. exit).

REM  Important assumptions used to simplify the 1-D governing compressible
REM  flow equation are: 1) constant stagnation temperature; 2) constant
REM  cross sectional area; 3) condensation at the main stream axial velocity
REM  In addition, there are no internal bodies present to produce drag.
```

Appendix C

Sample Calculations for a Parametric Study for the Vibration Response Technique for Measuring Mass Migration in a Heat Pipe

The Influence of Pipe Diameter, Wall Thickness and Pipe Length on the First Two Modes of Vibration

k1 := 10 k2 := 10 k1 & k2, spring constants, lb/in

Ro := 0.25 tube radius, inches δ := 0.010 wall thick., in.
Ri := Ro - δ

ζ := .1128 Mass moment of inertia about the C.G. for for an eccentric load. In this case two 5 oz. accelerometers, spaced 8.35".

i := 1 ..100

$l1_i := 1.\cdot i$ $l2_i := l1_i \cdot 1.001$ $L_i := l1_i + l2_i$ total length

ρ := 0.29 density, stainless steel lb/in^3

$$ma_i := \rho \cdot \pi \cdot \left[Ro^2 - Ri^2 \right] \cdot L_i$$ tube weight, (force: lbm)

$$m_i := \frac{ma_i}{386.4}$$ tube mass, lbf*s^2/in

$$J_i := \frac{m_i}{4} \cdot \left[Ro^2 + Ri^2 + \frac{L_i^2}{3} \right] + \zeta$$ mass moment of inertia for a tube,in-lb-s^2/radian

$$r_i := \frac{\sqrt{J_i}}{\sqrt{m_i}}$$

$$a_i := \frac{1}{m_i} \cdot (k1 + k2)$$

$$b_i := \frac{1}{m_i} \cdot \left[k2 \cdot l2_i - k1 \cdot l1_i \right]$$

$$c_i := \frac{1}{J_i} \cdot \left[k1 \cdot l1_i^2 + k2 \cdot l2_i^2 \right]$$

$$\omega 1_i := \sqrt{a_i - \left[\frac{b_i^2}{2 \cdot \left[r_i \cdot \left[c_i - a_i \right] \right]} \right]}$$

$$\omega 2_i := \sqrt{c_i + \left[\frac{b_i^2}{2 \cdot \left[r_i \cdot \left[c_i - a_i \right] \right]} \right]} \quad \text{rad/second}$$

$$f1_i := \frac{\omega 1_i}{2 \cdot \pi} \qquad f2_i := \frac{\omega 2_i}{2 \cdot \pi} \quad \text{cycles/sec. (Hz)}$$

$$rat_i := \frac{f2_i}{f1_i}$$

$L_{12} = 24.012$

$f1_{12} = 42.733$

$f2_{12} = 24.061$

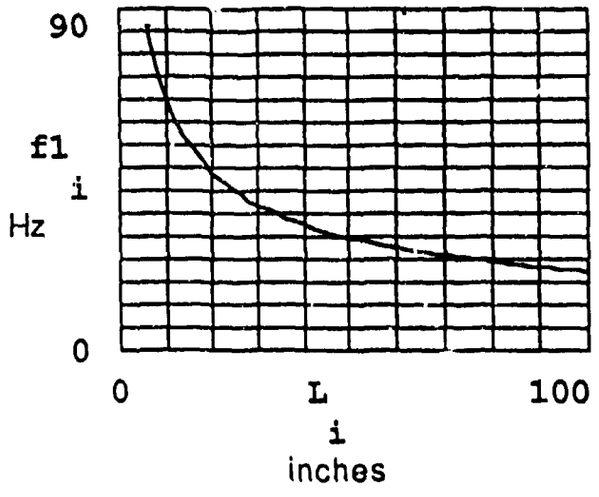

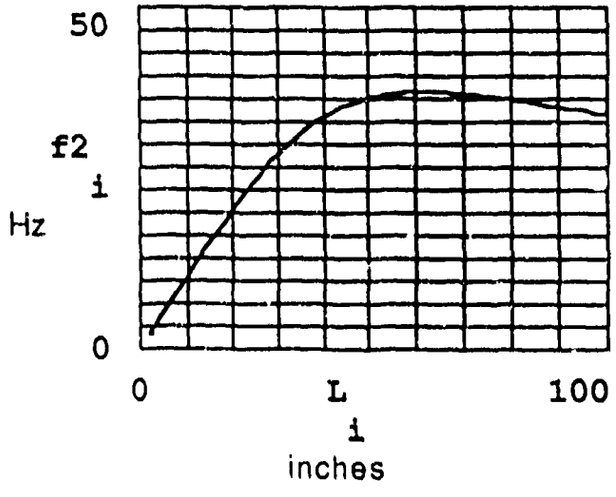

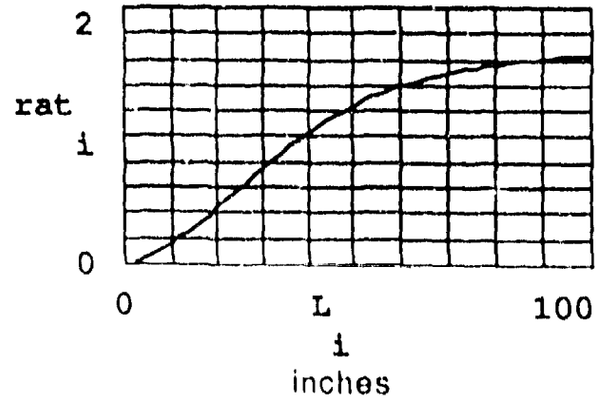

Appendix D

Thermophysical Properties for Octadecane

Vapor Pressure

T (K)	(N/m2)
392.773	1.33e+2
425.351	6.67e+2
442.870	1.33e+3
460.617	2.67e+3
480.538	5.33e+3
492.854	8.00e+3
509.165	1.33e+4
533.618	2.67e+4
561.167	5.33e+4
590.319	1.01e+5

Latent Heat

T(K)	(J/kg)
310.000	3.071e+5
340.000	2.983e+5
370.000	2.891e+5
400.000	2.794e+5
430.000	2.692e+5
460.000	2.585e+5
490.000	2.219e+5
510.000	2.165e+5
540.000	1.992e+5
570.000	1.844e+5
600.000	1.683e+5

Liquid Viscosity

T (K)	(centi Poise)
330.000	2.1740
350.000	1.5919
370.000	1.2074
390.000	0.9421
410.000	0.7531
430.000	0.6147
450.000	0.5109
470.000	0.4313
490.000	0.3692
510.000	0.3200
530.000	0.2803
550.000	0.2479
570.000	0.2211
590.000	0.1988

Vapor Viscosity

T (K)	(micro Poise)
330.000	40.4240
350.000	42.8300
370.000	45.2600
390.000	47.7120
410.000	50.1840
430.000	52.6730
450.000	55.1760
470.000	57.6930
490.000	60.2200
510.000	62.7550
530.000	65.2960
550.000	67.8410
570.000	70.3880
590.000	72.9360

Liquid Density

T (K)	(gm/cm3)
330.000	0.7563
350.000	0.7419
370.000	0.7276
390.000	0.7132
410.000	0.6988
430.000	0.6843
450.000	0.6697
470.000	0.6549
490.000	0.6397
510.000	0.6242
530.000	0.6083
550.000	0.5919
570.000	0.5749
590.000	0.5573

Vapor Density

T (K)	(gm/cm3)
330.000	2.200e-7
350.000	9.000e-7
370.000	3.100e-6
390.000	9.100e-6
410.000	2.400e-5
430.000	5.600e-5
450.000	1.200e-4
470.000	2.400e-4
490.000	4.600e-4
510.000	8.200e-4
530.000	1.400e-3
550.000	2.200e-3
570.000	3.500e-3
590.000	5.300e-3

Surface Tension

T (K)	(dyne/cm)
330.000	25.0342
350.000	23.5935
370.000	22.1673
390.000	20.7563
410.000	19.3611
430.000	17.9824
450.000	16.6212
470.000	15.2783
490.000	13.9548
510.000	12.6519
530.000	11.3711
550.000	10.1139
570.000	8.8822
590.000	7.6785

References

1. Woloshun, K. A.; Sena, J. T.; Keddy E. S.; and Merrigan, M. A., "Radial Heat Flux Limits in Potassium Heat Pipes: An Experimental and Analytical Investigation," *Proceedings of the 7th Symposium on Space Nuclear Power Systems, The Institute for Space Nuclear Power Studies,* Chemical/ Nuclear Engineering Department, University of New Mexico, Albuquerque NM 87131, January 7-11, 1990.

2. Brown, G. P.; DiNardo, A.; Cheng, G. K.; and Sherwood, T.K., "The Flow of Gases in Pipes at Low Pressure," *Journal of Applied Physics*, Vol.17, 1946, pp. 802-813.

3. Perry, R. H. and Green, D., *Perry's Chemical Engineers' Handbook*., Sixth ed., Sec. 5, McGraw-Hill Publishing Co., NY, 1984.

4. Cotter, T.P., *Heat Pipe Startup Dynamics*, Thermionic Conversion Specialist Conference, Oct. 30 - Nov. 1, 1967, Palo Alto, CA

5. Deverall, J.E., Kemme, J.E., Florschuetz, L.W., *Sonic Limitations and Startup Problems of Heat Pipes*, Los Alamos Scientific Laboratory, LA-4518, 1970

6. Busse, C.A., *Theory of the Ultimate Heat Transfer Limit of Cylindrical Heat* Pipes, Int. J, Heat Mass Transfer, vol. 16, pp 169-186, Pergamon Press 1973

7. Deverall, J.E., Salmi, E.W., Knapp, R.J., *Orbital Heat Pipe Experiment*, Los Alamos Scientific Laboratory Report LA-3714, June 1967

8. Shapiro, Ascher H., *The Dynamics and Thermodynamics of Compressible Fluid Flow*, Ronald Press Co. vol. I, 1953

9. Merrigan, M.A , Keddy, E.S., *High Temperature Heat Pipes for Waste-Heat Recovery*, Journal of Energy, v. 6, no. 5, Sept.-Oct. 1982, p. 298

References (Cont.)

10. Deverall, J.E., *Mercury as a Heat Pipe Fluid*, Los Alamos Scientific Laboratory Report LA-4300-MS, Jan. 5, 1970

11. Dunn, P.D., Reay, D.A., Heat Pipes, 3rd. ed, Pergamon Press, 1982

12. Brennan, P.J., Krolicsek, E.J., Heat Pipe Design Handbook, prepared for NASA Goddard Space Flight Center, Contract No. NAS5-23406, June 1979

13. Chi, S.W., Heat Pipe Theory and Practice: A Sourcebook, Hemisphere Publishing Co. 1976

14. Merrigan, M. A.; Keddy, E. S.; and Sena, J. T., "Transient Performance Investigation of a Space Power System Heat Pipe", 4th Joint Thermophysics and Heat Transfer Conference, June 2-4, Boston, Mass., AIAA-86-1273